The putative role of HERC5 in NSCLC metastasis and its potential utility as a liquid biopsy marker

Dissertation

With the aim of obtaining a doctoral degree (Dr. rer. nat.)
at the Department of Biology
Faculty of Mathematics, Informatics and Natural Sciences
University of Hamburg

submitted by:

Svenja Schneegans

Hamburg, May 2020

Reviewers of the dissertation:

Prof. Dr. Susanne Dobler
Fakultät für Mathematik, Informatik und Naturwissenschaften
Fachbereich Biologie
Institut für Zoologie
Molekulare Evolutionsbiologie
Martin-Luther-King-Platz 3
20146 Hamburg

Prof. Dr. Harriet Wikman-Kocher
Institut für Tumorbiologie
Zentrum für Experimentelle Medizin
Universitätsklinikum Hamburg-Eppendorf
Campus Forschung N27, 4. Etage
Martinistraße 52
20246 Hamburg

Date of oral defense: June 26$^{\text{th}}$ 2020

„Je mehr ich weiß, desto mehr erkenne ich,
dass ich nichts weiß.“

Albert Einstein

Contents

Abstract

Non-small cell lung cancer (NSCLC) accounts for the majority of lung cancer cases, with the overall five-year survival rate being only around 15%. Metastasis remains the primary cause for all cancer-related deaths, including NSCLC. Metastatic relapse is caused by disseminated tumor cells (DTCs), which have been able to escape the primary tumor and outgrow at distant organs. Recently, HERC5 has been identified as a potential metastasis suppressor gene in NSCLC, as its loss was correlated with positive DTC status as well as occurrence of brain metastasis and shortened both disease-free and overall survival.

This thesis investigated the role of the putative metastasis suppressor HERC5 in early dissemination. In lung cancer cell lines, low HERC5 expression was significantly associated with an elevated aggressive phenotype including increased migratory potential, as well as clonogenic and anchorage-independent growth, while proliferative capacity was not altered. These characteristics indicate that HERC5 harbors metastasis-suppressing function rather than onco-suppressing properties. Since HERC5 has been associated with increased metastasis formation in brain and bone, the microenvironmental influence of these tissues was analzyed as well, but were shown to have no effects on the HERC5-mediated carcinogenic traits in the model systems.

Interestingly, RNAseq analysis of HERC5 overexpressing and control cell lines did not show alterations in downstream pathways, as only two genes were found to be differentially regulated. This indicates that the oncogenic function of HERC5 might be regulated more at the protein level via its E3 ligase activity.

Previous studies linked HERC5 function mainly to viral defense mechanisms and regulation of the innate immune response. In endothelial cells HERC5 is upregulated by inflammatory cytokines such as TNFα or interferons, hereby catalyzing the transfer of the ubiquitin-like modifier ISG15 onto target proteins as an E3 ligase. The ISGylation of target proteins induces pleiotropic effects such as DNA repair, interference with the ubiquitin system and exosome secretion.

The present study aimed at identifying novel interacting and ISG15 target proteins in NSCLC cell lines after activation by inflammatory cytokines. SILAC-based proteomic analysis revealed 42 HERC5 ISGylation targets. However, no specific pathway was found to be altered when performing gene annotation enrichment analysis, possibly indicating a lower impact of IFNγ and TNFα in protein ISGylation on immune-related processes in NSCLC.

Extracellular vesicles (EVs) are important mediators of cell-cell-communication. Tumor-derived EVs have been previously shown to prime the so-called pre-metastatic niche by inducing e.g. vascular leakage, remodeling of the extracellular matrix, and

immunosuppression. The here presented study demonstrated that under inflammatory conditions, the secretion of EVs is enhanced in HERC5-depleted lung cancer cells. Moreover, preliminary results indicated that EV protein cargo is specifically altered in these cells. In contrast to the limited amount of intracellular pathways affected by ISGylation, functional annotation analysis of EV proteins revealed an enrichment of pathways connected to innate immune responses as well as cell adhesion showing a possible link between HERC5 expression and an immunomodulatory function of the vesicles.

Early detection of cancer is highly important for prevention of primary and metastatic disease. Liquid biopsies from blood of cancer patients can give important information on the tumor state and evolution without the necessity of invasive procedures. Moreover, the combined analysis of different liquid biomarkers can give complimentary information on disease state compared to single analysis. A prerequisite for clinical utility is also the development of standard operating procedure (SOPs) for these highly sensitive assays. Here, we show the feasibility of a combined liquid biopsy assay, obtaining results from circulating tumor cells (CTCs), circulating tumor DNA (ctDNA), and miRNAs from a single blood draw. The outcome of the analysis, however, strongly depends on the selection of blood-collection tube and normalization methods of next-generation sequencing data, indicating the importance of strict SOPs. Furthermore, a method for standardized, semi-automated detection of CTCs from cancer patients was established. Combined, these results are important prerequisites for the establishment of a HERC5-based liquid biopsy assay in the future.

Taken together, the results indicate that low HERC5 levels elevate metastatic potential *in vitro*. Its impact on extracellular signaling via EVs in an immunomodulatory context is increased while intracellular pathways are less affected by HERC5 levels and ISGylation of proteins. Further analysis needs to be performed to evaluate the exact nature of tumor and immune cell cross talk. Liquid biopsy experiments could validate whether HERC5 could become a blood-based biomarker aiding in early detection of relapse in NSCLC.

Zusammenfassung

Das Nicht-kleinzellige Bronchialkarzinom (NSCLC) stellt die Mehrheit aller Lungenkrebs-fälle dar, dessen Fünf-Jahres-Überlebensrate bei lediglich circa 15% liegt. Metastasen bilden den Hauptgrund für alle krebsbedingten Todesfälle, einschließlich NSCLC. Rück-falle der Metastasierung werden durch disseminierte Tumorzellen (DTCs) verursacht, die es geschafft haben, dem Primärtumor zu entweichen und in entfernten Organen herauszuwachsen. Aktuelle Studien identifizierten HERC5 als potentielles Metastase-Suppressorgen, denn es korreliert sowohl mit positivem DTC-Status als auch Gehirn-metastasierung und einem verkürzten krankheitsfreien- und Gesamtüberleben in Lun-genkrebspatienten.

Die vorliegende Studie untersucht die Rolle des potentiellen Metastasesuppressors HERC5 im Zusammenhang mit früher Disseminierung. In Lungenkrebs-Zelllinien wurde HERC5 mit einem erhöhten aggressiven Phänotyp assoziiert, welcher ein erhöhtes Migrationspotential, klonogenes Überleben und Wachstumsfähigkeit in Suspension beinhaltet. Unverändert bleibt dabei die proliferative Kapazität. Diese Charakteristika deuten darauf hin, dass HERC5 eher Metastase-supprimierende als onkogene Funk-tionen besitzt. Aufgrund der erhöhten Metastasierungsrate in Gehirn und Knochen durch geringe HERC5 Expression wurde der Einfluss dieser Mikroumgebungen ebenfalls analysiert. Es wurden keine Effekte auf HERC5 vermittelte, karzinogene Eigenschaften in den Modellsystemen festgestellt.

Bemerkenswert ist, dass durch RNA-Sequenzierung von HERC5-überexprimierenden und Kontrollzelllinien keine Veränderungen in nachgeschalteten Signalwegen nachge-wiesen wurden, denn nur zwei differentiell reguliert Gene wurden identifiziert. Daher könnte die onkogene Funktion von HERC5 viel mehr auf Proteinebene anhand seiner E3 Ligaseaktivität reguliert sein.

Vorherige Studien brachten die Funktion von HERC5 hauptsächlich mit viralen Ab-wehrmechanismen und Regulation der angeborenen Immunantwort in Verbindung. In Endothelzellen wird HERC5 durch inflammatorische Zytokine wie TNFα oder Interfer-one hochreguliert, wodurch der Transfer der Ubiquitin-ähnlichen Modifikation ISG15 auf Zielproteine katalysiert wird. Die ISGylierung von Zielproteinen bewirkt pleiotropis-che Effekte, wie unter anderem DNA-Reparatur, Beeinträchtigung des Ubiquitin-Systems und Freisetzung von Exosomen.

Die vorliegende Studie zielte darauf ab, nach Aktivierung durch inflammatorische Zytokine neue Interaktionspartner und ISG15 Zielproteine in NSCLC zu identifizieren. SILAC-basierte Proteomanalysen ergaben 42 von HERC5 ISGylierte Zielproteine. Jedoch wurde kein spezifischer Signalweg beeinflusst, was auf einen geringeren Einfluss von

IFNγ und TNFα auf Protein ISGylierung in Immun-bezogenen Prozessen in NSCLC hindeutet.

Extrazelluläre Vesikel (EVs) sind essentielle Mediatoren der Zell-Zell-Kommunikation. Von Tumoren freigesetzte EVs wurden beschrieben, die sogenannte prä-metastatische Nische zu etablieren, beispielsweise durch Induktion von Gefäßdurchlässigkeit, Remodulierung der extrazellulären Matrix und Immunsuppression. Die gegenwärtige Studie demonstrierte eine verstärkte Sekretion von EVs in HERC5-dezimierten Lungenkrebszellen unter inflammatorischen Bedingungen. Darüber hinaus deuten vorläufige Ergebnisse darauf hin, dass der Inhalt von EVs spezifisch in diesen Zellen verändert ist. Im Gegensatz zum geringen Einfluss durch ISGylierung auf Signalwege in der Zelle, zeigten Analysen von funktionalen Annotationen in EVs eine Anreicherung von Signalwegen, die sich sowohl mit der angeborenen Immunantwort als auch Zelladhäsion verknüpfen lassen. Dies weist auf eine immunmodulatorische Funktion der Vesikel hin.

Früherkennung von Krebs ist entscheidend zur Prävention von Primärtumoren sowie Metastasen. Flüssigbiopsien aus Blut von Krebspatienten können nicht nur relevante Informationen über den Zustand des Tumors, sondern auch dessen Evolution beinhalten, ohne die Notwendigkeit von invasiven Eingriffen. Im Vergleich zu Einzelanalysen kann die Kombination von verschiedenen Biomarkern zusätzlich ergänzende Informationen geben. Die Voraussetzung zur klinischen Nutzung dieser hoch sensitiven Analysen ist ferner die Entwicklung von Standardvorgehensweisen. Hier zeigt die vorliegende Forschung die Durchführbarkeit einer kombinierten Analyse von zirkulierenden Tumorzellen (CTCs), zirkulierender Tumor DNA (ctDNA) und miRNA aus einer einzigen Blutabnahme auf. Das Ergebnis dieses Tests hängt allerdings stark ab von der Wahl des verwendeten Blutentnahmeröhrchens und der Normalisierungsmethode von DNA Sequenzierungsdaten, was die Notwendigkeit von normierten Verfahren unterstreicht. Weiterhin wurde eine Methode zur standardisierten, halb-automatischen Detektion von CTCs aus Krebspatienten etabliert. Beide Ergebnisse schaffen gemeinsam die Voraussetzung zur zukünftigen Entwicklung eines auf HERC5 basierenden Flüssigbiopsie-Tests.

Zusammengefasst deuten die Ergebnisse darauf hin, dass anhand geringer HERC5 Expression das metastatische Potential verstärkt wird. Sein Einfluss auf extrazelluläre Signalwege durch EVs in einem immunmodulatorischen Kontext ist erhöht, während intrazelluläre Signalwege weniger durch HERC5 Level und ISGylierung von Proteinen beeinflusst werden. Weitere Analysen müssen durchgeführt werden, um die genauen Eigenschaften der gegenseitigen Wechselwirkung von Tumor und Immunzellen zu beurteilen. Zumal könnte mithilfe von Flüssigbiopsie-Studien überprüft werden, ob HERC5 zukünftig als Blut-basierter Biomarker zur Früherkennung von NSCLC-Rückfall fungieren kann.

1 Introduction

Cancer development is considered a multi-step process, which is often triggered by activation of oncogenes or loss of function of tumor suppressor genes [1]. There is, however, a vast complexity of different cancer entities, which all have distinct alterations in regulatory pathways. In 2000, Hanahan and Weinberg refined the definition of malignant transformation processes by introducing the so-called hallmarks of cancer. These essential alterations included six hallmarks which are characterized by self-sufficiency in growth signals, insensitivity to growth-inhibitory (antigrowth) signals, evasion of programmed cell death (apoptosis), limitless replicative potential, sustained angiogenesis, and tissue invasion and metastasis [2]. It was argued that all six steps are essential for complete tumorigenesis and that acquisition of these varies both in a mechanistical and chronological manner, meaning that specific genetic events may contribute to a different extent and the order of hallmark acquisition can vary [2]. During the multiple steps in carcinogenesis different abilities are acquired by the tumor. While oncogenes play an important role in early stages of tumor growth, so-called metastasis suppressor genes are able to inhibit dissemination from primary tumors and thus metastasis formation.

11 years after the original publication, these hallmarks were updated by the same authors implying that tumorigenesis is not merely a process triggered by the tumor itself but is also heavily influenced by the tumor microenvironment. The hallmarks were thus adjusted and now further include deregulation of cellular energetics, avoiding immune destruction, tumor-promoting inflammation, and genomic instability and mutation [3]. It becomes more and more evident that interactions with surrounding cells of the immune system are intricate and that they play an active part in tumorigenesis.

The best way to treat or prevent cancer still remains early detection or detection of minimal residual disease (MRD). Liquid biopsy approaches represent a new diagnostic concept in which low amounts of circulating tumor cells (CTCs) or circulating tumor DNA (ctDNA) can be analyzed from blood, enabling MRD detection in patients [4].

1.1 Lung cancer

According to global cancer statistics GLOBOCAN by Bray *et al.*, in 2018 lung cancer was the most commonly diagnosed cancer entity worldwide comprising an estimated 15% of all new cancer cases in men and 8% in women. Only prostate (14%), breast (24%) and colorectal (appr. 10%) cancers have similar or higher incidence rates in men and women, respectively [5]. To date, lung cancers represent the leading cause of all cancer-related deaths in men with a mortality rate of 22% and has the second highest mortality rate

of 14% in women, when comparing all cancer-related deaths (see Figure 1) [6]. Overall, lung cancer caused approximately 1.8 million deaths worldwide in 2018 according to GLOBOCAN [5].
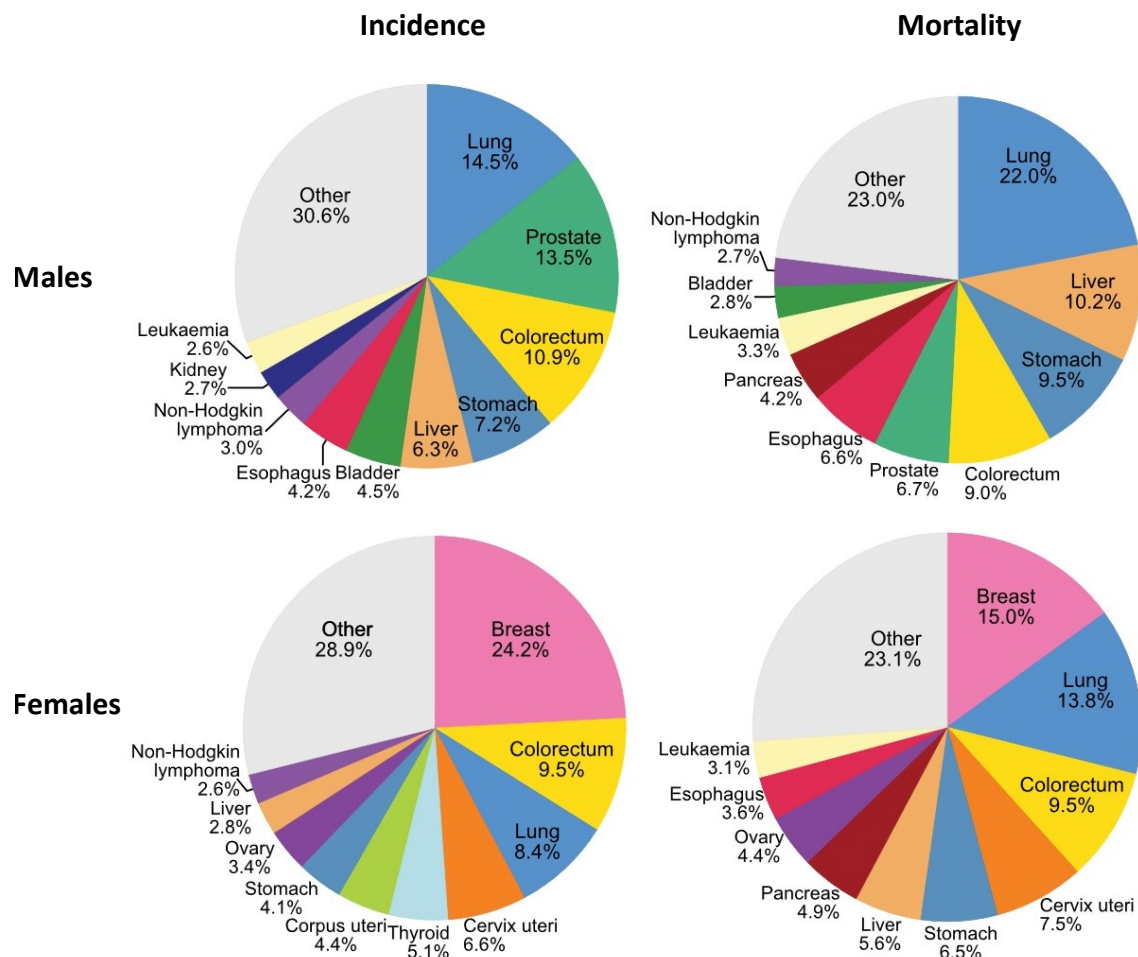
Figure 1: Estimated new cases and cancer deaths worldwide according to gender in 2018. Modified after Bray *et al.* [5].

The five-year survival rate of lung cancer patients is around 54% for localized stage disease and, like in all cancer entities, is drastically reduced when the tumor has already spread to distant sites with a 5-year survival rate of 4% [7, 8]. In contrast to most other cancer entities, the survival rates have not improved significantly during the last decades, as its 5-year survival rate increased from an average of 12.2% in 1975 to 18.7% in 2012 (see Figure 2) [9].

This high mortality rate can be explained by the fact that patients often present to the clinic at a late, often already in a metastasized state (57%), while approximately only 15% of cases are diagnosed in the localized stage [7, 8]. This is mainly due to the fact that symptoms occur late or are hardly distinguishable from a normal cough or other infection-related symptoms, which are also common for smokers. The vast
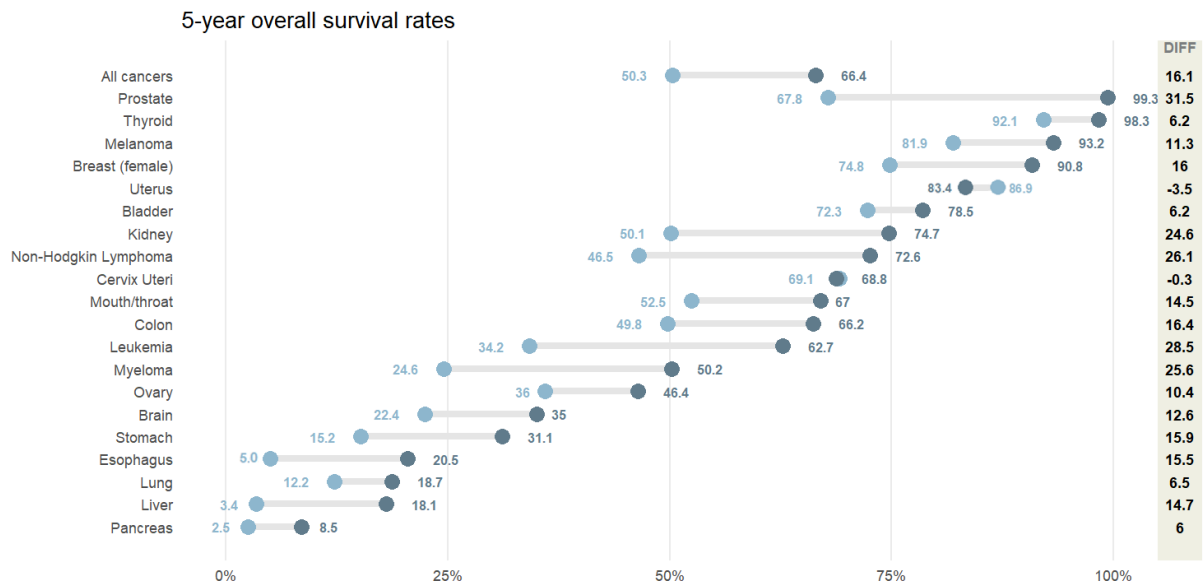
Figure 2: Five-year survival rates for the most common cancer sites. Modified after Jemal *et al.* Average values for the years 1975 - 77 are depicted in light blue; average values for the years 2006 - 12 are shown in dark blue [9].

majority of lung cancers (about 80% in the US and other developed countries) are caused by tobacco consumption [10]. Globally, lung cancer incidences are therefore highly correlated to smoking prevalence and are especially elevated in Europe, North America, Micronesia/Polynesia, and Eastern Asia [8]. Other risk factors besides smoking include passive smoking, occupational exposures to asbestos and other carcinogens, and urban and indoor air pollution [11]. Moreover, chronic obstructive pulmonary disease (COPD) as well as pneumonia, which are both associated with chronic inflammation of the lung, are risk factors for lung cancer development [12, 13].

1.1.1 Non-small cell lung cancer (NSCLC)

Lung cancers can be subdivided into two main types: small cell lung cancer (SCLC) and non-small cell lung cancer (NSCLC). The latter represents the majority of the two lung cancer subgroups (85%) [14] and it can be further subdivided based on its histology. Adenocarcinomas (AD; 40% [15]), which arise from alveolar, bronchial, or bronchiolar epithelial cells, are more peripheral and have glandular histology [14], while squamous cell carcinomas (SCC; 25-30% [15]) arise from the bronchial epithelium of the larger, more central airways, and are more strongly associated with smoking and chronic inflammation [16]. Large cell carcinomas (LCC; 10-15% [15]) are diagnosed by exclusion of the two previously mentioned subtypes [16].

1.1.2 TNM staging and treatment options

Irrespective of subtype, the so-called TNM staging has been established and is constantly re-evaluated by the Union for International Cancer Control (UICC) in order to standardize and accurately evaluate disease burden and treatment options [17]. The TNM staging represents a nomenclature for the anatomic extent of primary tumor (T), lymph nodes (N) and metastases (M). TNM classifiers are furthermore characterized by numbers representing the severity or extent of tumor growth or occurrence of metastases. Increasing tumor size and local invasion are correlated with higher T-descriptors, ranging from T1-T4, which are also influenced by the tumor location. Nodal staging is determined by the number of lymph node metastases and increases with higher numbers, also depending on the affected region in the body. M-descriptors are categorized into M0 for no distant metastasis while M1 is further subdivided into M1a-c depending on single or multi-organ involvement. In general, Tx and Nx are assigned if primary tumor or lymph nodes cannot be accessed [18]. After determination of the TNM descriptors, their combination can be used to assign an overall stage, ranging from stage I to IV. NSCLC is a molecularly heterogeneous disease and therefore understanding its biology based on its specific subtype and staging is necessary for assessment of the right treatment strategy. Surgical resection remains the recommended treatment for stage I-II patients [19] and is complemented for stage II patients with adjuvant chemotherapy [20]. If complete resection is not possible, postoperative radiation is recommended [20]. Treatment options in stage III NSCLC patients vary due to a large heterogeneity within the group. Patients with limited or moderate nodular involvement (N1-N2) undergo surgery, if possible, and treatment is combined with neoadjuvant chemotherapy or adjuvant chemoradiotherapy [21]. Without the option of surgical resection (N3), thoracic radiotherapy in combination with chemotherapy is the treatment of choice [19, 21]. Stage IV patient care largely consists of chemotherapy with platinum-based drugs and is complemented by palliative therapy but includes immunotherapies as well [22].

1.1.3 Molecular alterations in NSCLC

NSCLC represents a tumor entity with one of the highest tumor mutational burden [23], which is largely induced by carcinogenic tobacco consumption [11]. Due to this high amount of mutations present within the tumor, in addition to histological subtyping, specific genomic aberrations should be identified in order to analyze those patients who might benefit from a variety of molecular targeted therapies that are available. Today, several targeted treatment options are available for lung adenocarcinoma patients. Lung adenocarcinomas most frequently harbor activating mutations in driver oncogenes such as *KRAS*, epidermal growth factor receptor (*EGFR*) gene mutations, anaplastic

lymphoma kinase (*ALK*) gene rearrangements, reactive oxygen species proto-oncogene-1 (*ROS1*) gene rearrangements and B-raf proto-oncogene (*BRAF*) point mutations (see Figure 3) [20]. However, only a subset of these represent actionable molecular targets and could thus benefit from molecular targeted therapies. EGFR is a receptor tyrosine kinase which is in involved in signal transduction via the PIK3CA/AKT1/MTOR or RAS/RAF1/MAP2K1/MAPK1 pathways [24]. Both pathways are involved in cell proliferation, survival, invasion and angiogenesis [25]. Mutations causing constitutive EGFR activation and ligand independence [26] therefore lead to oncogenic transformation. EGFR specific tyrosine kinase inhibitors (TKI) such as gefitinib or afatinib can reversibly or irreversibly block the receptor, respectively [27]. The most commonly acquired resistance mechanism during treatment is a mutation arising in exon 20 and codon 790 (T790M) [28] for which a new generation of TKIs already exists. Osimertinib for example can inhibit both original sensitizing and T790M mutations [27]. There is an ever growing number of TKIs against these and other new targets that are already available or are currently being tested in clinical trials. However, emerging mutations in most tyrosine kinases lead to resistance against these drugs in patients and thus other options are needed.
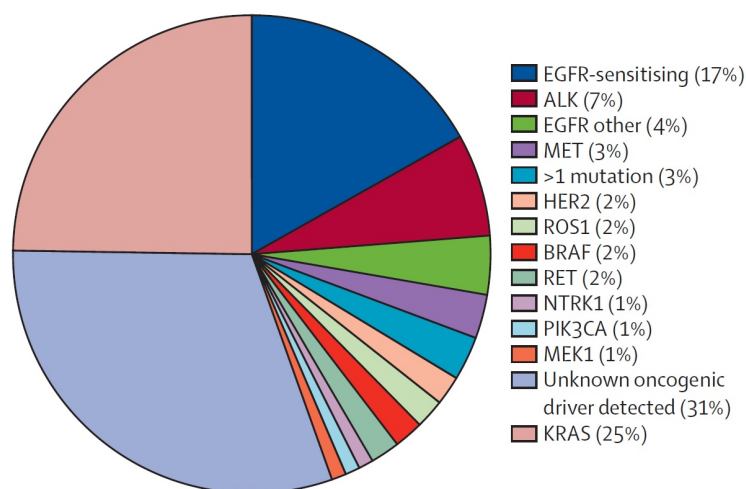
Figure 3: Frequency of molecular aberrations in driver oncogenes in lung adenocarcinomas. Taken from Hirsch *et al.* [19].

As more knowledge on the immune-landscape of tumors is available, immunotherapy is a novel revolutionary treatment option especially in advanced disease setting. In line with this, programmed death ligand-1 (PDL-1) expression should be assessed for therapy with immune checkpoint inhibitors. Adaptive PD-L1 expression within the tumor leads to binding of programmed death-1 (PD-1) expressed by T-cells. The formation of this immunological synapse thereby blocks T-cell specific immune rejection and allows tumor progression and dissemination [29]. Monoclonal antibodies targeting the PD-1/PDL-1

axis or cytotoxic T-lymphocyte antigen-4 (CTLA-4) have proven to successfully inactivate either of these targets, therefore restoring T-cell-mediated anti-tumor immunity [27, 30].

1.2 Early dissemination and metastasis

Metastatic spread is a hallmark of cancer and represents the main cause of all cancer-related deaths [31]. It occurs when tumor cells deriving from the primary site are able to detach and intravasate the surrounding tissue and blood vessels, circulate in the blood-stream whilst surviving pressure, extravasate, adapt to a new microenvironment at a secondary site, and evade immune defense mechanisms [32]. Still, the exact mechanisms of how cells are able to overcome all these various obstacles and furthermore colonize new organs are not yet fully understood to an extent that would allow to apply this information to the treatment of patients.

Two main mechanisms of detachment from the primary tumor site have so far been described, i.e. active and passive shedding. Shear forces, mechanical stress e.g. from surgery or tumor growth can lead to passive shedding of single or multiple cells, termed circulating tumor cells (CTCs), which then can be forced into the blood circulation. These cells are likely to keep their original expression patterns and might contribute to metastasis formation [33, 34]. Active detachment of tumor cells is another way of dissemination and includes acquisition of a more aggressive phenotype. Hence, in order for cells to adapt to the environmental changes during the course of metastasis, some plasticity in expression changes is thought to be required. The main process in which cells can transform from being immotile into a less differentiated state with elevated migratory and invasive capacities is called epithelial–mesenchymal transition (EMT). This process is believed to have a broad spectrum of transitional stages rather than an alternation between full epithelial and full mesenchymal states [35].

During EMT, differential activation of transcription factors Slug, Snail, Twist, ZEB1, and ZEB2 occurs [36], altering signaling pathways and converting their apico-basal polarity into front-back polarity by remodeling of their extracellular matrix [35]. Cell-cell contacts through adherens junctions, tight junctions or desmosomes become weaker through loss of expression of cadherins, claudins or plakoglobin [34, 37] but also other epithelial proteins such as EpCAM or cytokeratins are downregulated while mesenchymal markers like N-cadherin or vimentin are upregulated. EMT can be induced by autocrine and paracrine growth factors including transforming growth factor-β (TGF-β), Wnt, hepatic growth factor (HGF), epidermal growth factor (EGF), fibroblast growth factor (FGF) and platelet-derived growth factors (PDGF) which can be expressed by immune cells, fibroblasts or mesenchymal stem cells present in the microenvironment of the tumor [38, 39]. The reversion of the EMT process is called MET (mesenchymal

to epithelial transition) and facilitates outgrowth. It is therefore necessary in order for cells to be able to re-attach to new tissue, proliferate and outgrow at metastatic sites [39]. Cells that have successfully detached from the primary tumor and migrated to distant organs are called disseminated tumor cells (DTCs).

Even though in theory, cells having disseminated from a primary tumor could form metastases at any organ of the human body, individual carcinoma entities are known to colonize specific target organs. [40]. This organ tropism of metastases can derive from intrinsic alterations from the tumor cells, accessibility of target organs and paracrine interactions between tumor cells and stroma [40]. During this process, chemo-attractants such as cytokines are released which direct metastatic cells to certain organs, extracellular matrices are remodeled and the host cellular composition can be altered [15, 40]. In NSCLC, the main sites of metastasis are bone, lung, brain, liver and adrenal gland [41]. In a study by Riihmäki *et al.*, population-based data from over 20,000 lung cancer patients was analyzed to obtain a more detailed view on this tropism. It was demonstrated that also histology, age at diagnosis and sex have a significant impact on metastatic patterns in lung cancer [41]. For example, in comparison with other subtypes, SCC patients had the lowest occurrence of metastasis. AD metastasized preferentially to the bone and respiratory tract and metastases in women occurred more frequently in the nervous system [41]. It is therefore conceivable that metastatic patterns derive from survival advantages through expressional differences of histological subtypes. Furthermore, microenvironmental factors from secondary sites but also overall metabolic changes could influence tumor cells from the lung in the blood circulation which leads to a site specific colonization [42]. The exact underlying principles of organ tropism, cellular modifiers and possible therapeutic targets, however, remain to be elucidated.

1.3   Liquid biopsy

Early detection is highly important for prevention of both primary and metastatic disease. Still today, 10-50% of patients even with resectable primary tumors and no overt metastases experience relapse within 5 years [43], indicating the presence of early dissemination of tumor cells in NSCLC responsible for metastatic relapse which cannot be detected by high-resolution imaging technologies [44]. A common homing organ for DTCs is the bone marrow (BM). The presence of DTCs has been shown to correlate with poor prognosis in most solid tumors including NSCLC [45, 46]. In breast cancer even prognostic value of DTCs has been shown [47]. However, DTC analysis requires repeated invasive BM sampling which is not always possible. The so-called liquid biopsy is a new emerging field dealing with the detection of tumor state and evolution from body fluids of cancer patients [44]. Using blood as a liquid biopsy tool represents a

non-invasive method for detection. The information obtainable in blood from patients samples is diverse: circulating tumor cells (CTCs) present in the mononuclear cell fraction, and circulating tumor DNA (ctDNA), exosomes and platelets derived from the plasma fraction can all give additional information on the genomic, epigenomic, transcriptomic and proteomic state of heterogeneous tumor cell populations as well as distant metastases (see Figure 4) [48].
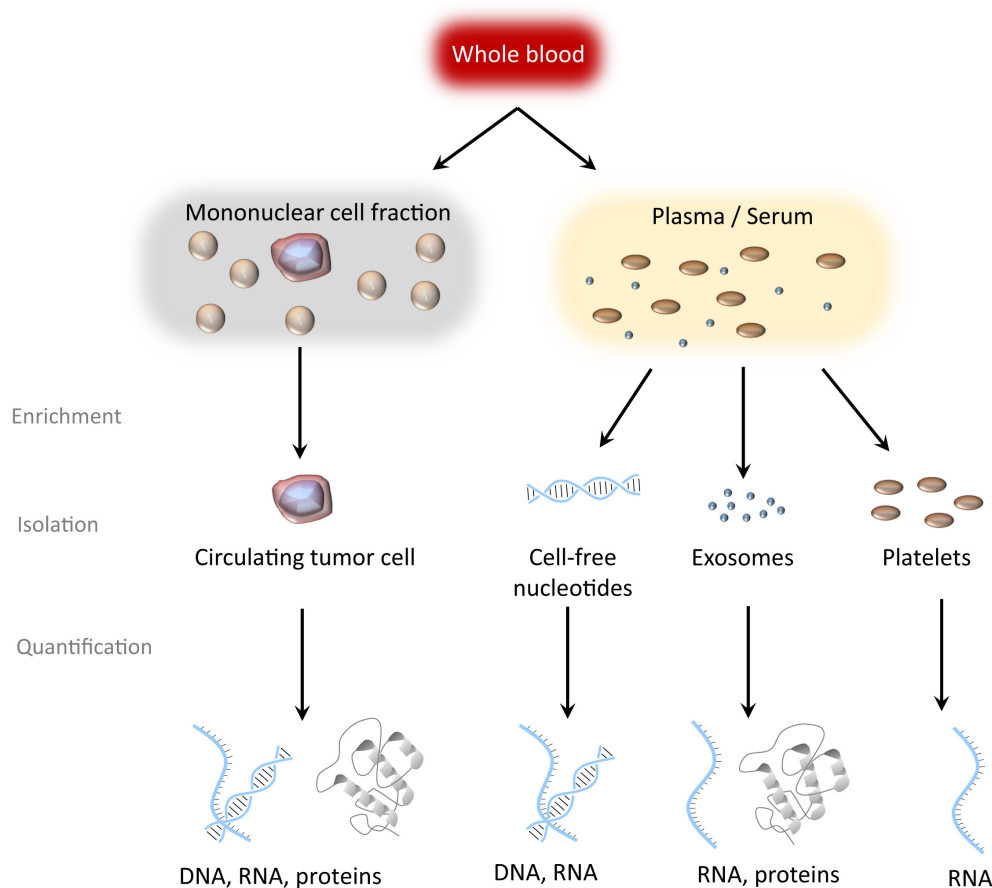
Figure 4: Overview of analytes present in blood and accessible by liquid biopsy. By centrifugation, whole blood can be separated into two parts. The mononuclear cell fraction contains CTCs for analysis of marker protein expression, as well as genomic and transcriptomic data. Plasma or serum components include cell-free DNA or RNA, exosomes and platelets, which all can give additional information on the disease state. Taken from Joosse *et al.* [48].

The versatile information obtained from liquid biopsies represents many advantages over classical tissue biopsies. During treatment, sequential biopsies for disease monitoring are also rarely possible and represent an increased burden for the patient. Since tissue biopsies from lung tumors are often hard to access surgically, requiring invasive procedures, the non-invasive analysis of biofluids could become an attractive alternative.

NSCLC tumors are known to exhibit a large intra- and inter-tumor (metastasis) variability. Therefore, even if tissue biopsies are feasible, they can only reflect a fraction of the largely heterogeneous tumor tissue while liquid biopsies can give rise to the overall state by detection of single clones or nucleic acids from theoretically any part of the tumor tissue [49]. Analytes present in the blood could not only mirror the real-time state of the patient but could become an important tool with respect to diagnosis, choice of treatment and therapy response and even resistance mechanisms [49]. Moreover, by sequential blood sampling tumor evolution can be tracked, therefore liquid biopsy has the potential to aid in understanding the metastatic cascade. It can furthermore indicate whether the disease is still present as micrometastases by assessing the so-called minimal residual disease (MRD) state [43]. Information on presence of CTCs or ctDNA can be thus be a predictive factor of progression and relapse [43].

1.3.1   CTCs, ctDNA, EVs and miRNA

Liquid biomarkers present in the blood can all give different, but complementary information on the current disease state and therefore represent valuable tools for monitoring treatment response, tumor evolution and presence of MRD [49]. In the following section, a short overview on the different analytes and their clinical relevance will be presented.

CTCs which have been shed from tumor tissue (both primary tumor and metastases) and are present in the blood circulation are exposed to harsh conditions such as immune surveillance, shear forces and apoptosis [50]. Their half-life is therefore short, estimated to be 1-2.4 h [51]. CTCs represent only a small fraction in the background of blood cells, usually in the range of 1 CTC per 10^6 - 10^8 leukocytes [52]. The number of CTCs depend on the type of tumor and disease stage. CTCs can be characterized by enumeration and molecular characterization by e.g. analysis of expression of specific tumor markers, RNA or DNA analysis with whole genome amplification tools and subsequent next generation sequencing (NGS) analysis. The CellSearch® device is considered the gold standard method for CTC detection as being the only US Food and Drug Administration (FDA)-approved device. CellSearch® makes use of epithelial cell adhesion molecule (EpCAM) expression on the cell surface by enriching EpCAM positive CTCs with magnetic labeled nanoparticles. Several studies have shown that CTCs can be present already at early disease stages, and can predict prognosis and response to therapy, in particular in breast and prostate cancer [49, 53]. Also in NSCLC, even though CTC numbers detected by CellSearch® and most other devices are low [54], positive CTC status correlates with lymph node metastasis and tumor stage, as well as shortened DFS and OS [55]. Furthermore, emergence of possible mutations in *KRAS*, *EGFR* e.g. its drug resistant T790M substitution could already be validated on CTCs [56].

Circulating tumor DNA (ctDNA) derives mostly from apoptotic and necrotic tumor cells and represents only a small fraction of total free circulating DNA (cfDNA) present in the blood of cancer patients [57]. Their half-life is comparable to CTCs, with an estimated 1.5 h [58]. Analysis of ctDNA can in principle reveal any type of DNA alteration, including mutations, structural variation and epigenetic changes, deriving from primary tumors, CTCs, micrometastases, or overt metastases. The alterations are mostly analyzed by either PCR- or NGS-based techniques [57]. Identification of EGFR mutations in plasma of NSCLC patients was for example shown to be of clinical relevance for patients since dynamic changes of the mutations and occurrence of mutations causing resistance against EGFR TKIs correlate with DSF and OS and can be assessed without the necessity of tissue biopsy [59]. It enables earlier diagnosis and therefore changes of treatment options and has been approved by the FDA [59]. Genomic abberations can furthermore include epigenetic changes, and thus alterations of methylation patterns, a common trait among tumor suppressor or metastasis suppressor genes. Their detection can also give valuable information on gene silencing in connection to resistance to therapy and is still most commonly performed by PCR after bisulfite-conversion of the DNA [50].

Further information on the current disease state can be obtained by analysis of free circulating miRNAs or miRNAs present in extracellular vesicles (EVs) or exosomes. MiRNAs are single-stranded, short (19–25 nt) non-coding nucleic acids which are sequentially processed from precursor pri-miRNAs to pre-miRNAs and finally to mature miRNAs [60, 61]. Within the RNA interference pathway, they are important post-translational regulators of gene expression and are thus not surprisingly often deregulated in various cancer entities. They are associated with downregulation of tumor suppressors or oncogenes [61]. Due to their rather high stability and bio-availability (24 h [62]), expression of single cancer-associated miRNAs or whole miRNA profiles could become biomarkers or indicators for disease state [61]. It seems that even though miRNA families such as hsa-miR-200 are frequently deregulated in cancer [63], every entity has their own pattern of distinct miRNAs, which furthermore varies when comparing cell free miRNA and miRNAs derived from exosomes [61]. Their evaluation as biomarkers therefore requires more research.

Exosomes represent a subgroup among EVs and are characterized by their size of approximately 50-150 nm, surface protein markers such as tetraspanins, TSG101 or Alix, and are derived from endosomes [64]. Besides miRNA, exosomes furthermore include other nucleic acids such as DNA, mRNA and long non-coding RNA, as well as proteins [65]. They are involved in cell-cell communication in an autocrine and paracrine manner and are capable of reprogramming of the recipient cells as well as their metabolism [64]. Through their function, they have been associated with tumorigenesis, growth,

progression, dissemination and therapy resistance [66]. During cancer progression, the amount of exosomes released from tumor cells is increased [64]. They have been recognized as important mediators of priming the metastatic niche by signal transduction directed at immune cells and stromal cells [66]. Moreover, exosome uptake by recipient cells seems to be organ-specific and is therefore linked to metastatic organotropism [67].

1.3.2   Influence of pre-analytical factors on liquid biopsy

As varied the information obtainable from blood can be and as promising the prognostic and therapeutic value for treatment seems, several aspects of data acquisition in liquid biopsy approaches need to be further evaluated. So-called pre-analytical factors, dealing for example with the identification and choice of tests, sample collection and sample handling, can influence analyses in many ways [68]. In order to be able to compare assays and to implement liquid biopsy into routine patient care, standardized procedures are indispensable but not completely validated yet.

One of the most crucial influences when analyzing analytes from blood are blood collection tubes. There are numerous tubes available which all contain preservatives influencing the stability of biomarkers in a different way [69]. Furthermore, varying blood volumes for analysis or wrong storage parameters, transportation issues or technical mistakes can have an impact on results as well [70]. For each analyte, various studies have been performed aiming at standardizing pre-analytical conditions. Mesquita *et al.* reported the establishment of storage of CTCs enriched by the CellSearch device for up to two years, whose genomic integrity remains suitable for subsequent whole genome amplification [71]. Regarding ctDNA analysis, differences in sample collection, storage, centrifugation, isolation, and quantification methods were compared by van Ginkel *et al.* revealing optimal conditions of blood sampling and choice of DNA extraction kits [72]. Moreover, in a study by Kloten *et al.*, extraction protocols for free circulating and EV-associated miRNAs analyzed by NGS were compared in a multicenter approach and revealed differences in miRNA yield and quality which might introduce bias in the data [73]. Since in principle, every pre-analytical step has an influence on results, evaluations are necessary regarding both single parameter and multiparameter analysis as well as testing at several laboratories in e.g. ring trials in order to overcome these biological and technical challenges.

1.4   HERC5

HERC5 (HECT and RLD domain containing E3 ubiquitin protein ligase 5) belongs to a family of proteins which comprises six members in total. Depending on their size and domain architecture, they can be further subdivided into two groups. While HERC1 and HERC2 represent large proteins containing one HECT (Homologous to the E6AP carboxyl terminus) and several RLDs (regulator of chromosome condensation 1 (RCC1)-like domain) functional domains, HERC3-6 belong to the small members of the protein family with only one HECT and RLD domain each [74]. Their common HECT domain feature has been proven to exert active ubiquitin ligase function, as it has the ability to form thioester bonds with ubiquitin [75]. Ubiquitination is a process which requires the action of three main proteins, constituting of ubiquitin-activating E1 enzyme, ubiquitin-conjugase E2 and E3 ligases [74]. HERC proteins belong to the latter group. In addition to HECT domains, the general functions of RLD structural components include guanine nucleotide-exchange factor activity for the small GTPase Ran and interaction with chromatin through histones H2A and H2AB [74].

HERC5 is a 117 kDa protein consisting of 1024 amino acids, which was initially identified in a yeast-two hybrid screening study with cyclin E-p21 as bait proteins [76]. *HERC5* gene is located at chromosome 4q22 and spans 23 exons [77]. It is mainly located in a punctuate manner in the cytoplasm and to a lesser extent in the perinuclear region [76]. Except for testis and fetal brain tissue, HERC5 mRNA has low basal expression levels in other tissues [76, 77, 78]. However, a vast variety of stimuli have been described to quickly increase its expression as a response to e.g. pro-inflammatory cytokines or presence of viral proteins [79]. Hence, a tight regulation of *HERC5* expression under inflammatory conditions has been proposed.

Kroismayer *et al.* have confirmed E3 ubiquitin ligase activity in combination with E2 enzyme UbcH5a also for this member of the HERC protein family [78]. HERC5 E3 ligase activity has, however, so far predominantly been connected to transfer of ubiquitin-like modifier (Ubl) ISG15 (interferon-stimulated gene 15) [80, 81]. Ubls harbor often structural similarities to ubiquitin but can be functionally divers. Ubiquitin ligase activity has been ascribed to the HECT domain of HERC5 [80, 81], however, its other structural component RLD was shown to also be of importance for overall ISG15 conjugation due to its association with polyribosomes and thus the translational machinery [82].

1.4.1   HERC5 as mediator of co-translational ISGylation

As stated previously, the main known function of HERC5 protein is its role as an E3 ligase mediating the transfer of Ubl ISG15 onto newly synthesized proteins. The ISGylation machinery consists of a three-step hierarchical cascade. ISG15 is expressed as a 17 kDa precursor molecule [83], which after cleavage is covalently transferred to E1 activating enzyme Ube1L [84]. UbcH8 acts as an E2 conjugase for ligation of ISG15 onto E3 ligase HERC5 [85]. HERC5 is the single major E3 ISG15 ligase within the cell and its conjugation targets newly synthesized proteins in a co-translational manner [82] while the only two other known E3 ligases TRIM25 and ARIH1 catalyze the ligation of specific substrates. An active cysteine residue is required for the catalysis of transferring ISG15 molecules onto target proteins. The active site of HERC5 is located at cysteine residue 994 [78]. ISGylation is a reversible process and its cleavage is catalyzed by de-ISGylating enzyme USP18 [86] (see Figure 5).

To date, numerous ISGylation target proteins have been identified by the means of mass spectrometry proteomics. In a study by Zhao *et al.* HeLa cells (cervical adeno-carcinoma cells) were treated with IFNβ for 24 h, transfected with ISG15 (6xHis and FLAG-tagged), Ube1L and UbcH8, and ISGylated proteins were purified by pull-down with Ni-NTA and anti-FLAG beads and subjected to mass spectrometry. With this approach, in total 158 targets from diverse cellular pathways were detected. These include association with the cytoskeleton, defense against bacterial infections and stress response pathways [87]. Moreover, Giannakopoulos *et al.* conducted a study with human U973 cells (histiocytic lymphoma), treated with IFNα for 24 h as well as murine Usp18$^{-/-}$ (mouse embryonic fibroblasts) treated with mouse IFNβ for 36 h. After immunoprecipitation (IP) with ISG15 and mass spectrometry analysis, 76 targets were identified, of which 21 were found in both cell lines. PANTHER classification system revealed that targets share, among others, pathways of protein modification and metabolism, carbohydrate metabolism, stress response and cell structure and motility [88]. Finally, after IFNβ treatment of A549 cells for 48 h while stably expressing FLAG-ISG15 and subsequent ISG15-IP, Wong *et al.* identified 174 targets involved in ISGylation [81]. While some of the targets are known IFN-inducible proteins, an analysis of affected pathways was not reported in this study [81].

Combined, around 300 unique ISG15 target proteins have been identified in these three studies [89]. Contrary to beliefs that this identification will give rise to assigning biological function to ISGylation, pathway analyses were not very revealing in terms of this prediction. The data suggests thus a broad range of functions rather than a single biological effect.

Figure 5: The ISG15 conjugation pathway. After cleavage of 17 kDa ISG15 precursor, mature ISG15 protein is transferred onto E1 activating enzyme Ube1L in an ATP-dependent manner. ISG15 is subsequently transferred to the active-site cysteine residue of E2 conjugase UbcH8 before transfer to E3 ligase. HERC5-dependent ISG15-conjugation is performed during association with polyribosomes and appears to target mainly newly synthesized proteins. Finally, de-ISGylase USP18 is able to cleave ISG15 from conjugated proteins. Modified after Perng *et al.* [79].

1.4.2   Involvement of HERC5 in innate immunity

As described previously, upregulation of HERC5 expression is highly connected to inflammatory responses. In endothelial cells for example, HERC5 expression can be highly induced by tumor necrosis factor α (TNFα), interleukin 1β, and lipopolysaccharides (LPS) [78]. Therefore, its upregulation was described to occur mainly by induction of NF-κB signaling pathway and is furthermore dependent on de novo protein synthesis upon infection [78]. Also in cancer cells expression of HERC5 could be induced by cytokines that are involved in antiviral immunity. In A549 NSCLC lung cancer cells and HeLa cervical adenocarcinoma cells these cytokines include IFNα and IFNβ, respectively [80, 81]. In line with these findings, all other proteins of the ISGylation machinery are upregulated under IFNs and thus levels of ISGylated proteins are strongly increased in an inflamed cellular state [90]. Antiviral activity exerted by ISGylation of target proteins has been shown for a variety of viral proteins with different functions. ISGylation of NS1/A protein of Influenza A virus occurs during viral replication and disrupts interaction with several binding partners [91, 92]. Disruption of function and geometry of viral complexes has been described for HPV protein L1 resulting in significant decreases of number and infectivity of viral particles [82]. Furthermore, ISGylation inhibits ubiquiti-

nation of Gag protein of HIV-1, therefore interaction with host TSG101 is disrupted and viral egress and budding of HIV-1 was shown to be inhibited [93]. Several viruses have developed immune-evasion mechanisms against ISGylation as a defense to the host antiviral response, including NS1 protein of influenza B, which sequesters ISGylated viral proteins in order to restore viral RNA synthesis [94], or ISG15 deconjugating proteases of coronaviruses MERS and SARS [95]. Taken together, viral ISGylated protein function can be impaired with respect to replication, oligomerization of capsid structures, and interaction with host pathways [79].

1.4.3 Role of HERC5 and ISGylation in cancer

HERC5 was described in the context of cancer through multiple interaction partners. Interestingly, HERC5 expression increases when tumor suppressors p53 and Rb are downregulated by viruses expressing viral oncoproteins [76]. Due to the initial finding of interaction with cyclin E-p21, a role in cell cycle progression has been proposed [76]. Furthermore, HERC5 was shown to not only interact but also to be involved in ubiquitination of Non-metastatic cells 23B (Nm23B) in HEK293 cells [96]. Its ubiquitination, however, does not lead to proteasomal degradation [96]. Through its role in receptor endocytosis, Nm23B regulates transcription of the *MYC* gene, which is in turn involved in cellular proliferation [97]. This all repeatedly implies that HERC5 plays a role in proliferation and cell cycle regulation. In two cancer entities clinical evidence for HERC5 deregulation has been shown i.e. hepatocellular carcinoma and NSCLC, which will be described in the following section in more detail [98, 99]. Xue *et al.* have discovered that HERC5 plays a crucial role in hepatocellular carcinoma progression. In this study, low mRNA expression levels could be correlated with shorter time to tumor recurrence as well as overall survival (OS) and furthermore led to immune evasion by indirectly increasing infiltration by regulatory T-cells [98].

In addition to HERC5, most other proteins involved in the ISGylation process have also been implied the be involved in malignant transformation or metastatic spread [100]. Specifically, altered expression patterns and chromosomal aberrations have been identified as the main cause for this dysregulation. For example, the chromosomal region of *UBE1L* gene was frequently lost in SCLC and NSCLC as well as other solid tumors [101]. Promoter hypermethylation was furthermore detected in lung cancer cells which led to reduction of Ube1L expression [102]. DeISGylase USP18 was also implicated in tumorigenesis as Guo *et al.* discovered that low expression or loss correlated with reduced cyclin D1 stability and therefore promoted apoptosis and inhibited cell cycle progression [103]. Moreover, augmented expression of USP18 was found in diverse human cancers [103]. Due to its dual role as a Ubl, as well as an unconjugated free intra-

and extracellular molecule, ISG15 exerts both oncogenic or tumor-suppressive roles in different types of cancers [104].

In conclusion, both tumor suppressive and activating functions have been ascribed to all members of the ISGylation machinery. The exact mechanisms of its deregulation therefore remains under investigation and the precise consequence of deregulation remains to be elucidated in each cancer context.

1.4.4 HERC5 in early NSCLC dissemination

Recently, HERC5 has been connected to early dissemination of lung cancer. Its chromosomal region 4q12-q32 is frequently lost in NSCLC patients who harbor DTCs in their bone marrow [105]. This genomic instability in connection to DTC-positive status was shown by comparative genomic hybridization data in combination with expression profiling as well as by FISH (fluorescence *in situ* hybridization) analysis on primary NSCLC samples. Furthermore, loss of this region could be detected especially in brain metastases of NSCLC patients showing a higher frequency of chromosomal loss compared to primary lung carcinomas [105]. These results indicate the importance of genomic integrity in this chromosomal region for prevention of metastatic spread and outgrowth.

Based on these results, this previously identified rather broad region could be narrowed down to 4q21.23-22.1 by allelic imbalance and FISH analysis [106]. Prognostic relevance could furthermore be assigned to loss of this region. Copy number loss at 4q22.1 could be correlated with the occurence of lymph node metastases and advance in tumor staging. Moreover, both disease free survival (DSF) as well as OS have been significantly associated with loss of this 4 Mb spanning chromosomal region (Figure 6). Occurrence of loss of 4q21.23 in DTCs derived from patients was shown to be a common feature as well [106], underlining once more its clinical relevance.

Within this region, methylation dependent expression array-screening analyzed genes regulated by methylation and by RT-qPCR on primary tumor samples, identified *HERC5* as the main target gene responsible for its association of 4q loss with prognostic relevance [99]. Methylation of a CpG-island containing promoter segment of *HERC5* was correlated with occurrence of brain metastases, as well as positive DTC status and was only present in tumor tissue but not in the adjacent normal lung tissue. Furthermore, hypermethylation of a specific CpG was found to have a negative predictive value for OS in stage I adenocarcinoma patients and stage IV patients irrespective of histology (Figure 7) [99].

Taken together, recent studies have shown that *HERC5* might play an important role in early dissemination and could therefore function as a potential metastasis suppressor gene in NSCLC.
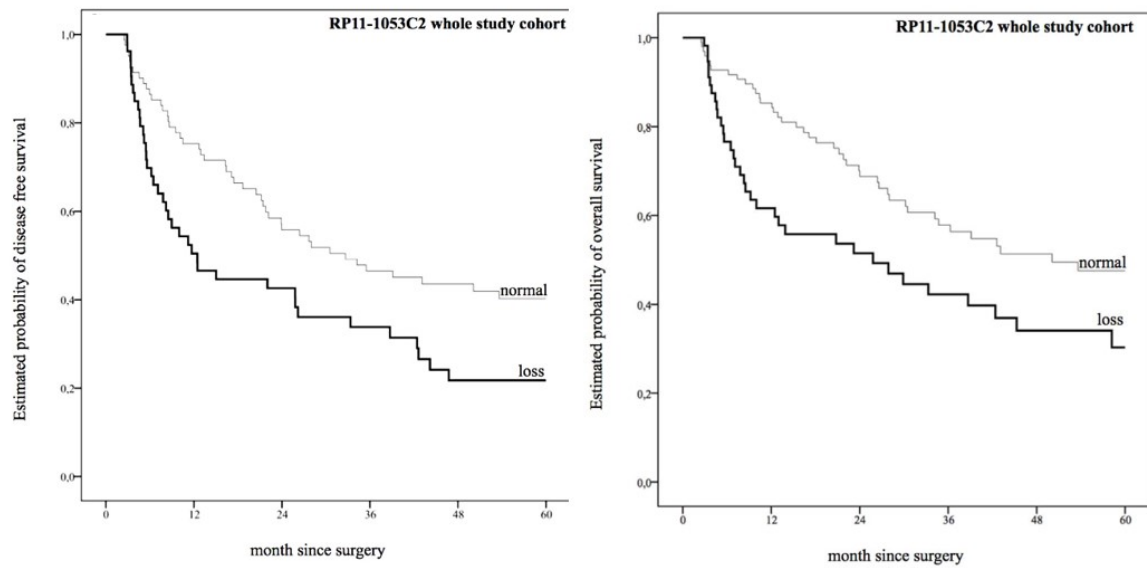
Figure 6: Clinical relevance of loss of 4q22.1 in NSCLC patients Left: Kaplan-Meier curves depict that DSF in patients harboring copy number loss at 4q22.1 is significantly reduced (p=0.012). Right: Loss of 4q22.1 is significantly correlated with OS in NSCLC patients (p=0.010) [106].
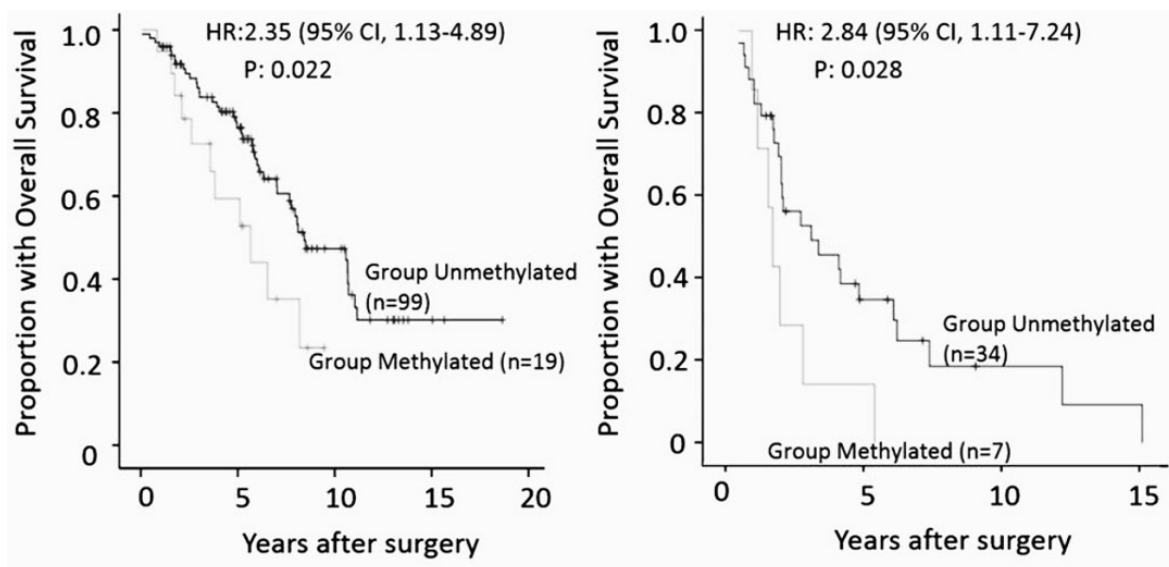
Figure 7: Survival analyses in dependence of methylation status in NSCLC patients. Left: OS in stage I/adenocarcinoma NSCLC patients is significantly reduced when cg08750951 is methylated (p=0.022). Right: Promoter hypermethylation of the same CpG is significantly associated with shorter OS in stage IV patients (p=0.028) [99].

1.5   Aims of this thesis

The main aim of this thesis is to further elucidate the functional role of HERC5 as a potential mediator of early dissemination and/or metastasis. As its clinical relevance in NSCLC patients could already be validated by showing that loss or hypermethylation of a region on chromosome 4q is involved in increased metastatic spread and decreased survival [99], in this work, cell line based studies were performed to study functional alterations associated with differential HERC5 expression. Using different *in vitro* knockout or overexpression cell lines, assays connected to tumorigenicity and metastatic outgrowth could give more insight into HERC5-associated malignant transformation. In previous studies, two of the main metastatic sites of NSCLC, the brain and the bone, also showed an increase in occurrence in a clinical setting when HERC5 levels are low [99]. Functional studies were thus performed while simulating the presence of brain or bone microenvironment. Due to the current knowledge of HERC5 being the main E3 ISG15 ligase in human cells and its involvement in innate immune responses, HERC5-dependent ISGylation was assessed in several NSCLC cell lines under treatment with inflammatory cytokines. Therefore, a robust model system for ISGylation was established for subsequent analysis of HERC5-dependent ISGylation targets. With the aim of further elucidating the role of HERC5 in NSCLC metastasis formation, SILAC (stable isotope labeling by amino acids in cell culture)-based proteome analysis of ISGylated proteins could reveal possible pathways involved in early dissemination. As a recent publication has described involvement of ISGylation in EV particle secretion [107], investigations on the role of HERC5 in EV secretion and processing could help to understand the important crosstalk between tumor and host cells and the role of HERC5 within these processes.

Finally, with the overall aim of ultimately establishing a liquid biopsy assay for detection of HERC5 levels in the future, different pre-analytical parameters possibly influencing stability of biomarkers after blood draw were assessed. For this, analysis of CTCs, ctDNA, EVs and miRNA from blood drawn in different collection tubes should reveal the feasibility of obtaining information on all biomarkers from one single blood draw and furthermore whether blood collection tubes affect outcome of the analysis. Since the detection of CTCs present in the blood of patients remains unstandardized and time consuming, their analysis using a semi-automated scanning microscope was further established.

2 Materials

2.1 Cell lines

Supplements for cell culture media are described in chapter 13.

Table 1: Cell lines used in this study

Description	Tissue type & origin	Media	Source
Astrocytes	Primary human astrocytes	DMEM	N7805-100, Life Technologies
A549	Adenocarcinoma, non-small cell lung cancer	DMEM	ITB, UKE
A549 HERC5 KO	Adenocarcinoma, non-small cell lung cancer	DMEM	ITB, UKE
BEAS2B	Lung epithelial, SV40 transformed bronchus	BEBM	ITB, UKE
HEK293T	Embryonic kidney cells	DMEM	Volker Assmann, ITB, UKE
H2228	Adenocarcinoma, non-small cell lung cancer	RPMI-1640	ITB, UKE
H441	Adenocarcinoma, non-small cell lung cancer	RPMI-1640	ITB, UKE
H460	Large cell lung cancer, derived from lung: pleural effusion	RPMI-1640	ITB, UKE
H1395	Adenocarcinoma, non-small cell lung cancer	RPMI-1640	ITB, UKE
H1395 OE HERC5	Adenocarcinoma, non-small cell lung cancer	RPMI-1640	ITB, UKE
H1563	Adenocarcinoma, non-small cell lung cancer	RPMI-1640	ITB, UKE
H1573	Lung, derived from metastatic site: soft tissue	RPMI-1640	ITB, UKE
H1650	Adenocarcinoma, non-small cell lung cancer, derived from metastatic site: pleural effusion	RPMI-1640	ITB, UKE
H1792	Adenocarcinoma, non-small cell lung cancer, derived from metastatic site: pleural effusion	RPMI-1640	ITB, UKE
H1975	Adenocarcinoma, non-small cell lung cancer	RPMI-1640	ITB, UKE
H1993	Adenocarcinoma, non-small cell lung cancer, derived from metastatic site: lymph node	RPMI-1640	ITB, UKE
HTB56 (Calu-6)	Lung adenocarcinoma (anaplastic)	MEM	ITB, UKE
HTB56 OE HERC5	Lung adenocarcinoma (anaplastic)	MEM	ITB, UKE
HTB58 (SK-MES-1)	Lung squamous cell carcinoma, derived from metastatic site: pleural effusion	MEM	ITB, UKE
MC3T3-E1	Murine preosteoblast	αMEM	ITB, UKE
MCF-7	Breast adeno carcinoma, pleural effusion	DMEM	ITB, UKE

2.2   Laboratory devices

Table 2: Laboratory devices used in this study

Device	Company	Office
Analytical balance BP610	Sartorius	Göttingen, DE
Analytical balance BP6100	Sartorius	Göttingen, DE
Analytical balance CPA224S-OCE	Sartorius	Göttingen, DE
BioPhotometer, thermal printer DPU-414	Eppendorf	Hamburg, DE
Centrifuge 5417R	Eppendorf	Hamburg, DE
Centrifuge Biofuge fresco	Heraeus Holding	Hanau, DE
Centrifuge Multifuge 3 S-R	Heraeus Holding	Hanau, DE
Centrifuge Sorvall RC-5C Plus	Thermo Fisher Scientific	Waltham, MA, US
Centrifuge Rotofix 32	Hettich	Villingen-Schwenningen, DE
ClearBridge ClearCell® FX1 System	Biolidics Limited	Singapore
CO_2-cell culture incubator HERAcell150	Thermo Fisher Scientific	Waltham, MA, US
Electrophoresis power source 250 V	VWR International	Radnor, PA, US
Film developer Curix 60	AGFA HealthCare	Bonn, DE
Hoefer Dual Gel Caster	GE Healthcare	Chalfont St Giles, GB
Hoefer SE250	GE Healthcare	Chalfont St Giles, GB
Gel documentation system GeneGenius	Syngene	Cambridge, UK
Icemaker FM-120 DE	Hoshizaki	Amsterdam, NL
Magnetic stirrer MR 3001	Heidolph	Schwabach, DE
Mastercycler gradient	Eppendorf	Hamburg, DE
Microwave 800	Severin	Sundern, DE
Nanodrop ND-1000 spectrophotometer	PEQLAB Biotechnology GmbH	Erlangen, DE
NanoSight LM10instrument	NanoSight Technology	Malvern, UK
Parsortix	ANGLE plc	Guildford, UK
pH-Meter inoLab	WTW	Heidelberg, DE
Pipettes (2,5 µl, 10 µl, 200 µl, 1000 µl)	Eppendorf	Hamburg, DE
Pipette boy	Hirschmann Laboratory equipment	Eberstadt, DE
Platereader NanoQuant infinite M200Pro	Tecan	Männedorf, CH
Realplex mastercycler ep gradient S	Eppendorf	Hamburg, DE
Scanner	Epson	Suwa, JP
Semidry Blot-apparatus	Bio-Rad Laboratories	Hercules, CA, US
Sterile hood Herasafe HS12	Heraeus Kendro	Langenselbold, DE
Thermomix comfort	Eppendorf	Hamburg, DE
Ultracentrifuge Optima LE-80K	Beckman Coulter	Brea, CA, USA

Table 2 continued from previous page

Device	Company	Office
Ultrasound homogenisator	Hielscher Ultrasonics GmbH	Teltow, DE
Vortex-Genie 2	Scientific Industries	New York, NY, US
Water bath GFL-1002/03	GmbH für Labortechnik	Burgwedel, DE
Water bath Hl 1210	Leica	Nussloch, DE
XCyto 10 Quantitative Cell Imager	ChemoMetec	Lillerød, DN

2.3   Chemicals and reagents

Table 3: Chemicals and reagents used in this study

Chemical	Company	Office
AB-serum/PBS	BioRad	Rüdigheim, DE
Acetic acid (96%)	Merck	Darmstadt, DE
Acetone	J.T. Baker	Deventer NL
Agarose LE	Genaxxon Bioscience	Ulm, DE
Ampicillin	Sigma-Aldrich	Deisenhofen, DE
Ammoniumpersulfate (APS)	AppliChem	Darmstadt, DE
Antarctic phosphatase reaction buffer	New England BioLabs	Ipswich, MA, US
Aqua	B. Braun Melsungen	Melsungen, DE
Bacto-Agar	BD Biosciences	Franklin Lakes NJ, US
Bacto-Trypton	BD Biosciences	Franklin Lakes NJ, US
Bromphenol blue	Merck	Darmstadt, DE
BSA Fraction V (Bovines Serum Albumin)	Biomol	Hamburg, DE
Complete Protease Inhibitor	Roche Applied Science AG	Penzberg, DE
Crystal violet	Sigma-Aldrich	St. Louis, MO, US
DAPI (4',6-Diamidine-2-phenylindole)	Carl Roth	Karlsruhe, DE
DMEM High Glucose-Medium (Dulbecco's Modified Eagle's Medium)	PAN Biotech	Aidenbach, DE
DMSO (dimethyle sulfoxide)	Serva	Heidelberg, DE
DNA-Marker GeneRuler 1 kb DNA Ladder	Thermo Fisher Scientific	Waltham, MA, US
DNA-Marker GeneRuler 100 bp DNA Ladder	Thermo Fisher Scientific	Waltham, MA, US
dNTPs (desoxyribonucleoside triphosphate set)	Roche Diagnostics	Mannheim, DE

Table 3 continued from previous page

Chemical	Company	Office
DTT (dithiothreitol)	Sigma-Aldrich	St. Louis, MO, US
Dulbecco's PBS (1%)	Gibco	Eggenstein, DE
EDTA (Ethylendiamintetraacetat)	Sigma-Aldrich	St. Louis, MO, US
Ethanol absolute	Merck	Darmstadt, DE
Ethanol denaturated	Chemsolute/TH Geyer	Renningen, DE
FCS (fetal calf serum)	PAA Laboratories	Pasching, A
Fermacidal D2	IC products SA	Gordola, CH
GelRed Nucleic Acid Gel Stain	Biotium	Fremont, CA, US
Glycerole	Merck	Darmstadt, DE
Hydrochloride acid 1 N (HCl)	Carl Roth	Karlsruhe, DE
Hydrogen peroxide (H_2O_2)	Merck	Darmstadt, DE
Hyperladder I	Bioline	Luckenwalde
Isopropyl alcohol	Carl Roth	Karlsruhe, DE
L-glutamine	PAA Laboratories	Pasching, A
Luminol	Sigma-Aldrich	St. Louis, MO, US
MEM minimum essential media (1x)	Gibco BRL, Life Technologies	Eggenstein, DE
Methanol	J.T. Baker	Deventer, NL
Milk Powder	Carl Roth	Karlsruhe, DE
MTT	Sigma-Aldrich	St. Louis, MO, US
NEAA (MEM non-essential amino acid solution)	Sigma-Aldrich	St. Louis, MO, US
NP40 (Nonidet P-40)	Roche Diagnostics	Mannheim, DE
Nuclease-free Water	Qiagen	Hilden, DE
p-Coumaric acid	Sigma-Aldrich	St. Louis, MO, US
PFA (Paraformaldehyde)	Merck	Darmstadt, DE
PhosSTOP	Roche Applied Science AG	Penzberg, DE
Prolong Gold Antifade Reagent	Thermo Fisher Scientific	Waltham, MA, US
Protein Ladder 10 – 180 kDa Page Ruler Prestained	Thermo Fisher Scientific	Waltham, MA, US
Rnase A	Thermo Fisher Scientific	Waltham, MA, US
RPMI 1640 Medium	PAN Biotech	Aidenbach, DE
Rotiphorese Gel 40%	Sigma-Aldrich	St. Louis, MO, US
SDS-solution 20% (sodium dodecyl sulfate)	AppliChem	Darmstadt, DE
Sodium chlorid (NaCl)	Carl Roth	Karlsruhe, DE

Table 3 continued from previous page

Chemical	Company	Office
Sodium hydroxide (NaOH)	Merck	Darmstadt, DE
Sodium-pyruvate	Gibco BRL, Life Technologies	Eggenstein, DE
TEMED (Tetramethylethylenediamine)	Sigma-Aldrich	St. Louis, MO, US
Tris-acetate	Sigma-Aldrich	St. Louis, MO, US
Tris-EDTA (TE) buffer; pH 8.0	Sigma-Aldrich	St. Louis, MO, US
Triton X-100	Sigma-Aldrich	St. Louis, MO, US
Trizma base	Sigma-Aldrich	St. Louis, MO, US
Trypsin-EDTA solution 0.25% (w/v)	Gibco	Eggenstein, DE
Tween-20	Fluka (Thermo Fisher)	Waltham, MA, US
Wester nova 2.0	Cyanagen	Bolonga, IT
Yeast extract	BD Biosciences	Franklin Lakes NJ, US

2.4 Consumables

Table 4: Consumables used in this study

Consumable	Company	Office
6-well plate	Sarstedt	Nümbrecht, DE
24-well plate	BD Falcon	Heidelberg, DE
96-well microtiter plate	Eppendorf	Hamburg, DE
Cell culture inserts (8 µm pores)	BD Falcon	Heidelberg, DE
Cell culture inserts with matrigel (8 µm pores)	Corning	Corning, NY, US
Cell scraper	bioswisstec	Schaffhasuen, CH
FastGene PAGE Gel, 4-20%	NIPPON Genetics Europe	Dueren, DE
Leucosep™ pre-enrichment	Greiner Bio One	Kremsmünster, AT
Millex HV 0.45 µm PVDF syringe filter	Merck	Darmstadt, DE
Serological pipettes	Sarstedt	Nümbrecht, DE
Super RX films	Fujifilm	Minato, JP
T25 cell culture flask	Sarstedt	Nümbrecht, DE
T75 cell culture flask	Sarstedt	Nümbrecht, DE
Pipette tips	Sarstedt	Nümbrecht, DE

2.5   Commercially available kits

Table 5: Commercially available kits used in this study

Kit	Company	Office
First strand cDNA Synthesis Kit	Thermo Fisher Scientific	Waltham, MA, US
miRCURY LNA miRNA PCR assays	Qiagen	Hilden, DE
miRCURY LNA RT Kit	Qiagen	Hilden, DE
Maxima SYBR Green/Fluorescein qPCR Master Mix	Thermo Fisher Scientific	Waltham, MA, US
NucleoSpin Gel and PCR Clean-up	Macherey Nagel	Düren, DE
NucleoSpin Plasmid (No Lid)	Macherey Nagel	Düren, DE
NucleoSpin RNA	Macherey Nagel	Düren, DE
NucleoSpin RNA Plus	Macherey Nagel	Düren, DE
NucleoSpin Tissue (gDNA Isolation)	MachereFy Nagel	Düren, DE
Pierce BCA Protein Assay Kit	Thermo Fisher Scientific	Waltham, MA, US
Venor GeM Classic Mycoplasma Detection Kit	Minerva Biolabs	Berlin, DE

2.6   Enzymes

Table 6: Enzymes used in this study used in this study

Enzyme	Company	Office
AmpliTaq Gold polymerase	Applied Biosystems	Darmstadt, DE

2.7   Cytokines

Table 7: Cytokines used in this study

Cytokine	Catalog#	Company	Office
IFNγ	300-02	PeproTech	Rocky Hill, NJ, US
TNFα	300-01A	PeproTech	Rocky Hill, NJ, US

2.8 Antibodies

Table 8: Primary antibodies used in this study

Antigen	Clone	Species	Company	Office
HERC5	polyclonal H00051191	mouse	Abnova	Taipei, TW
HSC-70	clone B-6	mouse	Santa Cruz	Dallas, TX, US
ISG15 (IP)	F-9	mouse	Santa Cruz	Dallas, TX, US
ISG15	polyclonal #2743	rabbit	CST	Danvers, MA, US
pSTAT1 Tyr701	58D6	rabbit	CST	Danvers, MA, US

Table 9: Secondary and conjugated antibodies used in this study

Antigen	Clone	Species	Conjugate	Company	Office
rabbit-IgG	polyclonal	goat	HRP	CST	Danvers, MA, US
mouse-IgG	polyclonal	horse	HRP	CST	Danvers, MA, US
CD45	REA747	human	APC	Miltenyi Biotec	Bergisch Gladbach, DE
pan-keratin	AE1/AE3	mouse	AF488	eBioScience	San Diego, CA, US
pan-keratin	C11	mouse	AF488	CST	Danvers, MA, US

2.9 PCR primers and oligonucleotides

Table 10: PCR primers and oligonucleotides used in this study

Description	Target gene	Sequence	Tm
Crisp guide 5 fwd	HERC5	5' ACCAGGCGTTCTCTCCTCTC 3'	63 °C
Crisp guide 5 rev	HERC5	5' GCTGGGAAAGAGCCAGAGC 3'	63 °C
IRF1 fwd	IRF1	5' AGACCCTGGCTAGAGATGCAG 3'	59 °C
IRF1 rev	IRF1	5' TTGGGATCTGGCTCCTTTTCC 3'	59 °C
RPLP0 fwd	RPLP0	5' ACCCAGCTCTGGAGAAACTGC 3'	58 °C

Table 10 continued from previous page

Description	Target gene	Sequence	Tm
RPLP0 rev	RPLP0	5' TGAGGTCCTCCTTGGTGAACA 3'	58 °C
HERC5 RT8 fwd	HERC5	5' GAGCTAAGACCCTGTTTGG 3'	58 °C
HERC5 RT8 rev	HERC5	5' CCACCTTCCACATGCTATC 3'	58 °C
Slug fwd	Slug (SNAI2)	5' CAGACCCCCATGCCATTGAA 3'	58 °C
Slug rev	Slug (SNAI2)	5' TTCTCCCCGTGTGAGTTCTA 3'	58 °C

2.10   Vectors and expression plasmids

Table 11: Vectors and expression plasmids used in this study

Plasmid	Vector backbone	Addgene#	Source
Empty	LEGO-IG2-HA		Stefan Werner, ITB, UKE
HERC5 OE	LEGO-IG2-HA		Annkathrin Hanssen, ITB, UKE
VSV-6 envelope expression plasmid	pMD2.G	12259	Addgene, Cambridge, MA, US
Lentiviral packaging plasmid	psPAX2	12260	Addgene, Cambridge, MA, US

2.11   Buffers and solutions

Table 12: Buffers and solutions used in this study

Description	Composition
2% SDS sample buffer	2% SDS
	10% glycerol
	62.5 mM Tris/HCl, pH 6.8
6x loading dye	0.15% bromophenol blue
	0.15% xylene cyanol FF
	3% 150 mM Tris/HCl (pH7.6)
	60% glycerol

Table 12 continued from previous page

Description	Composition
Cell culture medium BEBM	500 mL BEBM
	0.5 ng/mL epidermal growth factor ligand
	500 ng/mL hydrocortisone
	0.005 mg/mL insulin
	0.035 mg/mL bovine pituitary extract
	500 nM ethanolamine
	500 nM phosphoethanolamine
	0.01 mg/mL transferrin
	6.5 ng/mL triiodothyronine
	500 ng/mL epinephrine
	0.1 ng/mL retinoic acid
Cell culture medium DMEM	500 mL DMEM
	10% FCS
	2 mM L-Glutamine
	200 U/mL Pen/Strep
Cell culture medium DMEM for astrocytes	500 mL DMEM
	20% FCS
	2 mM L-Glutamine
	200 U/mL Pen/Strep
Cell culture medium αMEM	500 mL αMEM
	10% FCS
	2 mM L-Glutamine
	200 U/mL Pen/Strep
Cell culture medium MEM	500 mL MEM
	10% FCS
	2 mM L-Glutamine
	200 U/mL Pen/Strep
	1% sodium-pyruvate
	1% non-essential amino acids
Cell culture medium (RPMI-1640)	500 mL RPMI-1640
	10% FCS
	2 mM L-Glutamine
	200 U/mL Pen/Strep

Table 12 continued from previous page

Description	Composition
Dulbecco's Phosphate Buffered Saline (DPBS)	2.7 mM KCl
	1.5 mM KH_2PO_4
	137.9 mM NaCl
	8.1 mM Na_2HPO_4 7 H_2O
Electrochemoluminescence (ECL) solution 1	0.1 M Tris-HCl (pH 8.5)
	2.5 mM Luminol
	0.396 mM p-Coumarine acid
Electrochemoluminescence (ECL) solution 2	0.1 M Tris-HCl (pH 8.5)
	0.018% (v/v) H_2O_2
Laemmli buffer	19.2 mM Glycine
	0.01% SDS
	2.5 mM Tris base
10 x PBST	1,37 M NaCl
	27 mM KCl
	32 mM Na_2HPO_4 x 12 H_2O
	15 mM KH_2PO_4
	Tween-20 0,05%
SILAC dilution buffer	50 mM Tris/ HCl
	0.4% NP-40
SILAC lysis buffer	50 mM Tris/HCl pH 8
	0.4% NP-40
	300 mM NaCl
	10 mM $MgCl_2$
	Protease & Phosphatase inhibitors
SILAC wash buffer	50 mM Tris/HCl pH 8
	0.4% NP-40
	150 mM NaCl
	5 mM $MgCl_2$
50 x TAE buffer, pH 8.0	40 mM Tris base
	20 mM acetic acid
	50 mM EDTA, pH 8.0

Table 12 continued from previous page

Description	Composition
TBS-T, pH 7.6	150 mM NaCl
	50 mM Tris base
	0.05% Tween 20
Transfer buffer	39 mM glycine
	20% methanol
	0.037% SDS
	48 mM Tris base

2.12 Software

Table 13: Software used in this study

Software	Application	Source
Bio-Rad CFX Manager (3.1)	Analysis of RT-qPCR data	Bio-Rad Laboratories, Hercules, CA, US
BioRender	Online tool for creating scientific figures	`https://biorender.com/`
Bowtie	Read mapping to miRBase	`http://bowtie-bio.sourceforge.net/index.shtml`
Cell Colony Edge macro for ImageJ	Analysis of anchorage-independent growth	see ref [108]
ColonyArea plugin for ImageJ	Analysis of clonogenic growth	see ref [109]
cutadapt	Trimming of NGS data	`http://cutadapt.readthedocs.io/en/stable/guide.html`
DAVID	Functional annotation database	`https://david.ncifcrf.gov/`
GIMP (2.8)	Image processing	`www.gimp.org`
Axiovision	Image processing	`www.zeiss.de`
ImageJ (1.52a)	Image processing	`https://imagej.nih.gov/ij/`
Image Studio Lite	Western blot quantification	`https://www.licor.com/bio/image-studio-lite`

Table 13 continued from previous page

Software	Application	Source
NCBI	Database for literature (PubMed)	`www.ncbi.nlm.nih.gov`
NCBI Blast	Search of homologous sequences and primer design	`https://blast.ncbi.nlm.nih.gov/Blast.cgi`
NanoSight NTA 3.0	Analysis of particle size and concentration	Malvern Instruments Ltd, Worcestershire, UK
R	Statistical analysis	`https://www.r-project.org/`
R Studio	Integrated development environment for R	`https://rstudio.com/`
SnapGene Viewer	Analysis of DNA sequences	`https://www.snapgene.com/snapgene-viewer`

3 Methods

3.1 Cell culturing methods

In order to avoid contaminations that could influence results, all cell culture experiments have been performed under sterile conditions. Possible contaminations include bacteria, fungi, yeast or proteins (e.g. DNases). Therefore, consumables such as pipette tips, micro-centrifuge tubes and other vessels were autoclaved beforehand. Furthermore, working benches were disinfected with 70% ethanol or Fermacidal before and after the experiments. Cell culture experiments were performed under a laminar flow hood.

3.1.1 Analysis of mycoplasma contamination

Cells in culture were tested for possible contamination of mycoplasma by analysis of cell culture supernatant using Venor GeM Classic Mycoplasma Detection kit according to manufacturer's instructions. Cells were analyzed at least once per month and directly before cryopreservation.

3.1.2 Standard cultivation of eukaryotic cell lines

Eukaryotic cell lines were cultured in sterile cell culture flasks in media as shown in table 2.1. Depending on the culture media, cells were incubated in Hera150 incubator at 37 °C and 5% or 10% CO_2. Depending on their growth rates, cells were passaged twice or three times a week. Adherent cells were washed in PBS and through the addition of trypsin/EDTA solution (0.05%/ 0.02%) and by incubation for 5 min at 37 °C, cells were detached from culture flasks. The reaction was stopped with additional media and cells were centrifuged at 1200 g for 3 min. After resuspension of the pellet, cells were seeded at 30% density into new culture flasks or at specific cell numbers for specific assays as described below.

3.1.3 Cryopreservation of eukaryotic cell lines

For long-term storage purposes cells were resuspended in freezing media consisting of 90% culture media and 10% DMSO (dimethylsulfoxide) as a cryo-conservative and stored at -80 °C. The tubes were subsequently stored in liquid nitrogen to further enhance their conservation. For re-culturing of frozen cells, cells were thawed at 37 °C and resuspended immediately in 9 mL of pre-warmed media. After centrifugation at 1200 g for 3 min, cell pellets were resuspended in fresh media and cultured in new culture flasks.

3.1.4   Lentiviral particle production

The production of lentiviral particles was conducted by culturing HEK293T cells which are subsequently transfected using a three plasmid packing system. Cells at approximately 80% confluency were transfected with 3 µg of either LEGO-iG2-HERC5-HA or LEGO-iG2-HA plasmid, 3750 ng of psPAX2 packaging plasmid and 1250 ng of pMD2.G envelope plasmid in addition to 20 µl of Lipofectamine2000 reagent and 500 µl Opti-MEM. The backbone of LEGO-iG2 vector additionally carries a GFP sequence coupled with an IRES (internal ribosomal entry site). The transfection mix was replaced with standard medium 12-15 hours after transfection. The virus-containing supernatant was collected after an additional 48 h and filtered using 0.45 µm Millex Filters syringe filters. Virus stocks were stored at -80 °C.

3.1.5   Generation of *HERC5* overexpression cell lines

For the generation of *HERC5* overexpressing cell lines, 200 µL of lentiviral LEGO-iG2-HERC5-HA or corresponding empty vector control LEGO-iG2-HA particles were added dropwise to cultured H1395 cells at approximately 80% confluency. Cells were cultivated in 6-well plates in 2 mL media containing 2 µL polybrene (1:1000) to enhance transduction efficiency. 24 h after viral transduction, media was refreshed. Each day, cells were monitored for GFP positivity. After 7 days cells were seeded into T25 flasks.

3.1.6   FACS sorting of LEGO-iG2-positive cells

In order to select cells overexpressing HERC5 or an empty vector control, FACS (fluorescence-activated cell sorting) was performed. For this, cells were washed, trypsinized and resuspended in 500 µL PBS containing 1 mM EDTA. Because of the IRES-coupled GFP sequence present in the backbone of the LEGO-iG2 vector, those cells expressing HERC5 also express GFP and signal intensities therefore correlate. Using FACS Aria Fusion III device, cells were sorted according to their GFP positivity at a wavelength of 488 nm and re-cultured for further experiments.

3.1.7   Allowance of GMOs

In this study, several genetically modified (GMO) cell lines were generated under the registration numbers for genetic engineering facilities IB24-20/07 (S1) and IB24-21/07 (S2).

3.2 Molecular biological methods

3.2.1 Isolation of genomic DNA (gDNA) from cultivated cells

Genomic DNA from human cell culture cell lines was performed with NucleoSpin Tissue kit according to the manufacturer's instructions. Measurement of gDNA concentration and quality was performed using the Nanodrop ND-1000 system. For quality control, quotients of photometric absorption at 260 nm and 280 nm are calculated. Resulting absorption coefficients between 1.8 and 2.0 were considered acceptable for further downstream experiments.

3.2.2 Agarose gel electrophoresis

Agarose LE with a final concentration of 1% was heated in 1x TAE buffer until all of the agarose was dissolved. After cooling down to approximately 50 °C either ethidiumbromide (1:10000) or GelRed Nucleic Acid Gel Stain (1:10000) were added to the agarose solution. DNA samples were mixed with 6 x DNA loading-dye and were loaded on the gel after polymerization. For analytic uses of plasmid detection, approximately 400 ng of DNA was loaded on the gel, whereas 1 μg of DNA was used for subsequent gel extraction. For PCR analysis, 10 μL were loaded. The electrophoresis was run in 1x TAE buffer at 100 V for 30 min to separate the DNA according to its molecular weight. The DNA was detected by exposing the gel to UV light at 234 nm in a trans-illuminator. Analysis of the gel was performed with the documentation system 'Gene Genius 2'.

3.2.3 Extraction of DNA fragments from agarose gels

DNA extraction from agarose gels was performed using NucleoSpin Gel and PCR Cleanup kit in order to remove residual contaminations such as primers, unbound nucleotides, enzymes or unspecific side-products after PCR. The protocol was performed according to the manufacturer's instructions. After agarose gel electrophoresis the DNA was exposed to UV-rays for only a few seconds during the excision to avoid any damage. DNA was eluted from the column using 20 μL NE-buffer and stored at -20 °C.

3.2.4 Polymerase chain reation (PCR)

The amplification of target DNA sequences with specific primers was performed by polymerase chain reaction (PCR). Here, PCR was used in order to verify DNA sequences of A549 HERC5 KO clones which had been previously raised after transfection with CRISPR-Cas9 plasmid. Reations were set up according to table 14 using AmpliTaq Gold polymerase and Crisp guide 5 primers.

Table 14: Reagents used for PCR

Reagent	Volume
10 x AmpliTaq Gold buffer	5 µL
Forward primer (10 µM)	1 µL
Reverse primer (10 µM)	1 µL
DNA template	100 ng
AmpliTaq Gold polymerase	1 µL
DMSO	2.5 µL
sterile ddH$_2$O	to 50 µL

The corresponding PCR protocol is presented in table 15.

Table 15: PCR protocol

Step	Duration	Temperature	Cycles
Initial denaturation	10 min	95 °C	1
Denaturation	1 min	95 °C	
Annealing	1 min	63 °C	30
Extension	3 min	72 °C	
Final extension	7 min	72 °C	1

3.2.5   RNA isolation

RNA extraction from cell lines using NucleoSpin RNA or NucleoSpin RNA Plus kit was performed according to the manufacturer's protocols. After application of the lysis buffer, detached cells were scraped off with a cell scraper prior to RNA isolation. Measurement of RNA concentration and quality was performed using the Nanodrop ND-1000 system, with an acceptable absorption coefficient ranging between 1.8 and 2.0. The absorption coefficient is the quotient of photometric absorption at 260 and 280 nm.

3.2.6   RNA sequencing

HTB56 OE/EC cell lines were grown in triplicates in T75 flasks to a confluency of approximately 80%. After RNA isolation, concentrations and absorption coefficients were analyzed. For further quality control, electrophoretic separation of total RNA is performed for analysis of RNA integrity. For this, RNA ScreenTape Analysis kit from Agilent and Agilent 4200 TapeStation instrument was used according to the manufacturer's instructions. Here, RNA integrity numbers (RIN) are assessed which is a measurement

for the amount of degradation of ribosomal RNA in the sample. RNAseq was performed by CeGaT, Tübingen, Germany using 500 ng of RNA.

3.2.7   cDNA synthesis

For quantification of expression of particular genes, first RNA has to be reverse transcribed into cDNA. First Strand cDNA Synthesis kit was used according to the manufacturer's instructions and Table 16. For this, 500 ng of total RNA were transcribed using random hexamer oligo nucleotides. For further analyses the cDNA was diluted in a range from 1:2 to 1:10 in ddH$_2$O and subsequently stored at -20 °C.

Table 16: Program used for cDNA synthesis

Step	Duration	Temperature
Annealing	5 min	65 °C
Reverse transcription	60 min	37 °C
Inactivation of transcriptase	5 min	70 °C

3.2.8   Real-time quantitative polymerase chain reation (RT-qPCR)

In order to quantify the mRNA expression of genes of interest, real-time quantitative PCRs (qPCR) were performed using Maxima SYBR Green/Fluorescein qPCR Master Mix kit. Previously reverse transcribed cDNA was used as a PCR template, and by binding of SYBR Green fluorescent dye, double-stranded DNA generated during the PCR is detected in which the signal increases with higher amounts of PCR products. Once signal intensities reach logarithmic phase, the specific cycle number is detected as the so-called C$_q$-value (quantitation cycle). The reaction was set up according to Table 17 and to manufacturer's instructions.

Table 17: Reagents used for RT-qPCR

Reagent	Volume
SYBR Green	5 µL
Forward primer (10 µM)	0.3 µL
Reverse primer (10 µM)	0.3 µL
Nuclease free ddH$_2$O	1.9 µL
cDNA template	2.5 µL

The amplification was performed in triplicates using Realplex mastercycler ep gradient S. The corresponding RT-qPCR protocol is presented in Table 18. Melting curves

were analyzed to confirm primer binding specificity. Quantification of PCR products was subsequently performed using $\Delta\Delta C_q$ method. Here, genes of interest are first normalized against expression levels of housekeeping gene *RPLP0* by calculating $\Delta C_q = C_q$ (target gene) - C_q (reference gene). This value is then normalized once more in order to quantify expression levels relative to a control (e.g. untreated cell lines or reference cell lines) by $\Delta\Delta C_q = \Delta C_q$ (sample) - ΔC_q (control). The fold change of expression is assessed by calculation of $2^{-\Delta\Delta C_q}$. MiRNA analysis on patient samples are described in chapter 3.6.

Table 18: RT-qPCR protocol

Step	Duration	Temperature	Cycles
Initial denaturation	10 min	95 °C	1
Denaturation	15 s	95 °C	
Annealing	30 s	58 °C	40
Extension	30 s	72 °C	
Denaturation	15 s	95 °C	1
Final extension	55 s	60 °C	1
Melting gradient	+0.5 °C/5 sec	60 °C to 95°C	1

3.2.9 Protein isolation of cultured cells

The generation of whole protein lysates was performed after first washing cells at approximately 90% confluence with PBS. Subsequently, 1 mL of PBS was added and cells were detached from the culture flask surface using a cell scraper. The resulting suspension was transferred into a 1.5 mL reaction tube, centrifuged (3 min, 750 g, 4 °C) and the pellet was resuspended in 2% SDS sample buffer containing freshly added Complete Protease Inhibitor and PhosSTOP phosphatase inhibitor. Homogenization of the sample was achieved by degrading genomic DNA through sonication with an ultrasound homogenisator for 10 seconds (continuous cycle at an amplitude of 50%). After measurement of protein concentration, 1 μL of saturated bromophenol blue solution was added. Samples were denatured by incubation at 95 °C for 5 min .

3.2.10 Measurement of protein concentration

Pierce BCA Protein Assay Kit was used according to the manufacturer's instructions in order to quantify the protein concentration of whole cellular extracts. In general, samples were added to a mixture of reagents A and B (1:50). A calibration curve containing protein standards of 10 μg, 20 μg and 30 μg was generated by adding BSA

stock solution. 2 µL of protein sample were used for assessment of concentration. A purple-colored complex resulting from chelation of BCA (bicinchoninic acid) and copper ions is formed in the presence of proteins which intensifies over time and with increasing concentrations. After an incubation period of 15 min at RT, extinction at 562 nm of the samples was measured against a blank of reagent mixture of A and B. By performing linear regression of the BSA standards, protein concentrations were calculated.

3.2.11   Immunoprecipitation

Whole protein lysates designated for immunoprecipitation (IP) were produced by washing the cells with PBS, scraping them off in 1 mL PBS and centrifugation of the cell suspension at 750 g for 3 min at 4 °C. After removal of the supernatant, cells were gently lysed in 300 µL IP lysis buffer and incubated on ice for 15 min. Nuclei and cellular debris were removed by centrifugation at 4 °C at 19,000 g for 5 min. The supernatant was mixed with 300 µL of IP dilution buffer and protein concentration was measured. 500 µg whole protein lysate was added to spin columns and filled to a volume of 500 µL IP wash-buffer. 30 µL ISG15-agarose beads were resuspended carefully and added to the lysate. The lysate-beads mixture was incubated over night at 4 °C with gentle end-over-end mixing. By pulse centrifugation for 10 s the flow-through was discarded and beads were subsequently washed three times with 500 µL IP wash-buffer by pulse centrifugation and discarding of the flow-through. Immunoprecipitated proteins were eluted with 35 µL 2% SDS-buffer containing 1 µL of saturated bromophenol blue solution. For this, the beads were incubated with the buffer at 95 °C for 5 min before pulse centrifugation. The eluate was added to the beads for a second time and elution was repeated to increase overall yield.

3.2.12   SDS-PAGE

In order to visualize proteins on either Coomassie-stained polyacrylamide gels or western blot membranes, they were first separated according to their molecular weight by SDS-Polyacrylamide Gel Electrophoresis (SDS-PAGE). For this, total protein lysates or immunoprecipitated proteins were applied on an SDS polyacrylamide gel which was prepared according to table 19 or pre-made (4%-20% gradient gels). Whether self-made 8% gels or pre-made gradient gels were used depended on the antibodies used in subsequent western blot analysis. For the detection of ISG15 protein, gradient gels were used in order to visualize unconjugated ISG15 at 15 kDa as well as ISGylated proteins of higher molecular weight simultaneously.

For analysis of whole protein lysates, 80 µg were used while for IP analysis, eluate from 500 µg initial input was applied to each lane. SDS-PAGE was performed using

Table 19: Reagents used for self-made SDS-polyacrylamide gels

Reagent	6% stacking gel	8% separation gel
H_2O	1.46 mL	2.1 mL
1.0 M Tris (pH 6.8)	0.3 mL	-
1.0 M Tris (pH 8.8)	-	1.0 mL
Rotiphorese Gel 40%	0.3 mL	0.8 mL
10% SDS	20 µL	40 µL
10% ammonium persulfate	20 µL	40 µL
TEMED	2 µL	4 µL

Hoefer SE250 system in Laemmli buffer at 25 mA for 60 min for self-made gels or in MOPS buffer for pre-made gels at initially 40 mA for 30 min and 20 mA for further 30 min. PageRulerTM Prestained Protein Ladder was used as size standard.

3.2.13   Coomassie staining

SDS-gels subsequently used for control of IP elution efficiency or for SILAC analyses were subjected to Coomassie staining. After electophoresis, the gel was fixed in fixation buffer and subsequently stained for 1 h in Coomassie staining solution. The gel was then incubated in destaining solution for approximately 3 h until the bands were clearly distinguishable from the background.

3.2.14   Western Blotting

In order to detect proteins of interest through specific antibody binding, proteins separated according to their molecular weight by SDS-PAGE were transferred onto a nitrocellulose membrane via semi-dry transfer. For this, in total 4 Whatman filters and a nitrocellulose membrane were soaked in transfer buffer and assembled on a Trans-Blot SD semi-dry transfer cell to form a sandwich consisting of two Whatman filters, a nitrocellulose membrane, an unstained SDS gel and two additional Whatman filters. After removal of air bubbles, the sandwich was subjected to an electrotransfer at 40 mA per gel for 2 h. By gentle shaking, the membrane was subsequently washed in TBS-T or PBS-T for 5 min before blocking of unspecific protein binding sites in 5% (w/v) milk powder/PBS-T or 5% (w/v) BSA/TBS-T for 1 h at RT. This was followed by an incubation of primary antibody in blocking solution at 4 °C over night. The next day, unbound primary antibody was removed by washing three times with TBS-T or PBS-T for 5 min. The membrane was then incubated with secondary antibody coupled with horseraddish peroxidase (HRP) in 5% (w/v) BSA/TBS-T or 5% (w/v) BSA/PBS-T for 1 h

at RT followed by additional washing of excess antibody for three times with TBS-T or PBS-T for 5 min. Detection was performed by adding ECL solution (consisting of freshly combined parts 1 and 2 in equal amounts) to the membrane. The detection is based on enzymatic catalyzation by HRP of the secondary antibody of luminol oxidation by H_2O_2. The emitted photons are captured on x-ray films which are subsequently developed with Film developer Curix 60.

3.3 Functional assays

In order to assess phenotypical differences in cancer-related behavior deriving from differential HERC5 expression, several functional assays were performed. For this, HTB56 HERC5 OE/empty vector control (EC), H1395 HERC5 OE/empty vector control (EC) and A549 HERC5 KO/parental model cell lines were used. The establishment of an HTB56 HERC5 overexpression cell line as well as the generation of different A549 HERC5 KO clones had already been previously completed by Dr. Annkathrin Hanssen. All functional assays were performed in at least triplicates, each time using different passages of cells to ensure technical and biological replicates for statistical testing.

3.3.1 Generation of conditioned media

In order to analyze the influence of a bone or brain micro-environment on cells harboring differential HERC5 expression, assays were also performed using conditioned media from MC3T3-E1 or primary human astrocytes instead of standard culture media where indicated. For this, either MC3T3-E1 or astrocytes were grown to a confluency of 80% for 48 h and cell culture supernatant was filtered using 0.45 μm Millex Filters syringe filters. Conditioned media was subsequently diluted in a 1:1 ratio with the corresponding cell culture media to avoid growth inhibition by insufficient amount of growth factors depleted by the cells.

3.3.2 MTT assay

For examining proliferative capacities of cell lines MTT (3-(4,5-dimethylthiazol-2-yl)-2,5-diphenyltetrazolium bromide) assays were performed. In this assay, the metabolic activity of cells is indirectly measured by assessing the capability of converting tetra-zolium dye MTT to its insoluble form formazan. First, 1000 single cells of each cell line were seeded into 96-well plates in 100 μL standard or conditioned media. The proliferation was measured at days 0, 3, 5 and 7 for HTB56 and H1395 and at days 0, 3, 4 and 5 for A549 cell lines. Subsequently, growth curves were compared. For the measurement, 20 μL of MTT was added to the individual wells. After an incubation

period of 3 h, media was carefully removed and formazan was dissolved in 100 μL of DMSO by gentle shaking. A NanoQuant infinite M200Pro ELISA plate-reader was used to measure absorption at 540 nm and 650 nm for reference wavelength correction. In order to monitor the growth changes of cells at different time points, absolute values after correction were plotted against time and by t-testing, absorption at end-points were compared. For the evaluation of growth rate of KO clones, ratios of absorption at day x and day 0 are calculated. By calculating the $\log_2$ value of these ratios one can identify the amount of doublings that have taken place. Plotting time against doublings will give an equation in which the slope equals the time that was needed for the population of cells at the beginning of the experiment to double.

3.3.3   Clonogenic assay

The colony formation assay can be used to determine the ability of single cells to grow into a colony and therefore to undergo unlimited division. The assay was performed using either standard culture media for HTB56, H1395 or A549 or conditioned astrocytes or MC3T3-E1 media and their respective media to serve as a control. For this, 1000 cells were seeded in 6-well plates and detected after 7 days. After gently removing the media, cells were washed with PBS and colonies were fixed with 4% (w/v) PFA/PBS for 10 min. Subsequently, colonies were stained with 0.5% (w/v) crystal violet/H_2O solution for 30 min and generously washed with ddH_2O to remove excess staining solution. The plate was scanned and colonies were detected using ColonyArea plugin for ImageJ [109].

3.3.4   Anchorage-independent growth

The ability of cells to grow under anchorage independent conditions was studied by performing a soft agar assay. For this, 2 mL of bottom-agar consisting of standard cell culture media and heated agar solution (final concentration: 0.5% in ddH_2O) was produced by mixing both solutions at a temperature of 42 °C, poured into 6-well plates and left to harden. For each well, 1 mL of top-agar was prepared, consisting of 2/3 bottom-agar and 1/3 cell suspension (3000 cells). Every 3 days, 300 μL media was added to prevent drying of the agar. 14 days after seeding, 200 μL MTT was added dropwise to the wells and the plate was scanned 3 h later. Colonies exceeding a diameter of 100 μm were counted using Cell Colony Edge macro for ImageJ [108]. Detection parameters were changed to "Number of pixels/unit" = 0.0945; "Rolling Ball Radius" = 50; "Analyze Particles - Min size" = 7854 and "Analyze Particles - Min circ" = 0.5. Changes were made in order to adjust the detection to a suitable diameter of colonies according to cell numbers and growth time.

3.3.5   Migration assay

The influence of differential HERC5 expression on the migratory capability was analyzed in cell lines by seeding 500 µL media containing 20,000 cells of each modified NSCLC cell line into cell culture inserts (8 µm pores), so-called boyden chambers. The migration assay was performed by seeding either 100,000 astrocytes or MC3T3-E1 cells at the bottom of the wells 24 h prior to the experiments or by simply using culture media containing FCS while the cells in the boyden chambers were FCS deprived. The amount of migrated cells was counted 16 h after seeding. The media was then removed from the inserts, cells were washed in PBS and fixed with 4% (w/v) PFA/PBS for 10 min. Cells were permeabilized with methanol for 20 min and subsequently stained with 0.5% (w/v) crystal violet/H_2O solution for 10 min. Excess staining solution was removed by washing the chambers in PBS. Using a sterile cotton swab, non-migrated cells were scraped off from the inside of the inserts so that only those cells which have migrated through the pores remain on the surface on the porous membrane. The membrane was imaged under a brightfield microscope (Zeiss, Axiovision) and cells were counted manually.

3.3.6   Invasion assay

The invasive potential can be linked to the metastatic capacity of cells. To study this capacity, an invasion assay was performed. Similar to migration assays, commercially available cell culture inserts with 8 µm pores in the membrane were used which are covered with matrigel. First, inserts were thawed at RT and rehydrated by incubation with 500 µL FCS-free media in both the well and in the chamber each for 2 h at 37 °C. Subsequently, 20,000 cells of each modified NSCLC cell line in FCS-free media were seeded into chambers while media in the wells was replaced with media containing FCS. In parallel to the invasion assay, a migration assay was performed which served as a control for successful migration through the pores. The amount of cells which were able to invade through the matrigel and subsequently migrated through the pores was counted 22 h after seeding. Cells were stained and counted as described in 3.3.5.

3.4   Stable isotope labeling by amino acids in cell culture (SILAC)

In order to detect and quantify differences in HERC5 ISGylation in A549 HERC5 KO and parental cell lines, stable isotope labeling by amino acids in cell culture (SILAC) analyses was performed. SILAC is a mass spectrometry (MS) based method which uses *in vivo* metabolic incorporation of ^{13}C-labeled amino acids L-lysine and L-arginine into proteins. Here, A549 parental cell line was ^{13}C -labeled while A549 HERC5 KO cells remain unlabeled. Briefly, proteins were isolated from cell lysates which were then

subjected to immunoprecipitation using ISG15 antibody as bait. After ISG15 IP, equal concentrations of eluate from the cell lines are combined, separated by SDS-PAGE with subsequent Coomassie-staining, digested with trypsin and subjected to MS. So-called SILAC pairs were analyzed which consist of isotopic peptide pairs.

3.4.1 ^{13}C-labeling of A549 cell line

Media for SILAC analyses were set up according to table 13 in the materials section. Standard SILAC DMEM does not initially contain amino acids L-lysine and L-arginine. Both amino acids as well as L-proline were therefore carefully reconstituted by adding 1 mL of SILAC DMEM to the amino acids and subsequently more media was added to reach final concentration of stock solutions. Both A549 parental and HERC5 KO cell lines were seeded in T25 flasks. After reaching 90% confluence cells were split according to section 3.1.2 while A549 par cells were re-seeded in heavy SILAC DMEM and HERC5 KO cells in light SILAC DMEM. Both cell lines were passaged 5 times. In order to analyze the time and passaging needed for total incorporation of ^{13}C amino acids, cell lysates of each passage were produced simultaneously. Cell lysates were subjected to SDS-PAGE and were stained using Coomassie solution. Analysis of ^{13}C incorporation rate was kindly performed by Parinaz Mossahebi Mohammadi at Institute of Tumor Biology, UKE.

3.4.2   Set up of SILAC study

After analysis of ^{13}C incorporation rates, cell lines were grown in T75 flasks until passage 3 based on the results obtained in section 3.4.1. Upon confluence, cells were detached, split in a 1:6 ratio, then seeded in heavy or light SILAC DMEM for parental or KO cells, respectively, and treated with 10 ng/mL IFNγ and 50 ng/mL TNFα for 48 h. Cells were lysed in IP lysis buffer and IP using agarose beads-coupled ISG15 antibody was performed. After elution, BCA test was used to assess protein concentration and 25 μg of protein were mixed in a 1:1 ratio of each cell line and subjected to SDS-PAGE.

3.4.3   Mass spectrometry parameters

After SDS-PAGE, Coomassie-staining was performed in order to visualize proteins of different sizes eluted after ISG15-IP. Each lane of coomassie-stained gels was cut into 10 pieces and subjected to in-gel digestion. Proteins were digested with trypsin protease which specifically cleaves proteins after L-lysine and L-arginine residues to produces peptides of defined sizes. Digestion, mass spectrometry analysis and mapping to human database were kindly performed by Parinaz Mossahebi Mohammadi at Institute of Tumor

Biology, UKE. Proteins ISGylated by HERC5 were identified by sorting normalized ratios of heavy (H) and light (L). Using cut-off values of 1.5, proteins specifically ISGylated by HERC5 were dertermined. Subsequently, fold-changes of total peak intensities from mass spectrometry were calculated and included in the analysis as well. Only proteins enriched in parental cell lines were considered.

3.5   Analyis of extracellular vesicles from cell culture supernatant

For the analysis of extracellular vesicles (EVs) from cell culture supernatant, ultracentrifugation was performed which is still considered the gold standard for EV isolation [110]. Particle concentration was subsequently assessed by nanoparticle tracking analysis and protein content was analysed using a SILAC-based approach (see previous chapter).

3.5.1   Differential centrifugation of cell culture supernatant

Isolation of EVs was performed by multiple centrifugation steps. First, cell culture supernatant from cells at approximately 90% confluence was centrifuged at 1200 g for 3 min. During this step, cells that were not attached to the cell flask surface were removed by pelleting. The supernatant was then centrifuged at 1200 g at 4 °C for 15 min to increase removal of residual cells and debris. The resulting supernatant was subjected to centrifugation at 10,000 g at 4 °C for 20 min in order to deplete apoptotic bodies and large vesicles. The supernatant was then filtrated using 0.2 μm syringe filters. EVs were pelleted by ultracentrifugation using Optima LE-80K ultracentrifuge equipped with swinging bucket rotor at 100,000 g at 4 °C for 70 min and supernatant was carefully removed. The pellet was resuspended in 200 μL PBS and stored at -80 °C.

3.5.2   Nanoparticle tracking analysis (NTA)

Nanoparticle tracking analysis (NTA) was performed for quantification of total numbers of EVs after isolation by ultracentrifugation as well as their size distribution. Since EVs are known to exhibit a large heterogeneity in size, this measurement therefore also served as quality control. Particles of 10-1000 nm in size can be analyzed. NTA measurements are based on Brownian motion of particles in solution which can be assessed by laser illumination and subsequent detection of light scattering on a CCD camera. This is then used to track movements of each particle. By making use of the Stokes–Einstein equation, hydrodynamic diameters of individual particles can be calculated and based on total counts, concentrations are measured. Here, NanoSight LM10 instrument was used as well as NanoSight NTA 3.0 software for analysis. Samples were diluted 1:100 in

PBS prior to measurements. For each sample, 10 videos of 30 s duration were recorded and analyzed in batch-processing mode using capture screen gain 2, camera gain max, process screen gain 10 and detection threshold 6 parameters.

3.5.3   SILAC analysis of extracellular vesicles

In order to analyze differences in protein content in EVs derived from A549 par/KO cell lines by using SILAC-based proteome analysis, FCS for SILAC purposes needs to be depleted of EVs from bovine sources. For this, FCS was diluted in SILAC DMEM to a final concentration of 30% and ultracentrifuged at 100,000 g at 4 °C for 16 h. Supernatant was then removed and used for subsequent preparation of SILAC DMEM with FCS (final concentration: 10%). Cells were grown in 2 T175 flasks in order to obtain sufficient media for following analyses. Hence, 75 mL of heavy or light SILAC DMEM was used to grow cells until passage 3 for A549 par/KO cells, respectively. Cells were grown in 10 ng/mL IFNγ and 50 ng/mL TNFα for 48 h until removal of the supernatant and subjection to ultracentrifugation (see above). Supernatant from final centrifugation step was removed and pellets were resuspended in 75 µL SDC buffer. Mass spectrometry analyses and database search services were kindly provided by Prof. Schlüter and Hannah Voß from the mass spectrometry core facility, UKE.

3.6   Processing of patients samples

3.6.1   Blood sample collection

For both studies presented here, blood was drawn from cancer patients under written informed consent and approval by the local ethical committee (PV5932). Analysis of influence on analytes from different blood collection tubes was performed using blood samples from 20 metastatic melanoma (MM) (stage IV) patients collected by Centre of Dermatology, Elbe Clinics, Buxtehude, Germany as well as Department of Dermatology and Venereology (UKE). In addition to this, blood from healthy donors was used from the Department of Transfusion medicine (UKE). For evaluation of a semi-automated scanning approach of CTCs, blood from 7 metastatic breast cancer patients from Department of Gynecology (UKE) was drawn (see table 28) [111].

3.6.2   Tumor cell enrichment by the ClearCell® FX1 system

For analysis of plasma removal on recovery rates of circulating tumor cells from melanoma patients, first spiking experiments were performed using 50 H1975-GFP positive cells in EDTA and Streck blood from healthy donors. Experiments were performed

without (EDTA: n=4) and with (EDTA: n=4, Streck: n=2) plasma removal (1900 g, 15 min), and whole blood/ PBMC fraction was processed with the ClearBridge ClearCell® FX1 system using default settings according to the manufacturer's instructions. The Clearbridge device makes use of cell size, deformability and inertia characteristics of tumor cells. It is a label-free enrichment method and blood is processed through a microfluidic chip which uses Dean vortex flows to separate the cell populations through small curvilinear channels. After treatment of the blood with red blood cell lysis buffer and centrifugation, the pellet was resuspended in 4 mL resuspension buffer and processed by the ClearCell FX1 System. During this process, the majority of smaller PBMCs is discarded, while the output contains enriched tumor cells among contaminating PBMCs. Supernatant was removed after centrifugation of the output (500 g, 10 min) and the pellet was transferred into 96-well plates for visualization of fluorescence signal of the GFP-positive H1975 cells and subsequent enumeration.

3.6.3   Isolation and analysis of EVs from patients samples

Isolation of patient-derived EVs from melanoma patients, NTA measurements as well as transmission electron microscopy were kindly performed by Orion Pharma, Finland.

3.6.4   MiRNA extraction and sequencing

Isolation of miRNA from plasma and EV samples were performed by Qiagen. Briefly, after plasma isolation 200 µL plasma from EDTA and Streck tubes was used to extract miRNAs from 10 melanoma patients and five HDs by using miRNeasy Serum/Plasma Advanced Kit according to instructions. miRNeasy Serum/Plasma Kit was used for extraction of miRNAs from EVs. QIAseq miRNA Library Kit was used for construction of QIAseq miRNA libraries while Illumina NextSeq High Output sequencing runs were performed by Illumina NextSeq 550 with 5 µL of miRNA. Quality control of NGS data was performed with cutadapt by trimming of 3' adapter sequences and low quality bases (Phred score <10). Identical reads were collapsed according to their Unique Molecular Indices (UMIs) sequences. Reads were mapped to miRBase using bowtie.

3.6.5   Differential expression analysis

For the assessment of differential miRNA expression, raw UMI reads of MM patients were compared to the counts in the HD samples. Normalization was therefore performed with UMI counts of HD and MM samples for the groups EDTA plasma, EDTA EV, Streck plasma and Streck EV. Differences in UMI count medians between EDTA and Streck samples were analyzed by statistical testing using Wilcoxon signed-rank test in R. Samples

were normalized using both geNorm [112] (GeneGlobe Secondary Data Analysis Tool, Qiagen) and NormFinder [113] (GenEx7, MultiD Analyses AB, Gothenburg, Sweden) algorithms separately in order to reduce possible bias from the normalization method. UMI counts exceeding 3 reads were considered as references genes for the NormFinder algorithm only. Cut-off values of (p<0.05) for analysis of differential miRNA expression by t-testing as well as fold-change ratios of 2 for MM/HD samples were used. Only genes exceeding the parameter of averaged UMI counts >10 in at least one group were analyzed by both geNorm and NormFinder analyses.

3.6.6   Orthogonal validation of differentially expressed miRNAs

In order to validate differential miRNA expression from NGS data 2 µL from EDTA and Streck EV miRNA samples were reverse transcribed into cDNA using miRCURY LNA RT Kit according to instructions. Shortly before RT-qPCR set up, samples were diluted 1:30 and using 3 µL of template cDNA, and prepared according to Table 20. Hsa-miR-103a-3p and hsa-miR-93-5p were used as reference gene assays (miRCURY LNA miRNA PCR assays), and were chosen according to geNorm results and based on abundant expression profiles. Hsa-miR-375, hsa-miR-215-5p, and hsa-miR-200c-3p were chosen for orthogonal validation due to the findings of expression analysis in both algorithms. Assays were performed in triplicates according to the instructions. Using the $\Delta\Delta C_q$ method for analysis, with ΔC_q = C_q (average (hsa-miR-103a-3p + hsa-miR-93-5p)) - C_q (individual assay of each patient or healthy donor) and $\Delta\Delta C_q$ = ΔC_q (individual patients) - ΔC_q (average of healthy donors), differential expression was assessed [114].

Table 20: RT-qPCR protocol for miRNA validation

Step	Duration	Temperature	Cycles
Initial denaturation	2 min	95 °C	1
Denaturation	10 s	95 °C	
Annealing/ extension	60 s	56 °C	40
Melting gradient	+0.5 °C/5 sec	60 °C to 95°C	1

3.6.7   Spiking of healthy donor blood with cell line cells

MCF-7 cells were cultured as described in section 3.1.2. After detachment of cells by trypsin, cells were centrifuged at 190 g for 5 minutes and supernatant was discarded. Cells were then resuspended in fresh culture medium and pipetted into a petri dish for better separation and visualization of cells. Using light microscopy, cells were counted during uptake with pipette and a 10 µL pipette tip, and cells were collected until the

desired number was reached. PBMCs were isolated by collection of 7.5 mL healthy donor blood in EDTA tubes and subsequent Ficoll density-gradient-based Leucosep™ pre-enrichment according to the manufacturer's instructions. A defined number of 300,000 PBMCs was used for spiking.

3.6.8 Tumor cell enrichment by the Parsortix® system

The Parsortix system is a device used for the enrichment of CTCs in a background of leukocytes from whole blood samples. It makes use of differences in size as well as rigidity of the two cell populations. Using a microfluidic cassette and constant liquid flow, the blood sample is passed through the cassette in which step-wise narrowing down of the gap is present. This is used to hold back those cells exceeding a critical size of 6.5 μm and letting cells of smaller sizes pass through the gap. Cells that were able to pass through the gap are discarded, whereas larger cells are flushed out by the system by application of reverse flow. Cells which were flushed out remain intact and suitable for down-stream analyses such as immunofluorescence staining and were harvested by collecting the cell suspension in a cytospin funnel and subsequent centrifugation onto a glass slide at 190 g for 3 min. Slides were dried overnight and frozen at -80 °C.

3.6.9 Immunofluorescence staining

After processing of blood samples with the Parsortix® system and drying of the cytospin slides, slides were thawed at room temperature for subsequent immunofluorescence staining. Fixation of the cells was performed with 2% PFA (10 min) before washing with PBS and permeabilization with 0.1% Triton X-100 in PBS (10 min). Slides were washed twice with PBS and blocking of unspecific binding sites was performed with 10% AB-serum/PBS for 20 min. Pan-keratin antibodies (AE1/AE3 and C11; directly labeled with Alexa Fluor 488, 1:100) and CD45 antibody (clone REA747; directly labeled with APC, 1:50) in blocking solution were used for identification of tumor cells and leukocytes, respectively. After incubation for 1 h, DAPI staining solution (1 μg/ml) was added for an additional 5 min. Using Prolong Gold Antifade Reagent, slides were covered with a cover slip, sealed and stored at 4 °C until imaging.

3.6.10 Image analysis using the XCyto 10 automated scanning microscope

The XCyto 10 Quantitative Cell Imager was used for scanning of slides which contain 300,000 PBMCs spiked with 1000 MCF-7 cells. The slides have previously stained by immunofluorescence using AF488-labeled pan-keratin and APC-labeled CD-45 antibodies. The XCyto 10 is equipped with a CCD 2.8 MP camera, four LEDs and 9 emission

filters and can be optimized for the semi-automated detection of cells in suspension or adherent cells and was used here in order to develop a tool for the detection of CTCs. By applying acquisition times of 100 ms for DAPI, and 500 ms for Alexa Fluor 488 and APC fluorophores, as well as the default 4x objective, whole slides were scanned by sequential imaging of 68 images per slide. For this, the combinations of excitation light sources and emission filters LED405/430-475 nm (DAPI), LED488/513-555 nm (AF488) and LED635/665-676 nm (APC) were utilized. Prior to image scanning, pre-settings of "Xcyto 2-Sample 15-A v1" slide type and "Adherent, User defined – Fluorescence Mask" method for cell nucleus identification were applied in the XcytoView software. Threshold intensities of the DAPI input channel of 10,000 as well as a max area of 900 μm^2 of DAPI signal were set. APC intensities were plotted against intensities in the AF488 channel in order to be able to distinguish between pan-keratin tumor cells and CD45-positive PBMCs. By applying bi-exponential scaling for better visualization, it was possible to separate both cell populations by establishment of a gate around the tumor cells. The gating parameters were saved and re-applied to images of patients samples in order to evaluate the feasibility of establishing an automated scanning system. Positive hits can be subsequently analyzed by re-imaging using 20x objective to further improve detection.

3.7   Statistical analyses

True biological differences, e.g. functional behavior of two cell lines, can only be evaluated by using statistical testing. According to the study conducted, different tests were applied using R software. For unpaired samples, in general normal distributed samples were analyzed using t-testing. For non-normal distributed samples, wilcoxon-rank-sum was applied. If samples were paired, student's paired t-test for normal distributions and wilcoxon-signed rank test for non-normal distributions were used. An alpha level of 5 percent was used. Therefore, null-hypotheses were rejected only if p-values reached significance levels <0.05. All experiments were performed using at least three independent biological replicates, unless otherwise indicated. Statistical analysis of miRNA NGS are described in section 3.6.5.

4 Results

Previous studies conducted at the Institute of Tumor Biology, UKE, have shown a significant association between loss of chromosomal region 4q12-q32 and early tumor cell dissemination as well as poor prognosis. In a study by Wrage *et al.* it was shown that NSCLC patients with a positive DTC status more often harbor a loss of 4q in their primary tumors [105]. Within this region, HERC5 was identified as a potential target metastasis suppressor gene [99, 106]. Therefore, functional characterization was performed in order to further elucidate the observed phenotype and metastatic potential in cell culture based studies.

4.1 HERC5 expression levels in NSCLC cell lines

In order to investigate whether HERC5 is biologically working as a metastasis suppressor gene, *in vitro* systems have to be generated. Cell lines bearing low expression levels were designated for the establishment of overexpression models, while intermediate or high levels should be used as a knock-out (KO) system. For this, different NSCLC cell lines were screened for their HERC5 expression level (see Figure 8). mRNA expression was normalized against immortalized lung epithelial cell line BEAS2B. Protein expression was also analyzed in a subset of these cell lines by Western blot. HSC70 protein was used as loading control.

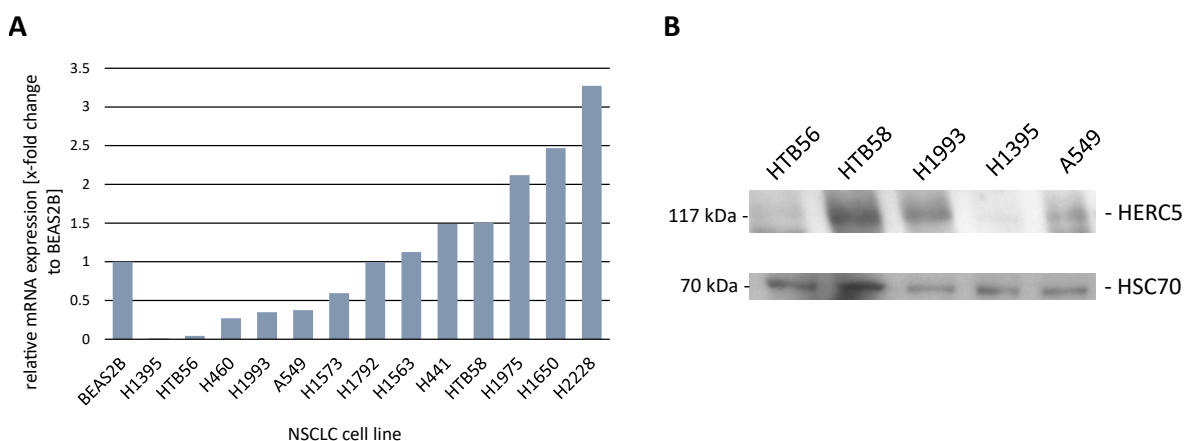**Figure 8:** *HERC5* **mRNA expression levels in different NSCLC cell lines.** Expression was measured by RT-qPCR and normalized first to *RPLP0* gene and subsequently to BEAS2B cell line. **A)** Relative expression levels are shown here as fold-change values in comparison to immortalized BEAS2B lung epithelial cell line. **B)** HERC5 protein levels in a subset of different NSCLC cell lines analyzed by Western blot.

4.2   Establishment of HERC5 KO and overexpression cell lines

Based on HERC5 mRNA and protein expression levels in section 4.1, different cell lines were chosen which served as model systems in the following experiments. Due to its low HERC5 expression, H1395 cell line was chosen as an overexpression model. In addition to the generation of a novel overexpression cell line, HTB56 HERC5 OE and HTB56 empty vector control (EC) cell lines had already been completed by Dr. Annkathrin Hanssen. A549 cells is an already well-described cell line frequently used in the context of NSCLC research. Furthermore, A549 cells were shown to have an intermediate level of HERC5 and were therefore chosen for the establishment of an additional KO system. After transfection with CRISPR-Cas9 plasmids, different A549 HERC5 KO clones had previously been raised by Dr. Annkathrin Hanssen but not yet validated for sequence integrity.

4.2.1   HTB56 HERC5 OE and H1395 HERC5 OE

HTB56 HERC5 OE and EC cell lines had been previously established by lentiviral transduction with LEGO-iG2-HERC5-HA or LEGO-iG2-HA, respectively. The vector backbone also contains an IRES-coupled GFP sequence so that by FACS analysis, GFP-positive, successfully transduced cells can be separated from untransduced cells. Both cell lines were subsequently screened for HERC5 expression. Differences in HERC5 expression levels were assessed by RT-qPCR in two independent replicates as well as Western blot by detection with HA- and HERC5 antibodies (see Figure 9). Compared to HTB56 EC cells, *HERC5* mRNA expression is upregulated 280-fold (SD=135) in HTB56 OE cells. Western blots show a strong upregulation of HERC5 protein as well.

Figure 9: *HERC5* mRNA expression levels in modified HTB56 cell lines.
Expression was measured by RT-qPCR and normalized to *RPLP0* gene.
A) Fold-change expression levels relative to empty vector control cells
(n=2). **B)** HERC5 protein levels analyzed by Western blot using anti-HA
antibody (left) and anti-HERC5 antibody (right).

H1395 cell line was transduced with LEGO-iG2-HERC5-HA or LEGO-iG2-HA in order to generate a second overexpression cell line with its corresponding empty vector control. After FACSing and therefore selection of GFP positive, successfully transduced cells, newly established cell lines H1395 HERC5 OE and H1395 EC were analyzed for HERC5 mRNA as well as protein expression (see Figure 10). RT-qPCR results show a 283-fold upregulation in HERC5 OE cells compared to EC cells, and Western blot analyses with HA and HERC5 antibodies support these results.
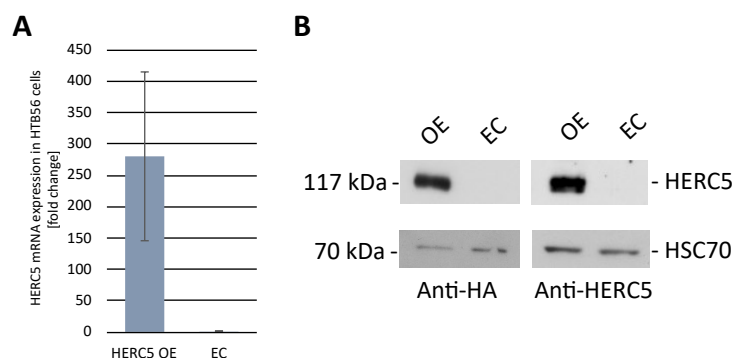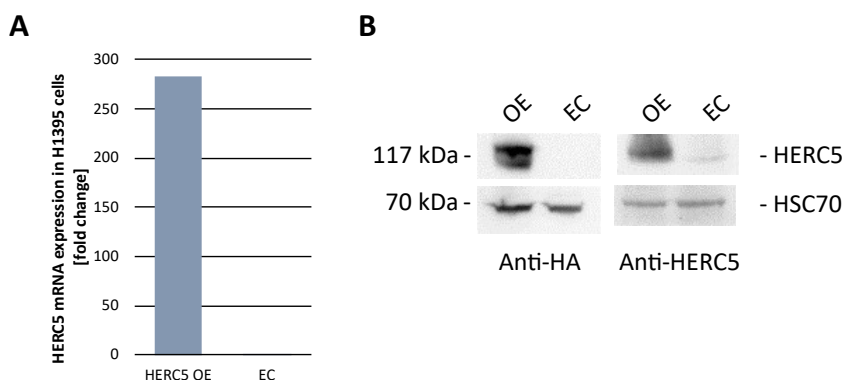

Figure 10: *HERC5* mRNA expression levels in modified H1395 cell lines. Expression was measured by RT-qPCR and normalized to *RPLP0* gene. **A)** Fold-change expression levels relative to empty vector control cells (n=1). **B)** HERC5 protein levels analyzed by Western blot using anti-HA antibody (left) and anti-HERC5 antibody (right). HSC70 served as loading control.

4.2.2   A549 HERC5 KO

By using CRISPR-Cas9 technology, total knock out of genes can be achieved if the induced double-strand break results in a frameshift mutation or premature stop codon formation [115]. Several A549 KO clones pre-established by Dr. Annkathrin Hanssen were analyzed for their sequence integrity to see whether transfection has resulted in knocking out *HERC5* gene completely. For this, gDNA was extracted from seven different clones and PCRs using Crisp #5 primers were performed. Subsequently, DNA was applied on agarose gels for visualization of product sizes (see Figure 11) and extracted from the gels. For unmodified sequences, the expected amplicon length is 138 bp. The purified PCR products were sequenced and analyzed with BLAST algorithm (see Table 21).
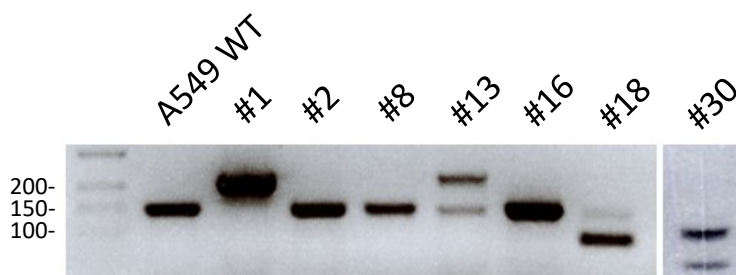
Figure 11: PCR analysis of different *HERC5* KO clones. After gDNA extraction, PCRs using Crisp #5 primers show expected bands of 138 bp for A549 par cells. *HERC5* KO clones show bands of various lengths.

Table 21: Sequence analysis of KO clone by BLAST algorithm

Clone	Induced mutation
#1	65 bp insertion
#2	2 bp deletion
#8	3 bp deletion
#13	lower band: 2 bp deletion, upper band: 78 bp insertion
#16	1 bp deletion
#18	52 bp deletion
#30	lower band: 26 bp deletion, upper band: 85 bp deletion

Due to the results of the sequencing reaction, clones harboring deletions that either do not result in frameshift mutations of *HERC5* gene or insertions that could lead to unclear gain of function were not considered suitable. Clones #2, #16, #18 and #30 were chosen for generation of a KO cell line since the mutations contain a genotype resulting in *HERC5* KO. In order to create a cell line that is more genetically heterogenous compared to a cell line stemming from a single clone and to furthermore reduce the influence of possible off-target effects, these four aforementioned clones were combined.

HERC5 KO on protein level was subsequently confirmed by Western blot (Figure 12A). A549 KO cells do not show any morphological differences compared to A549 par cells (Figure 12B). In order for a single clone not to overgrow the heterogenous cell population, average population doubling times of each clone were assessed by MTT measurements. Doubling times were highly similar (Figure 12C).
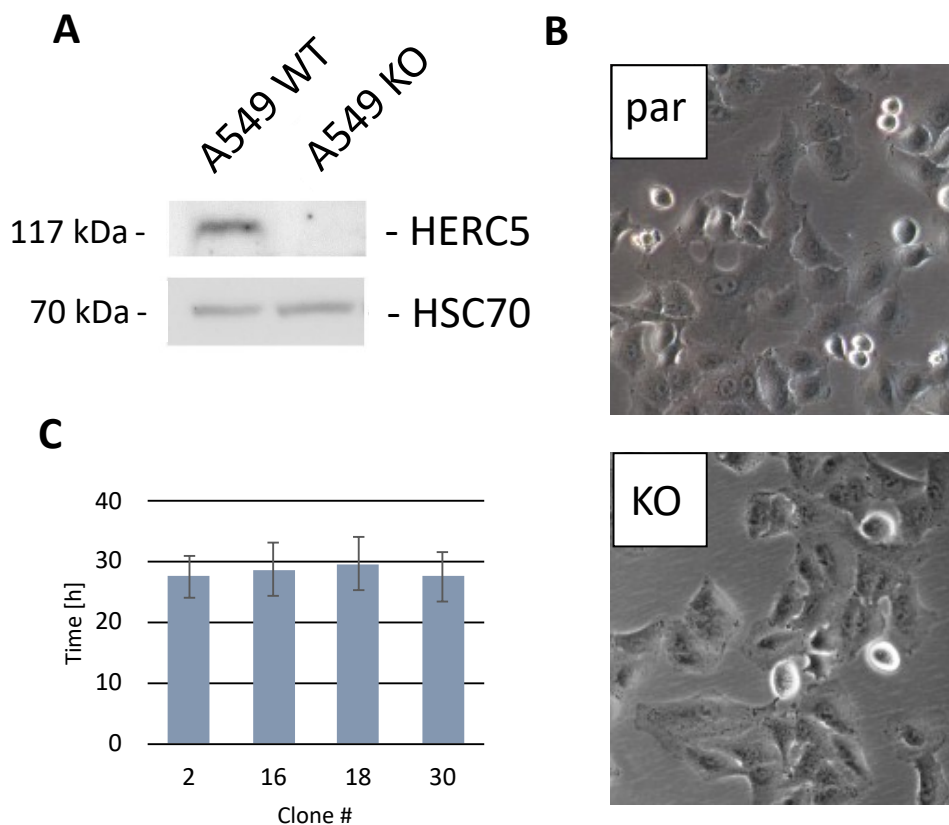
Figure 12: Analysis of A549 KO cell line. A) HERC5 protein levels analyzed by Western blot using anti-HERC5 antibody. **B)** Light microscopy images showing no morphological differences between parental (left) and KO (right) cells. **C)** Doubling times [h] of different knock out clones assessed by MTT analysis.

4.3 Functional analysis of differential HERC5 expression

After having successfully established different *in vitro* model systems, phenotypical alterations deriving from differential HERC5 expression levels in NSCLC cell lines were further investigated. Functional assays focusing on their connection to cancer and metastasis formation were hence performed using the different cell lines.

4.3.1 Proliferation capability

The ability of cells to undergo unlimited division is considered one hallmark of cancer [2]. In order to analyze a possible differential behavior in proliferative capacity an MTT assay was performed using HTB56 HERC5 OE/EC, H1395 HERC5 OE/EC and A549 KO/par cell lines. After seeding the cells, measurements were taken at days 0, 3, 5 and 7 (HTB56 and H1395) or at days 0, 3, 4 and 5 (A549). End point analysis of growth curves were compared by student's t-test but no statistical differences were observed in any of the cell lines (HTB56: $p=0.16$, H1395: $p=0.22$, A549: $p=0.64$; Figure 13). Thus, HERC5 did not influence the basal proliferation capacity of any of the different cell lines.
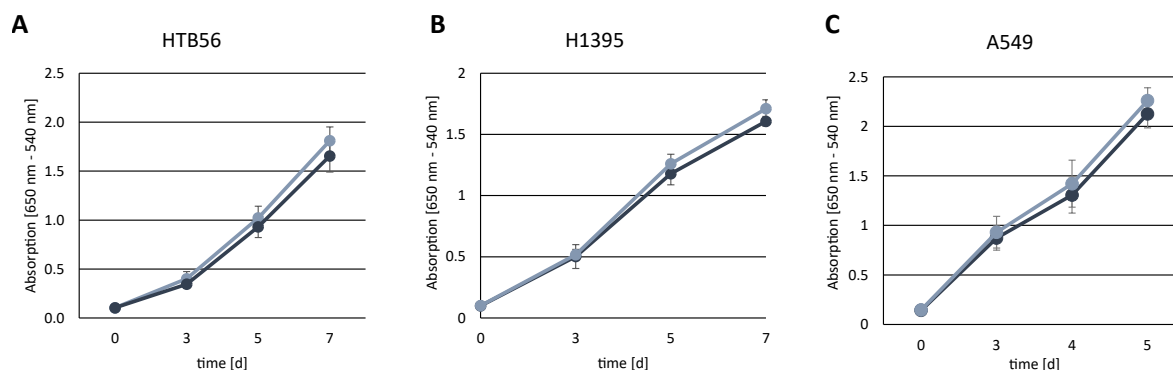
Figure 13: Analysis of proliferative capability by MTT assay. 1000 cells were seeded in 96-well plates, stained and detected after days indicated. Absorption [650 nm - 540 nm] was plotted against time and growth curves were compared. Standard deviations are indicated by error bars. **A)** HTB56 cell lines ($p=0.16$, $n=5$), light blue: EC; dark blue: OE **B)** H1395 cell lines ($p=0.22$, $n=3$), light blue: EC; dark blue: OE **C)** A549 cell lines ($p=0.64$, $n=3$), light blue: par; dark blue: KO

4.3.2   Clonogenic capacity

The capacity of single cells to grow into colonies can be examined in order to analyze the potential of metastasis formation from detached tumor cells [2]. For this, colony assays were performed. Using ColonyArea plugin for ImageJ, percentages of area covered in each well were calculated and compared by t-testing. HTB56 OE cells show a significantly lower clonogenic growth (mean: 3.3 ± 0.2) compared to EC cells (mean: 1.3 ± 0.5; p=0.0004, n=5, Figure 14 (left)) . Boxplots depict ranges of areas covered by the cells and exemplary images from the stained wells are shown above. The modified cell line A549 did not show any significant differences in clonogenic potential (A549 par: 10.0 ± 1.2, A549 KO: 8.6 ± 0.9; p=0.07 , n=5, Figure 14 (right)). Even though not significant, parental cells show a slightly increased clonogenic growth compared to KO cells. When using H1395 cells, hardly any colonies grew and were therefore not analyzed.
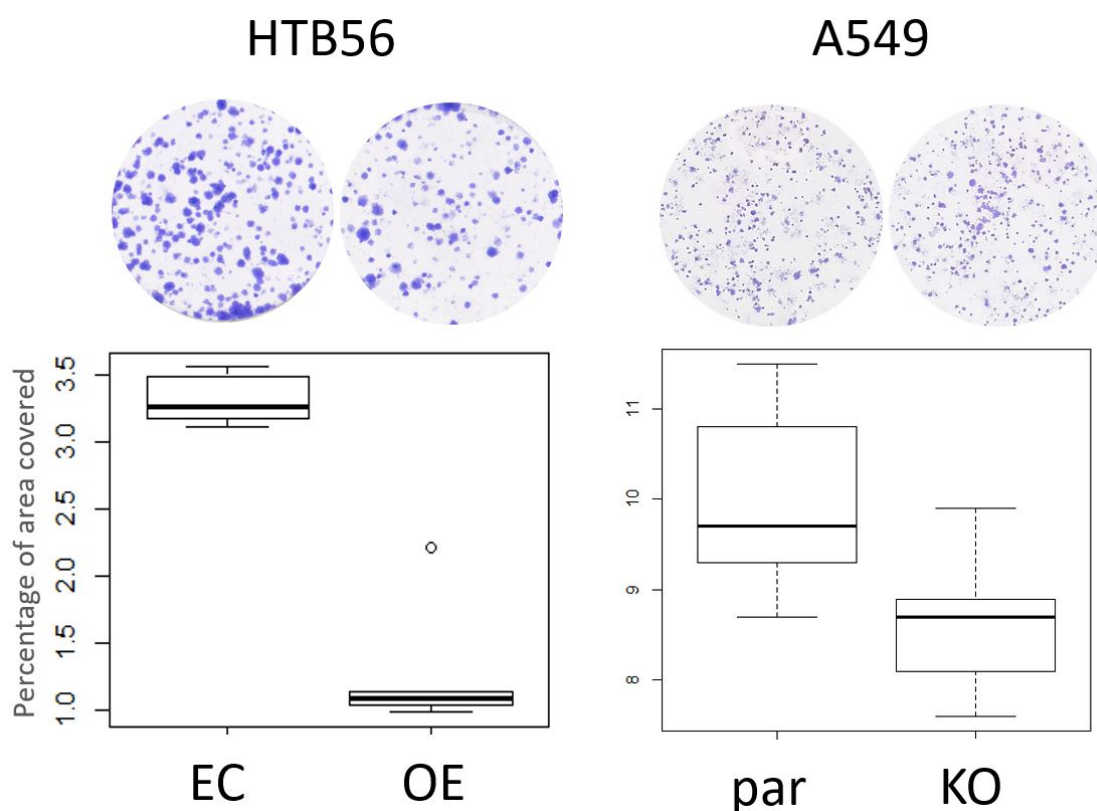
Figure 14: Clonogenic capacity of modified HTB56 and A549 cells. 1000 cells were seeded in 6-well plates, stained and detected after 7 days using ColonyArea plugin for ImageJ. Percentages of area covered are represented by boxplots. Statistical testing was performed by t-testing (HTB56: p=0.0004, n=5; A549: p=0.069 , n=5).

4.3.3   Anchorage-independent growth

By performing soft agar assays, assessment of growth under anchorage independent conditions was performed as it is described as a hallmark of carcinogenesis [2]. For this, 3000 cells were seeded in 6-well plates and analyzed 14 days after seeding using Cell Colony Edge macro for ImageJ. In comparison to EC cells, significantly less colonies were grown in HTB56 HERC5 OE cells (mean EC: 262 ± 70, OE: 143 ± 30; p=0.008; n=5, Figure 15) independently of a solid surface; indicating a less aggressive phenotype, whereas A549 KO/par cell lines did not show any significant differences (A549 par: 1527 ± 465, A549 KO: 1342 ± 391; p=0.52, n=5). Details of the stained colonies can be seen above the boxplots. Analysis of differential growth in H1395 cell lines was not possible since no colonies were formed in soft agar.
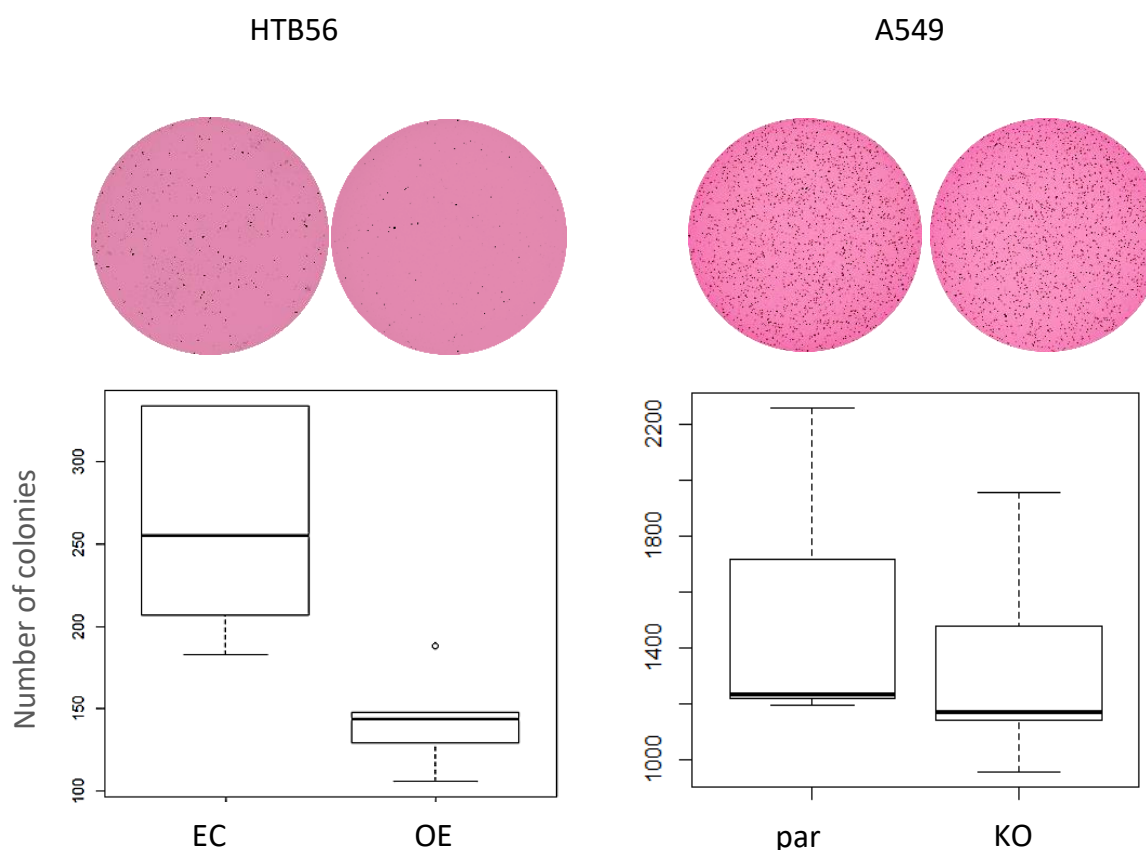
Figure 15: Anchorage-independent growth of modified HTB56 and A459 cells. Detection was performed by Cell Colony Edge macro for ImageJ 14 days after seeding of 3000 single cells. Number of colonies exceeding pre-defined parameters were counted and plotted. Statistical testing was performed by t-testing (HTB56: p=0.008; n=5, A549: p=0.52, n=5).

4.3.4   Migratory capability

The ability to directionally migrate towards different chemo-attractants is often studied in the context of cancer as it correlates with spreading to distant sites and therefore with metastatic progression [2]. This chemotactical behavior was examined by using boyden-chambers. Here, 20,000 cells were seeded in FCS-deprived media, while the bottom of the wells contained FCS as chemoattractant. Migrated cells were then stained and counted.

Applying Wilcoxon rank-sum test, HTB56 OE cells have a significantly lower migratory capability than the corresponding EC cells (mean EC: 1678 ± 338, OE: 785 ± 186; p=0.012, n=5, Figure 16 (left)). A549 parental cells also have a significantly lower migratory capability than HERC5 KO cells (mean par: 723 ± 249, KO: 1639 ± 824; p=0.0012, n=7, Figure 16 (right)). Exemplary sections of the membranes are illustrated above the boxplots. When using H1395 cells, no migrated cells were found in the FCS controls.
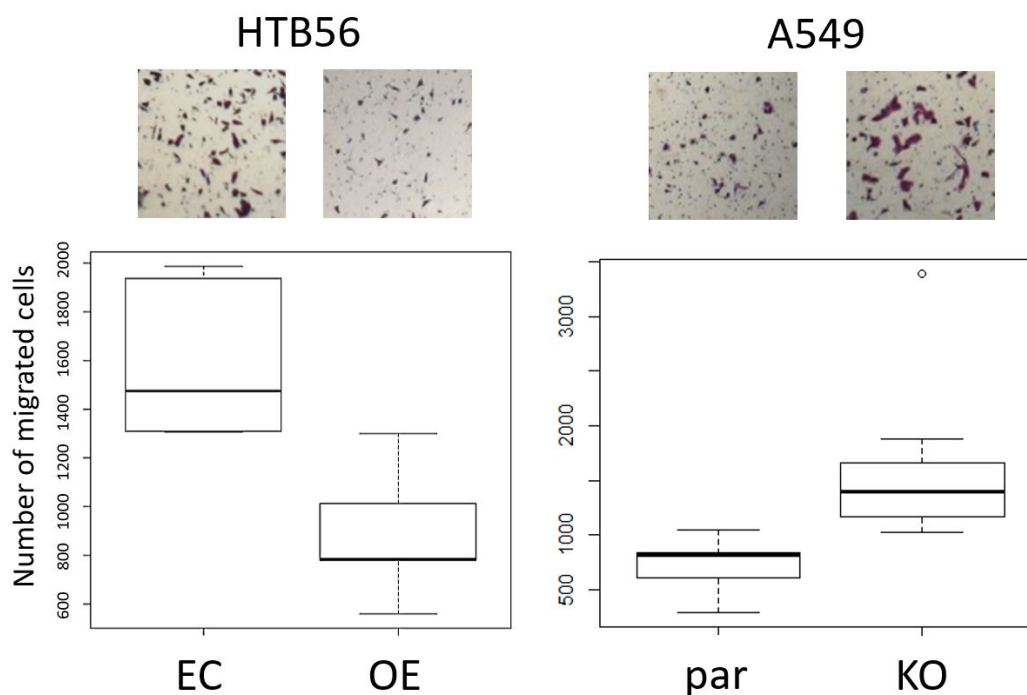
Figure 16: Migratory capability of modified HTB56 and A549 cells. By using boyden-chambers, migratory capabilities were assessed after seeding 20,000 cells and staining of those which migrated to the bottom of the membrane after 16 h. HTB56 EC cells show an enhanced migration (p=0.012, n=5) compared to OE cells. A549 KO cells also have an enhanced migratory potential (p=0.0012, n=7).

4.3.5   Invasive potential

Apart from being able to migrate, in order for cancer cells to successfully extravasate to distant organs, they have to overcome natural barriers and invade through extracellular matrices [2]. Boyden-chambers covered with matrigel mimic the extracellular matrix and are therefore suitable for the assessment of invasive potential. Here, 20,000 cells were seeded into the matrigel-covered chambers under FCS-free conditions. First invasion and then migration through the pores was observed due to chemo-attractant FCS in the wells. Cells were stained and counted afterwards in the same way as in migration assays.

Both HTB56 OE/EC and A549 KO/par cell lines did not show any significant differences in invasive potential when applying Wilcoxon rank-sum test, even though a trend is visible for A549 cells (HTB56: EC mean: 1303 ± 941, OE: 1211 ± 810; p=1.00, n=3; A549: par mean: 355 ± 285, KO: 687 ± 365; p=0.34, n=4; Figure 17). Due to the negative results for H1395 cells when analyzing anchorage-independent growth and migratory capacity, it was assumed that this rather non-aggressive cell line is not suitable for the assessment of invasive potential.
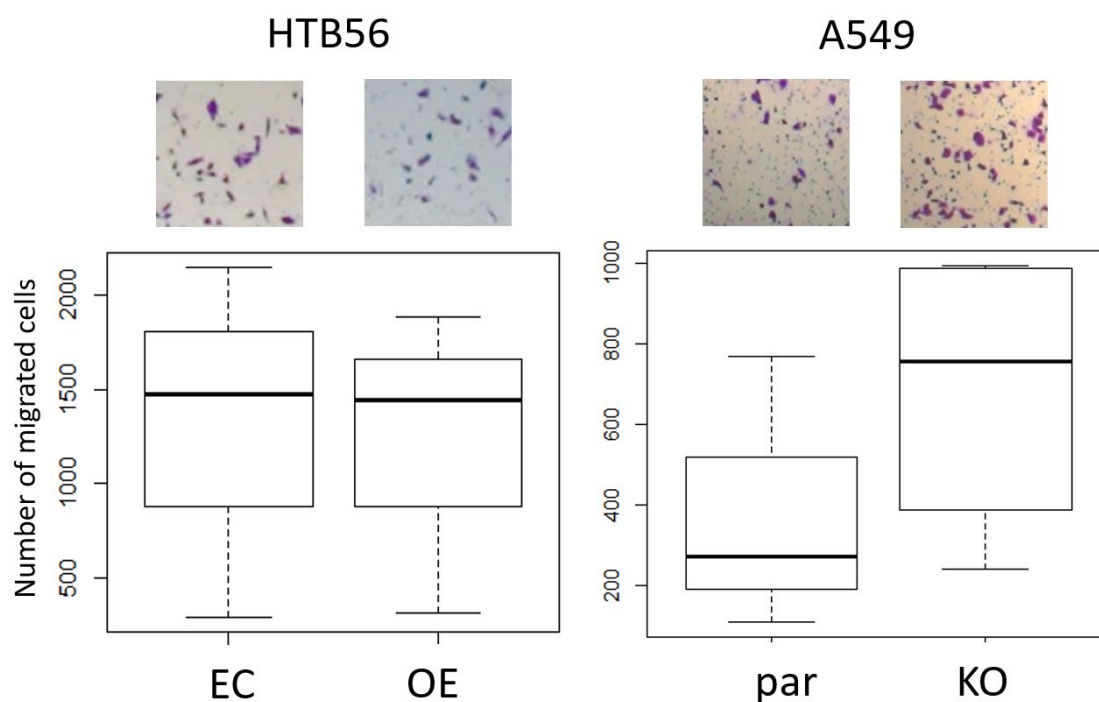
Figure 17: Invasive potential of modified HTB56 and A549 cells. 20,000 cells were seeded into matrigel-covered boyden-chambers and analyzed after 22 h. Neither HTB56 (p=1.00, n=3) nor A549 (p=0.34, n=4) modified cell lines showed differences in invasive potential.

4.4   Interaction with brain and bone microenvironment

Previous analyses by Wrage *et al.* had shown a specific effect of HERC5 loss on brain metastasis formation as well as a positive DTC status [99], therefore a possible influence of the brain or bone microenvironment on the cellular behavior of the tumor model cell lines was assessed. The aforementioned assays were thus adjusted to examine a possible influence of the brain or bone microenvironment on cancer-related phenotypes induced either by primary human astrocytes or immortalized murine pre-osteoblasts (MC3T3-E1).

4.4.1   Proliferation capability

Despite not having found any significant differences in proliferative capability of cells, MTT assays were repeated by incubating the cells in conditioned media from either astrocytes or murine osteoblasts to examine a possible influence of the brain or bone microenvironment on the proliferative behavior. After 0, 3, 5 and 7 (HTB56) or 0, 3, 4 and 5 (A549) days, measurements of absorption were taken. End point analysis of growth curves were compared by student's t-test but no statistical differences were observed in any of the cell lines (HTB56 astrocytes: p=0.81 , HTB56 MC3T3-E1: p=0.48, A549 astrocytes: p=0.59, A549 MC3T3-E1 p=0.48; Figure 18). Standard deviations are indicated by error bars. Thus, proliferation was not altered in any of the cell lines under brain or bone microenvironment. HTB56 and A549 show a slightly increased proliferation capability in astrocyte media compared to their standard growth media, which might be due to the elevated levels of FCS present in astrocyte media. In MC3T3-E1 media, however, growth is slightly decreased in HTB56 and even stronger in A549 cells compared to standard conditions possibly due to insufficient growth factors. Growth curves furthermore did not show strong variations between conditioned and standard media for the respective astrocytes or osteoblasts.

A

B
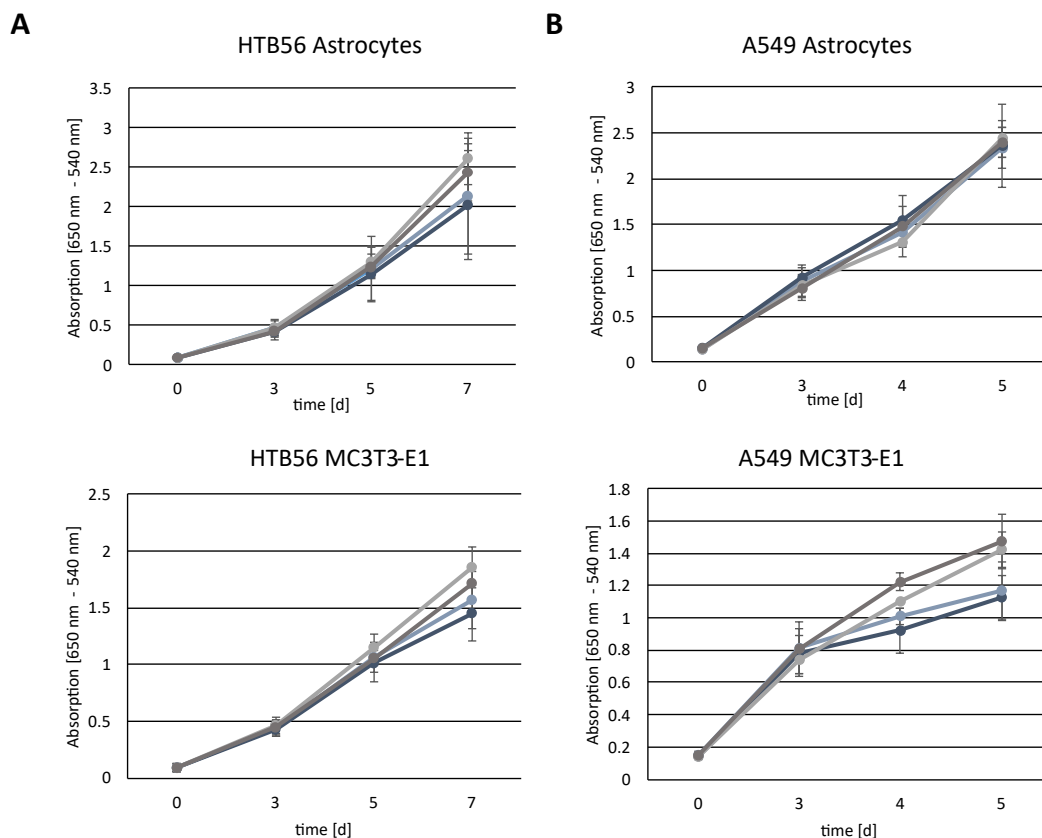
Figure 18: Influence of astrocytes or MC3T3-E1 cells on proliferation capability of modified HTB56 and A549 cells. 1000 single cells were seeded into 96-well plates with either MC3T3-E1 or astrocyte conditioned media for days indicated. Absorption [650 nm - 540 nm] was plotted against time and growth curves were compared by t-testing of absorption at end-points. **A)** Growth of HTB56 cell lines under brain (above) or bone (below) microenvironments (HTB56 astrocytes: p=0.81, HTB56 MC3T3-E1: p=0.48; n=5) (light blue: EC; dark blue: OE). Growth curves in light gray and dark gray represent growth in standard MC3T3-E1 media for EC and OE, respectively. **B)** Growth curves of A549 cell lines (A549 astrocytes: p=0.59, A549 MC3T3-E1 p=0.48; n=3) (light blue: par; dark blue: KO). Growth curves in light gray and dark gray represent growth in standard astrocyte media for par and KO, respectively.

4.4.2   Clonogenic capacity

Similar to MTT assay set up, clonogenic potential was assessed by incubation of the cell lines using conditioned media. After incubation of 3000 single cells in the respective conditioned media and analysis with ColonyArea plugin for ImageJ, the difference in clonogenic growth is not increased by the brain and bone microenvironment HTB56 (MC3T3-E1: EC mean: 4.8 ± 1.0, OE mean: 2.7 ± 1.2; p=0.08, n=3; astrocytes:

EC mean: 0.5 ± 0.4, OE mean: 0.3 ± 0.3; p=0.42, n=4), A549 (MC3T3-E1: par mean: 14.9 ± 2.6, KO mean: 12.6 ± 1.0; p=0.10, n=5; astrocytes: par mean: 11.6 ± 1.8, KO mean: 10.5 ± 2.2; p=0.40, n=5; see Figure 19). In comparison to standard conditions, HTB56 EC and OE cells grew less colonies in astrocyte conditioned media but more colonies in MC3T3-E1 media. A549 par and KO cells also showed an increase in colonies in MC3T3-E1 conditioned media, while in astrocyte conditioned media results remained similar. The increase of colony outgrowth in MC3T3-E1 conditioned media in both cell lines is already observable when using MC3T3-E1 standard media (data not shown) but is even more prominent in conditioned media, hinting at a possible influence of pre-osteoblast microenvironment on clonogenic outgrowth capacity. Clonogenic capacity with conditioned media in H1395 cells was not assessed due to the non-aggressive nature of these cells.
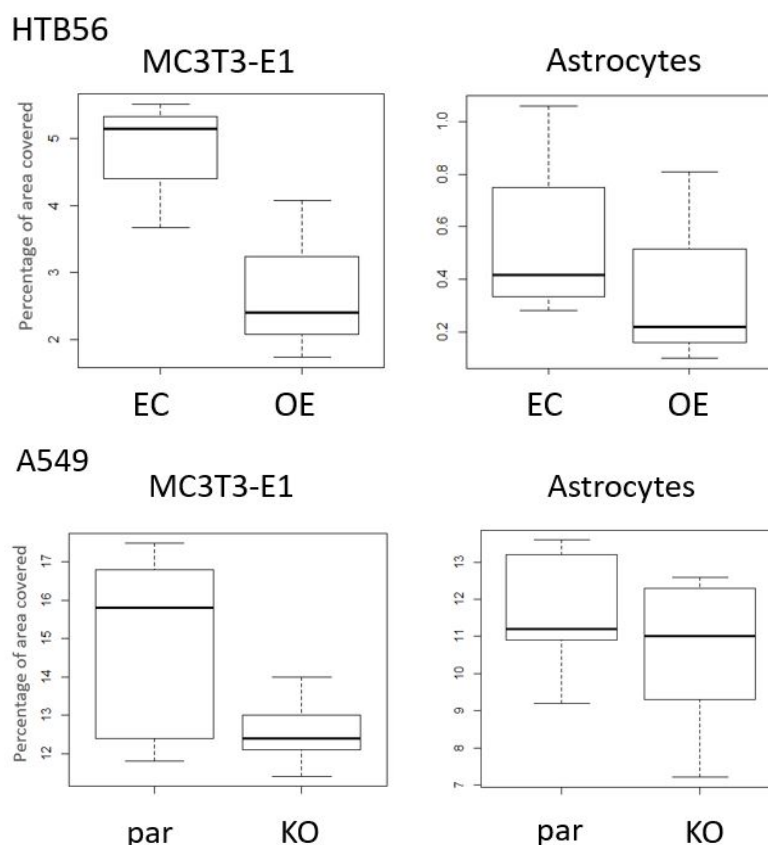
Figure 19: Influence of MC3T3-E1 cells or astrocytes on clonogenic capacity of modified HTB56 and A549 cells. 3000 single cells were seeded into 6-well plates with either MC3T3-E1 or astrocyte conditioned media for 7 days. Calculation of areas covered in the wells was done by using ColonyArea plugin for ImageJ. Neither HTB56 (MC3T3-E1: p=0.08, n=3; astrocytes: p=0.42, n=4) nor A549 (MC3T3-E1: p=0.10, n=5; astrocytes: p=0.40, n=5) modified cell lines showed differences in clonogenic capacity (t-test).

4.4.3 Anchorage-independent growth

During the set-up of the assay, agar has to be heated until dissolved in order to pour the different agar layers. This might lead to destruction of e.g. heat-sensitive cytokines secreted by the cells into the media. Furthermore, the amount of media subsequently added for prevention of drying of the agar is rather low. Therefore, soft-agar assays are not suitable for assessment of anchorage-independent growth with different conditioned media and were hence not performed here.

4.4.4 Migratory capability

For the assessment of migratory potential, either 100,000 astrocytes or osteoblasts were grown in the wells below the boyden-chambers instead of using FCS as chemoattractant. Here, only cell lines HTB56 and A549 were used, since H1395 cell lines did not show any migration when using an FCS controls. However, brain or bone microenvironments do not result in significant differences in migration in HTB56 (MC3T3-E1: EC mean: 848 ± 365, OE: 1003 ± 794; p=0.84, n=5; astrocytes: EC mean: 1125 ± 374, OE: 1191 ± 765; p=1.00, n=5) or A549 cells (MC3T3-E1: par mean: 809 ± 363, KO: 524 ± 567; p=0.40, n=3; astrocytes: par: 1903 ± 1486, KO: 1943 ± 1667; p=1.00, n=3; see Figure 20). Compared to FCS as a chemoattractant, HTB56 EC cells show a reduced migratory capacity, diminishing the difference between EC and OE cells in both pre-osteoblast and astrocyte microenvironments. A549 cells similarly show a decrease in migratory capacity in KO compared to par cells while overall migration was enhanced using astrocytes as a chemoattractant.
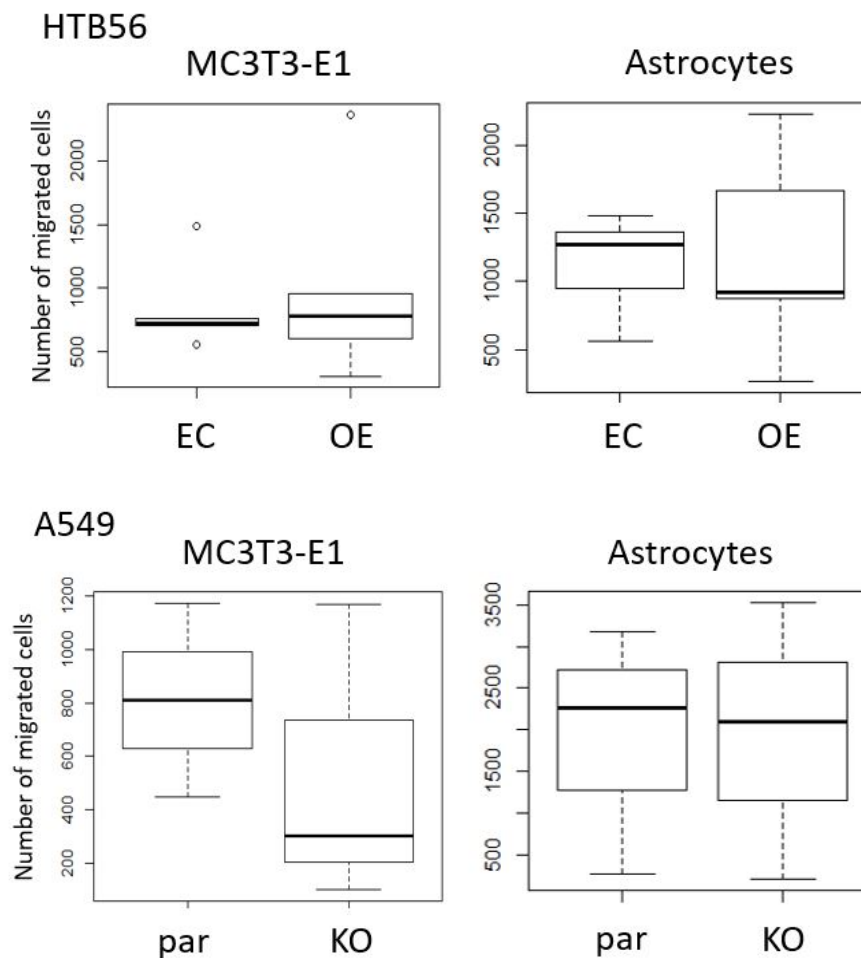
Figure 20: Migratory potential of modified HTB56 and A549 cells towards MC3T3-E1 cells or astrocytes. 20,000 cells were seeded into boyden-chambers with either 100,000 MC3T3-E1 or astrocytes below the chambers and analyzed after 16 h. Neither HTB56 (MC3T3-E1: p=0.84, n=5; astrocytes: p=1, n=5) nor A549 (MC3T3-E1: p=0.4, n=3; astrocytes: p=1, n=3) modified cell lines showed differences in migratory potential towards these cells.

4.4.5 Invasive potential

Since no migrated cells were found in the FCS controls of H1395 cell lines, migratory capacity was not assessed using astrocytes or pre-osteoblasts. As none of the cell lines showed a difference induced by astrocyte or pre-osteoblast environments in the previous studies, invasive capacity was not assessed.

4.5   RNAseq of HTB56-HERC5 OE/EC cell lines

In order to study potential alterations in downstream pathways resulting from HERC5 expression changes, which could explain phenotypical changes observed before, gene expression was assessed by RNAseq. For this, total mRNA of HTB56 HERC5 OE/EC cell lines were used from three independent biological replicates. After extraction, mRNA integrity was assessed by Tapestation measurements to ensure quality is suitable for subsequent downstream NGS analyses (Figure 21). RNA integrity numbers (RIN) were calculated which can range from 1 (completely degraded RNA) to 10 (highly intact RNA). During the measurements, separation by gel electrophoresis is used to visualize ribosomal proteins and their corresponding peak heights to calculate RIN scores. All of the 6 samples reached RIN scores between 9.9 - 10, indicating non-degraded RNA. NGS was performed by CeGaT, Tübingen, Germany. Fold changes of 2 and p-values<0.05 were considered significant. After correction for multiple testing, results show a significant upregulation of *HERC5* (control), *FGF7* and a significant downregulation of *COL12A1* (see Table 22). Due to the very low amount of differentially regulated mRNAs, the list of normalized counts was re-analyzed so that pathways possibly affected by differential HERC5 expression could be investigated nonetheless. For this, counts from the three replicates of each group were averaged and fold-change ratios of EC/OE were calculated. Genes were subsequently removed with less than ten counts in at least one of the groups and parameters for differential expression included fold-changes of <0.5 or >2. These parameters gave then rise to 303 identified mRNAs. Using DAVID database, functional annotation tool was used to look for enriched and functionally-related gene groups, but no significant cluster enrichment was found.
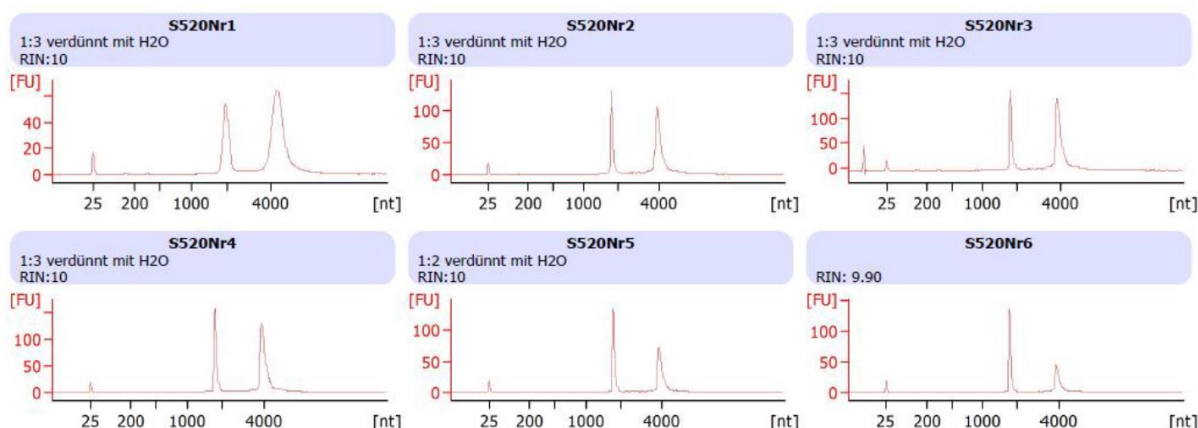
Figure 21: Assessment of RNA integrity. Samples designated for mRNA sequencing underwent quality control by Tapestation assessment of RIN scores. All samples reached scores between 9.9 - 10, confirming high quality and suitability for downstream NGS application.

Table 22: Significant RNAseq results of HTB56 HERC5 OE/EC cell lines

Gene	Fold change (OE/EC)	p-value (adj)
HERC5	44.12	2.34E-30
FGF7	3.96	0.0093
COL12A1	0.09	1.72E-08

A possible explanation for the low amount of significantly regulated genes could be that HERC5 might be predominantly regulated on the protein level rather than the mRNA level and is described to be only induced after viral infection or activation of the inflammasome.

4.6   Regulation of HERC5 expression by inflammatory cytokines

As previously stated, HERC5 has been mainly studied in the context of innate immunity. Its main function as an E3-ligase is conferring ubiquitin-like modifier (UBL) ISG15 to newly-synthesized proteins in a co-translational manner [82]. HERC5, as well as other proteins involved in ISGylation, have low basal expression levels, but are quickly upregulated during inflammation [78, 80, 81]. Due to the highly inflamed nature of the microenvironment in NSCLC primary tumors, we analyzed induction of HERC5 expression as well as ISGylation in different NSCLC cell lines under treatment with inflammatory cytokines IFNγ and TNFα over time by RT-qPCR and Western blotting. For this, A549 KO, A549 par, H1395, HTB56 and H1975 cell lines were used.

4.6.1   IFNγ-induced regulation of HERC5 expression

A549, H1975 and HTB56 cell lines were treated with 10 ng/mL IFNγ for 0 h, 24 h and 48 h to analyze *HERC5* levels under cytokine treatment (Figure 22). After normalization to *RPLP0* expression (ΔC_q) and 0 h of IFNγ stimulation ($\Delta\Delta C_q$), *HERC5* upregulation could be observed in three biological replicates (n=3) and all three cell lines after 24 h (Fold change values: A549: 1.6 ± 0.6, H1975: 1.6 ± 0.8, HTB56: 4.0 ± 1.5), with HTB56 showing the highest induction after 48 h (A549: 1.5 ± 0.3, H1975: 3.6 ± 1.9, HTB56: 17.4 ± 4.9). *IRF1* expression was examined to verify induction of canonical IFNγ pathways and confirmed successful stimulation.

Figure 22: mRNA analysis by RT-qPCR after IFNγ treatment. A549, H1975 and HTB56 par cell lines treated with 10 ng/mL IFNγ for 24 h (light blue) and 48 h (dark blue). *IRF1* indicates upregulation of IFNγ induced pathways. Expression was normalized to *RPLP0* and 0 h. Averaged values are shown from three biological replicates (n=3) with error bars depicting corresponding standard deviations.

To examine induction of HERC5 as well as overall ISGylation on protein level, A549 KO, A549 par, H1395 and HTB56 cell lines were used under the same conditions as mRNA analysis. Due to CRISPR-Cas9 induced deletions in the coding regions of *HERC5* gDNA, which was exploited for the establishment of A549 KO cell line, truncated *HERC5* mRNA is not suitable for analysis of expression level changes analyzed by RT-qPCR. However, protein levels were assessed by Western blotting of A549 KO cells to examine whether observed ISGylation is HERC5 dependent. Results were furthermore quantified from three independent replicates. Here, induction of ISGylation of proteins was most strongly observed in A549 par cells (24 h: 2.1 ± 1.2, 48 h: 3.5 ± 5.2; see Appendix) and slightly in H1395 cells (24 h: 2.0 ± 0.2, 48 h: 1.5 ± 0.9). While A549 KO cells do not show an upregulation of neither HERC5 (24 h: 1.4 ± 1.1, 48 h: 0.3 ± 0.3; Figure 23), nor ISGylation, induction of free, unconjugated ISG15 expression was observed indicating that HERC5 is responsible for the ISGylation of proteins in the corresponding A549 parental cells. In contrast to mRNA levels, neither ISGylation nor free ISG15 was observed in HTB56 cells under IFNγ stimulation (24 h: 0.9 ± 0.8, 48 h: 1.3 ± 0.5). Overall, HERC5 expression correlated with increasing ISG15 levels. Successful induction of canonical pathways by IFNγ was verified by upregulated pStat1 expression (Figure 23).

Figure 23: Protein analysis after IFNγ treatment. A549 KO, A549 par, H1395 par and HTB56 par cell lines treated with 10 ng/mL IFNγ for 0 h, 24 h and 48 h (n=3). Anti-ISG15 antibody detects ISGylated proteins as well as unconjugated ISG15. Anti-pStat1 indicates upregulation of IFNγ induced pathways. HSC70 serves as loading control.

Figure 24: Protein quantification after IFNγ treatment. A549 KO, A549 par, H1395 and HTB56 cell lines treated with 10 ng/mL IFNγ for 24 h (light blue) and 48 h (dark blue). Expression was normalized to 0 h (gray). Averaged values are shown from three biological replicates (n=3) with error bars depicting corresponding standard deviations.

4.6.2   TNFα-induced regulation of HERC5 expression
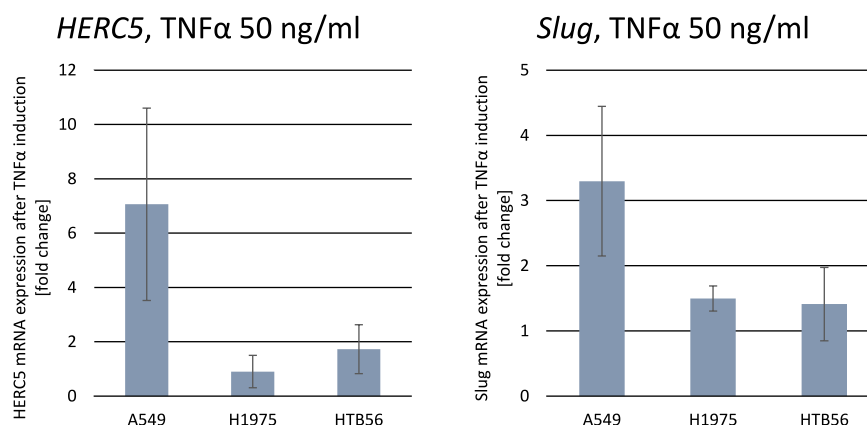
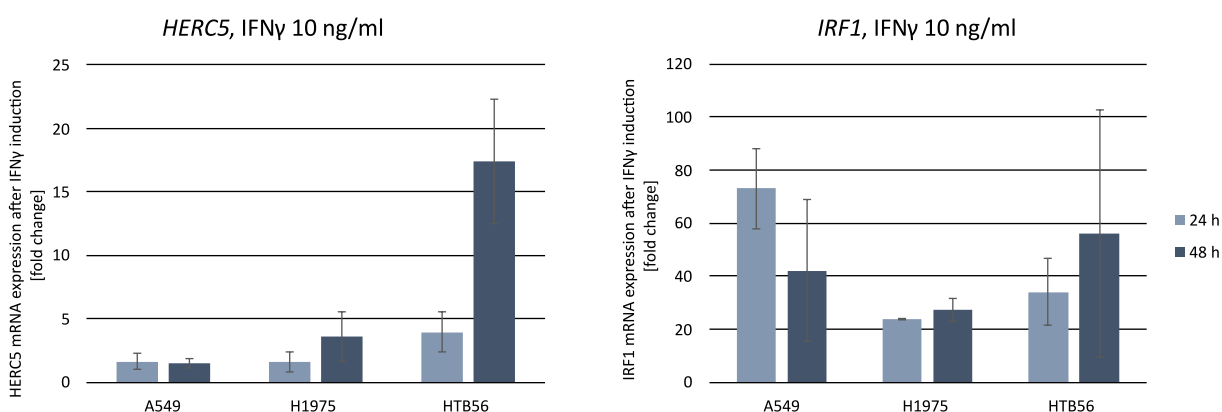**Figure 25: mRNA analysis by RT-qPCR after TNFα treatment.** A549, H1975 and HTB56 par cell lines treated with 50 ng/mL TNFα for 24 h. *Slug* indicates upregulation of TNFα induced pathways. Expression was normalized to *RPLP0* and 0 h. Averaged values are shown from three biological replicates (n=3) with error bars depicting corresponding standard deviations.

In order to analyze HERC5 expression and ISGylation under TNFα treatment, cells were incubated with 50 ng/mL TNFα for 0 h and 24 h. Using RT-qPCR to analyze mRNA expression, *HERC5* induction was assessed in cell lines A549, H1975 and HTB56 as well as *Slug* expression as a control of TNFα induction (Figure 25). Expression was normalized to *RPLP0* and no TNFα induction. *Slug* was induced in all three cell lines. *HERC5* expression levels were highest in A549 cells after 24 h, while H1975 and HTB56 showed little to moderate upregulation in comparison to lack of TNFα (A549: 7.1 ± 3.5, H1975: 0.9 ± 0.6, HTB56: 1.7 ± 0.9). Fold changes were calculated after averaging of three independent biological replicates.

Protein levels were analyzed by Western blots using A549 KO, A549 par, H1395 and HTB56 cell lines (Figure 26). ISGylation of proteins was most strongly induced in H1395 cells whereas the corresponding HERC5 expression remains hardly induced (24 h: 1.2 ± 1.6, 48 h: 2.0 ± 0.8; see Appendix). In A549 par cells, moderate upregulation of ISGylation was observed as well as strong HERC5 upregulation (24 h: 3.2 ± 3.5, 48 h: 4.3 ± 4.9). HERC5 expression, as well as ISGylation in A549 KO and HTB56 cells remain hardly affected (KO: 24 h: 2.2 ± 2.4, 48 h: 0.8 ± 1.4; HTB56: 24 h: 0.7 ± 0.4, 48 h: 0.0 ± 3.8). Induction of free ISG15, however, could be observed in A459 KO cells but hardly in parental cells, indicating transfer of newly synthesized ISG15 proteins to target proteins by HERC5, which is not visible in the KO cells.
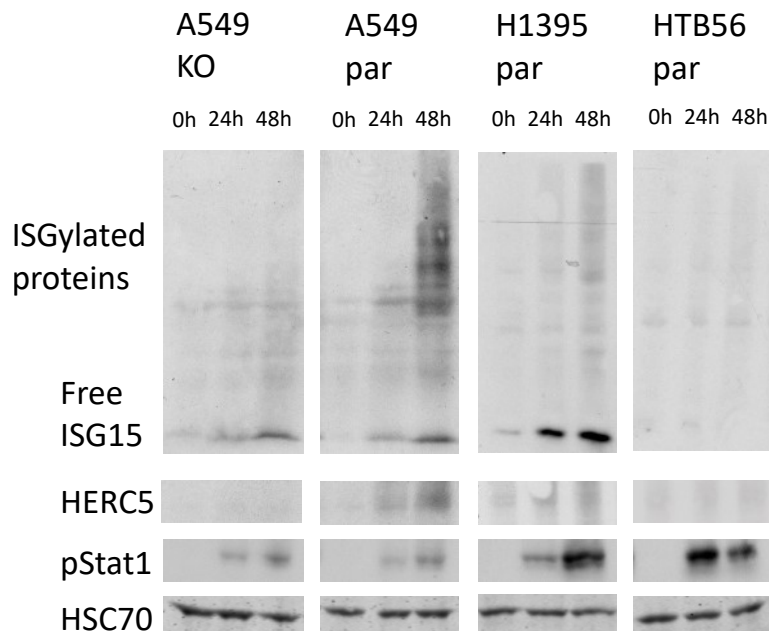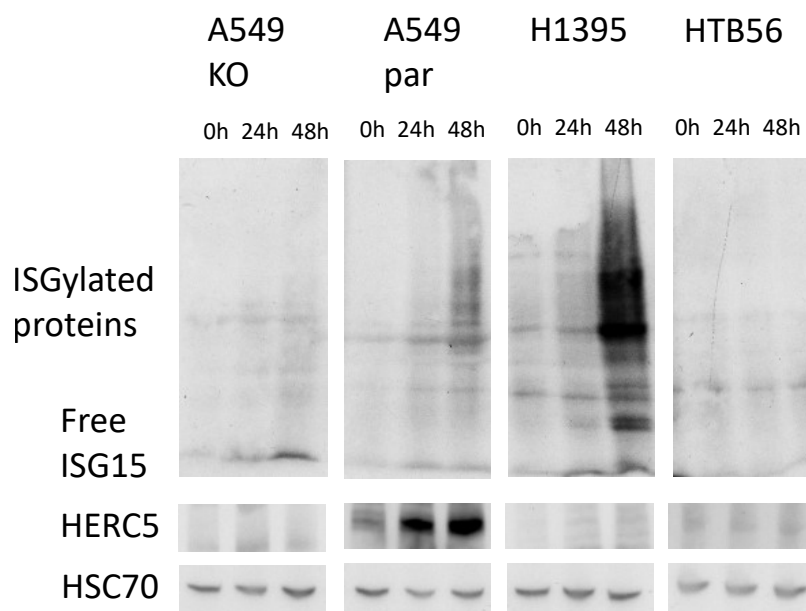

Figure 26: Protein analysis after TNFα treatment. A549 KO, A549 par, H1395 par and HTB56 par cell lines treated with 50 ng/mL TNFα for 0 h, 24 h and 48 h (n=3). Anti-ISG15 antibody detects ISGylated proteins as well as unconjugated ISG15. HSC70 serves as loading control.
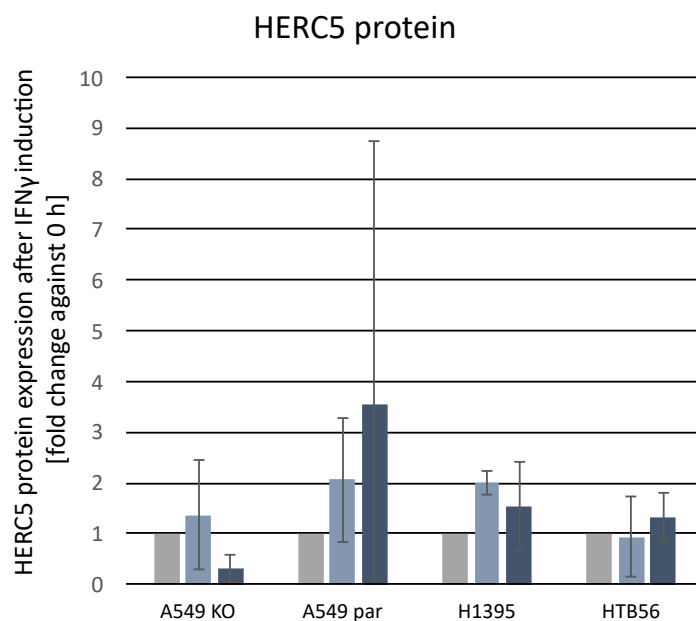
Figure 27: Protein quantification after TNFα treatment. A549 KO, A549 par, H1395 and HTB56 cell lines treated with 50 ng/mL TNFα for 24 h (light blue) and 48 h (dark blue). Expression was normalized to 0 h (gray). Averaged values are shown from three biological replicates (n=3) with error bars depicting corresponding standard deviations.

4.6.3 Regulation of HERC5 expression by combination of IFNγ and TNFα

Due to HERC5 and ISGylation induction observed in sections 4.6.1 and 4.6.2, a combination of both cytokines was performed since combining both cytokines is described to enhance their function in contrast to single use and has already been shown in A549 cells [116]. Whether this leads to enhanced HERC5 induction in NSCLC cell lines was analyzed first by RT-qPCR in A549, H1975 and HTB56 cells. Expression was normalized to *RPLP0* (ΔC_q) and no cytokine treatment ($\Delta\Delta C_q$). *Slug* and *IRF1* served for monitoring of successful TNFα and IFNγ induction. Both mRNAs were induced in all three cell lines but most strongly in A549. Similar to findings of TNFα induction, A549 cells showed the strongest overall *HERC5* expression, peaking at 24 h after induction but being still prominent after 48 h (fold changes after 24 h: 98.7 ± 44.2, 48 h: 29.4 ± 9.8). Sparse induction was observed in H1975 cells (24 h: 1.2 ± 0.6, 48 h: 2.1 ± 1.0), while HTB56 cells showed moderate induction (24 h: 2.5 ± 0.6, 48 h: 3.3 ± 0.4) (see Figure 28). Standard deviations are shown from three independent biological replicates.
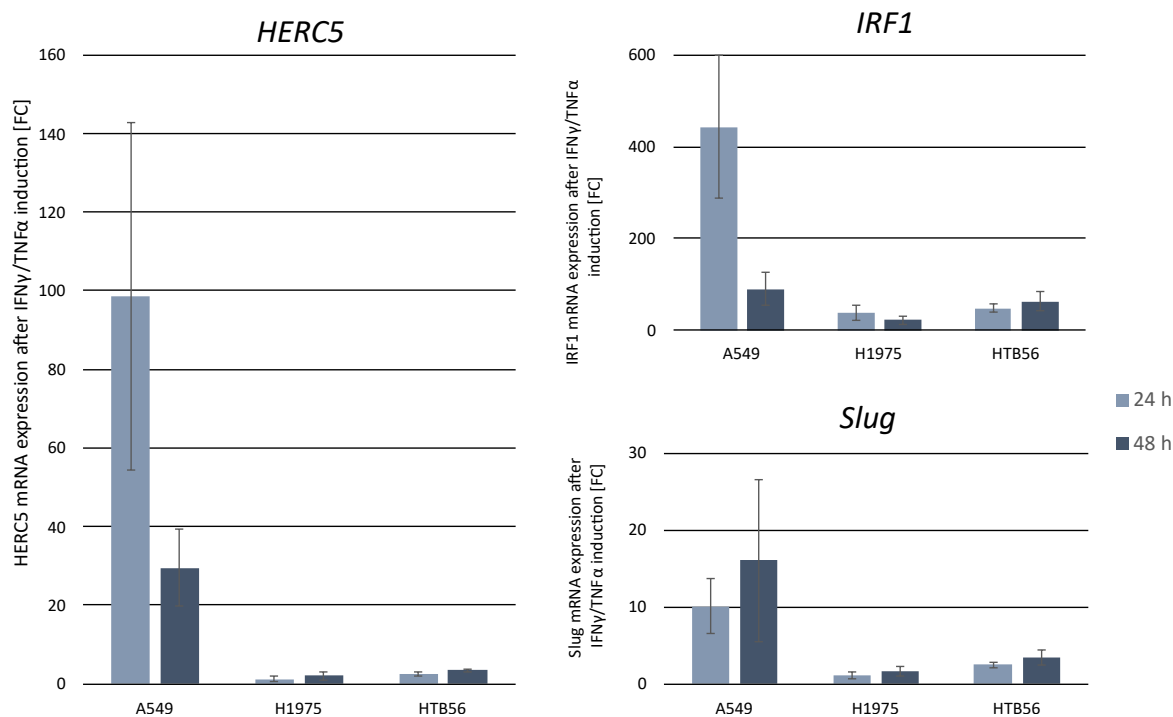
Figure 28: mRNA analysis by RT-qPCR after combined IFNγ and TNFα treatment. A549, H1975 and HTB56 par cell lines treated with 10 ng/mL IFNγ and 50 ng/mL TNFα for 24 h (light blue) and 48 h (dark blue). *IRF1* and *Slug* indicate upregulation of IFNγ/TNFα induced pathways. Expression was normalized to *RPLP0* and no cytokine treatment. Averaged values are shown from three biological replicates (n=3) with error bars showing corresponding standard deviations.

Subsequently, protein levels were analyzed by Western blot in A549 KO, A549 par, H1395 and HTB56 cells (Figure 29). A459 par cells showed the highest amount of ISGylated proteins of all cell lines as well as strong HERC5 expression both 24 h and 48 h after cytokine treatment (24 h: 4.3 ±3.8, 48 h: 4.5 ± 2.2), which reflects mRNA levels. Interestingly, ISGylation levels are highest after 48 h, which might be due to low basal HERC5 protein levels and therefore ligation of ISG15 to target proteins is delayed. H1395 cells furthermore showed high levels of ISGylation and HERC5 expression (24 h: 7.8 ± 8.5, 48 h: 6.4 ± 3.2; see Appendix) while HTB56 cells remained unaffected by combined treatment of IFNγ and TNFα in a similar way as single agents (24 h: 0.8 ± 0.4, 48 h: 0.5 ± 0.4). A549 KO cells showed hardly any HERC5 induction (24 h: 1.9 ± 1.6, 48 h: 1.0 ± 0.5; Figure 30), however, ISGylated proteins could be detected after 48 h. This might be due to the fact that although HERC5 has been described as the main, but not only E3 ISG15 ligase in the cell, ISGylation occurred by other E3 ligases [79].
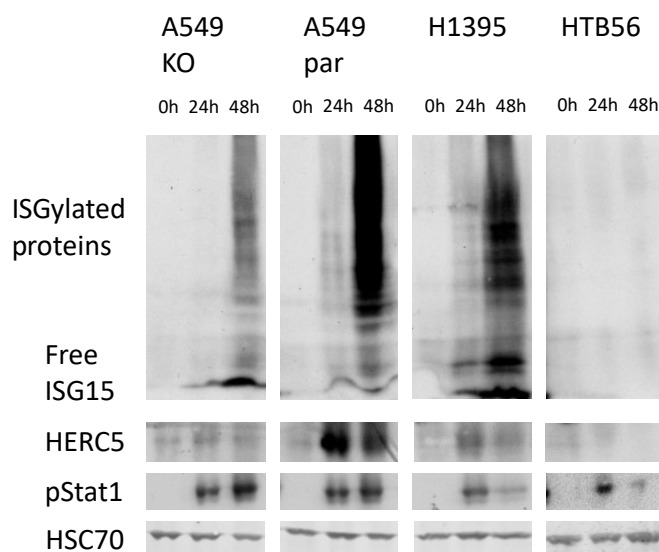
Figure 29: Protein analysis after combined IFNγ and TNFα treatment.
A549 KO, A549 par, H1395 par and HTB56 par cell lines treated with 10
ng/mL IFNγ and 50 ng/mL TNFα for 0 h, 24 h and 48 h (n=3). Anti-ISG15
antibody detects ISGylated proteins as well as unconjugated ISG15. Anti-
pStat1 indicates upregulation of IFNγ induced pathways. HSC70 serves as
loading control.

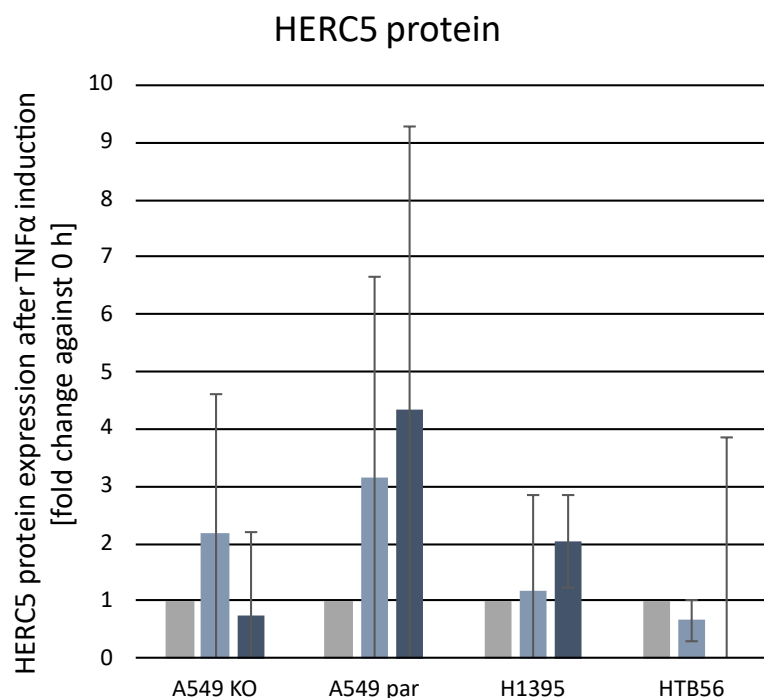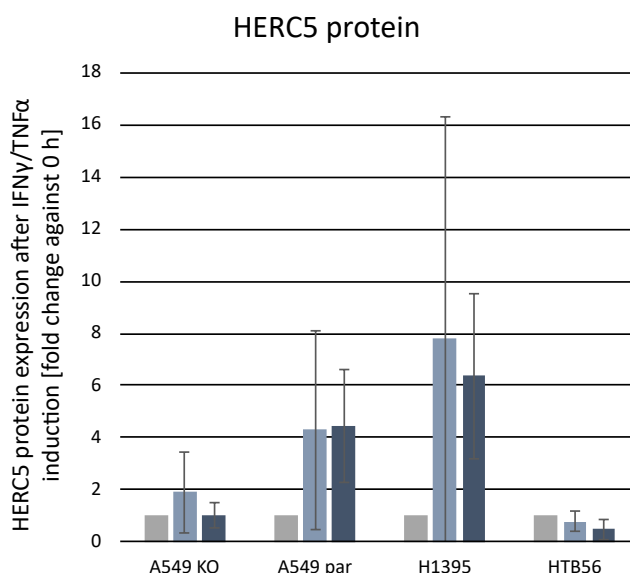**Figure 30: Protein quantification after IFNγ and TNFα treatment.** A549
KO, A549 par, H1395 and HTB56 cell lines treated with 10 ng/mL IFNγ
and 50 ng/mL TNFα for 24 h (light blue) and 48 h (dark blue). Expression
was normalized to 0 h (gray). Averaged values are shown from three bio-
logical replicates (n=3) with error bars depicting corresponding standard
deviations.

4.7   SILAC analysis of A549 par/HERC5 KO cell lines for identification of HERC5-dependent ISGylation

As previously shown in section 4.3, differential HERC5 can lead to a more aggressive phenotype in modified NSCLC cell lines. This behavior could not be explained by the differential mRNA expression as analyzed by the means of RNAseq, however, due to its main function as the main E3 ligase in the cell, it can be assumed that HERC5 might function on protein rather than mRNA levels.

Due to the results obtained in section 4.6, HERC5 expression as well as ISGylation has been shown to be strongly inducible by inflammatory cytokines. Since the main function of HERC5 is its ligation of ISG15 to target proteins, this function might also have an impact on rendering cells more aggressive when lacking HERC5. Whether this transfer of ISG15 is target-specific is currently still unknown. Therefore, interaction partners of HERC5 were assessed in the following section by using A549 par and A549 KO cell lines after combined induction by cytokines IFNγ and TNFα. In order to establish a suitable model for proteome analysis of HERC5-dependent ISGylation, first an immunoprecipitation (IP) approach was optimized using agarose-coupled ISG15 as bait. HERC5 antibody is unsuitable for IP due to binding of many unspecific proteins which is visible in Western blot application. In a second step, stable isotope labeling of amino acids in cell culture- (SILAC-) based mass spectrometry analyses were performed in order to identify those proteins specifically ISGylated by HERC5 under inflammatory stimulation. By using this approach, it should be investigated whether HERC5 is involved in metastatic spread through its interaction with immune environment deriving from its ISGylation funtion of interaction partners .

4.7.1   Establishment of ISG15-IP

Since interactions of bait antibodies with their targets are strongly dependent on their chemical environment, different washing buffers could lead to enhancement or reduction of target proteins bound to the antibody. Conditions such as pH, salt concentration or use of detergent and their concentration could therefore heavily influence binding properties. Here, different washing conditions were tested in order to find optimal parameters for the establishment of ISG15-IP.

In order to identify those conditions which lead to the highest difference in proteins bound to ISG15 antibody in the different cell lines, lysis and elution conditions remained constant. After treatment with IFNγ and TNFα for 48 h, cells were lysed with IP lysis buffer and 500 μg whole protein lysate was mixed with 30 μL ISG15 agarose beads. Four different washing buffers were tested (Figure 31). Washing buffer #1 led to the highest difference in ISGylated protein load while buffers #2-4 had too stringent washing conditions and seemingly have led to strongly reduced levels of ISGylated proteins both in A549 par and KO cells. Therefore, washing buffer #1 was chosen for subsequent SILAC-based proteome analysis (see Figure 32).
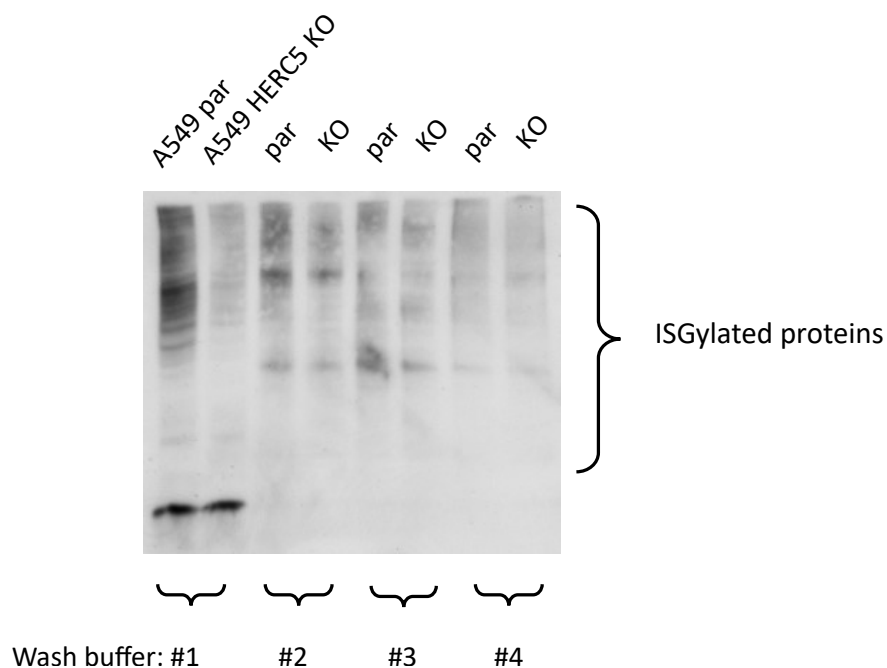
Figure 31: Western blot showing total eluates from IP using agarose beads-coupled anti-ISG15 as bait. Different washing buffers (#1-4) were used to determine the best conditions in which differences in ISGylation in A549 par and KO cells become most prominent. Detection was performed with anti-ISG15.
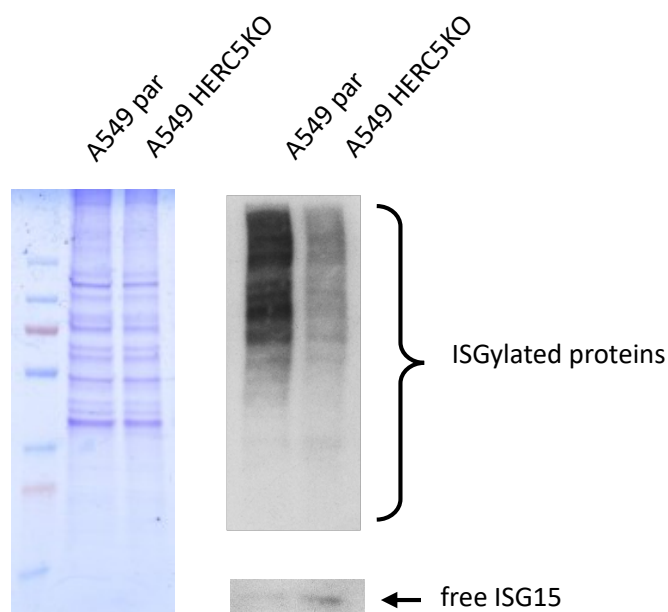
Figure 32: Final IP parameters established for SILAC-based proteome analyis. Left: Coomassie-stained SDS-gel shows total eluates from IP using agarose beads-coupled anti-ISG15 as bait. No difference in total protein concentration can be observed. Right: Western blot showing proteins from the same eluate after IP, detection was performed with anti-ISG15. Enrichment of total ISGylated proteins can be seen in A549 par samples as well as enhanced free, unconjugated ISG15 in A549 KO samples.

4.7.2 Determination of incorporation rate of ^{13}C-labeled amino acids

SILAC experiments are based on the incorporation of heavy labeled amino acids into proteins. In order to be able to distinguish between proteins derived from A549 par and KO cell lines, complete incorporation of heavy amino acids into proteins has to be ensured. Here, A549 parental cells were chosen for heavy labeling, while A549 KO cells remained unlabeled. This incorporation was monitored by continuously growing A549 par cells in heavy SILAC media while splitting cells into two flasks for lysate preparation and further passaging. Incorporation was analyzed for five subsequent passages by generation of whole cell lysates, followed by measurement of protein concentration. 25 µg protein of each passage were subjected to SDS-PAGE and stained with Coomassie. For each passage, two bands containing proteins of equal molecular weight were excised, digested with trypsin, and analyzed by mass spectrometry. Regions of excised proteins chosen for analysis can be seen in Figure 33. Performance of mass spectrometry and data analysis were executed by Kai Bartkowiak and Parinaz Mossahebi Mohammadi at ITB, UKE.
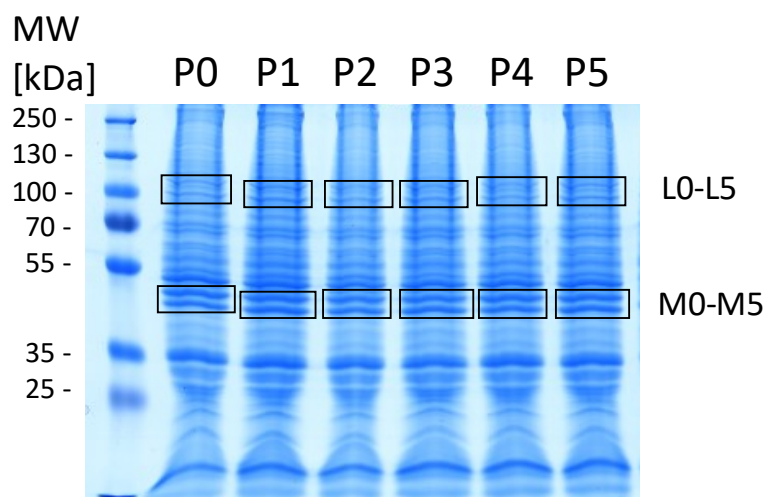
Figure 33: Coomassie-stained SDS-gel containing total protein lysates from different passages of A549 par cells after growth in heavy SILAC DMEM. Each lane contains 25 μg of lysate. The first lane contains only light proteins (P0), while the following lanes contain protein lysates from passages P1 to P5. Gel pieces excised for analysis of ^{13}C incorporation rate are indicated by squares and denoted as L0-L5 and M0-M5. Molecular weight marker PageRulerTM Prestained Protein Ladder was used for size reference.

Successful incorporation of ^{13}C-labeled amino acids is characterized by disappearance of signals from light peptides as well as an increase of signals from heavy peptides in the different mass spectra and was analyzed for several peptides, here shown for Heat Shock Protein HSP90AB1 in Figure 34. The mass peak at m/z=675.3692 in passage 1 is diminished in passage 3. Heavy labeling was thus achieved after passage 3.

For SILAC-based analyses, it is important that differences in protein ratios derive from differential HERC5 expression and not from influences induced by growth in heavy-labeled media. Therefore, whether heavy labeling has an influence on cell morphology was examined by light microscopy. Both A549 par (P3 heavy) and A549 KO (P3 light) were compared but no morphological differences could be observed (Figure 35) and furthermore show no differences in comparison to normal DMEM growth media as seen in Figure 12B. Influence of growth rates by heavy SILAC media could neither be observed.
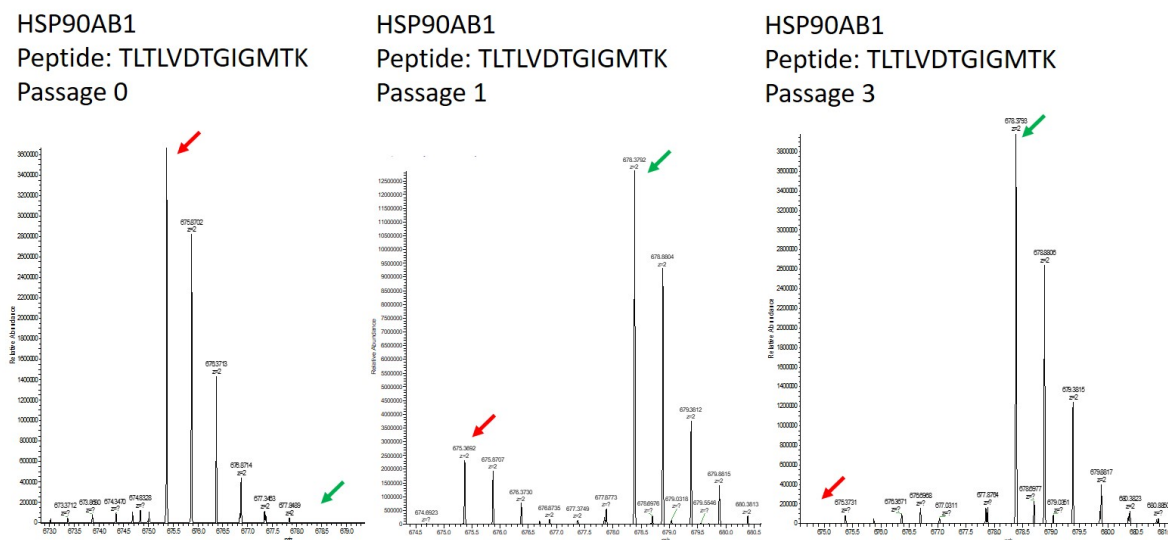
Figure 34: Exemplary HSP90AB1 mass spectra for analysis of incorporation rate of ^{13}C-labeled amino acids Left: Mass spectrum of passage 0 after growth in heavy-labeled SILAC media shows peak for the light peptide at m/z=673.4 (red arrow) and no peak for the heavy peptide (green arrow). Middle: The light peak in the mass spectrum of passage is strongly diminished while the heavy peak appears at m/z= 678.4. Right: The light peak in mass spectrum of passage 3 is completely diminished and the heavy peak shows a high intensity.
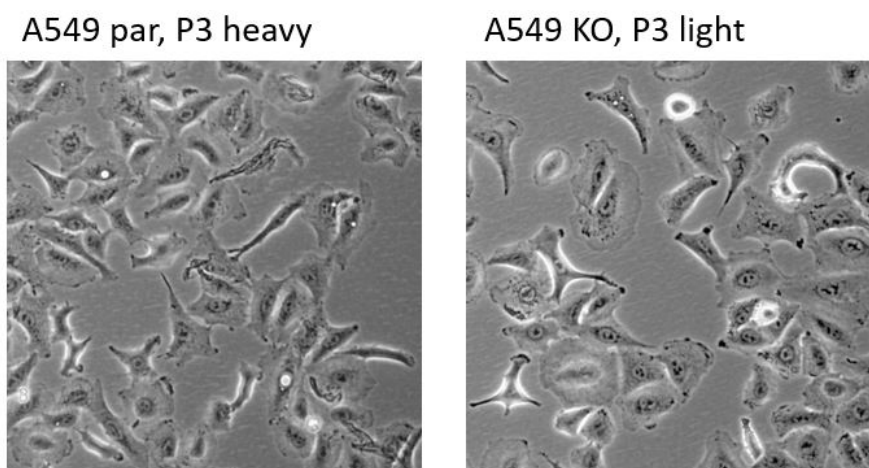
Figure 35: Light microscopy images of A549 cell lines. Left: A549 par cells after three passages in heavy SILAC DMEM. Right: A549 KO cells after three passages in light SILAC DMEM. Both cell lines show similar morphological traits.

4.7.3   HERC5 ISGylation targets

For SILAC-based quantitative proteomic analysis, cells were grown to passage 3 according to results from section 4.7.2 in either heavy or light media and seeded into their corresponding media including 10 ng/mL IFNγ and 50 ng/mL TNFα for 48 h. Cells were lysed in IP lysis buffer and proteins were quantified by BCA test. Immunoprecipitation was performed with 500 µg protein using agarose beads-coupled anti-ISG15 antibody. Protein concentrations were once more measured from IP eluates. Equal amounts of heavy labeled A549 par eluate and light A549 KO eluate were mixed (25 µg per replicate) and subjected to SDS-PAGE with subsequent Coomassie staining (see Figure 36). Lanes from the three different replicates, denoted as L, M and R were cut into 10 gel pieces each and analyzed by mass spectrometry, performed by Parinaz Mossahebi Mohammadi. Using Maxquant software, peptides analyzed from raw data were mapped to the human Uniprot database. After database search, two different search parameters were applied. Ratios of H/L proteins as well as the ratios of peak intensities determined from the mass spectra are listed below. Those proteins fitting to parameters of 1.5-fold enrichment in at least one of the groups were chosen for GO-term analysis and functional annotation and PANTHER pathway analysis. Using these parameters, 42 proteins are observed to be ISGylated by HERC5 in A549 par cell line and are listed in Table 23. 20 of these proteins were upregulated >2-fold in at least one of the search parameters. Missing values occur when the light peptides were not detected on the mass spectrometer. They therefore have the value 0, and results from this division are undefined. GO term analysis show a multitude of proteins with different functions within the cell. When using PANTHER GO term enrichment analysis, however, no significantly enriched pathway could be identified after FDR (False discovery rate)-correction for multiple testing.
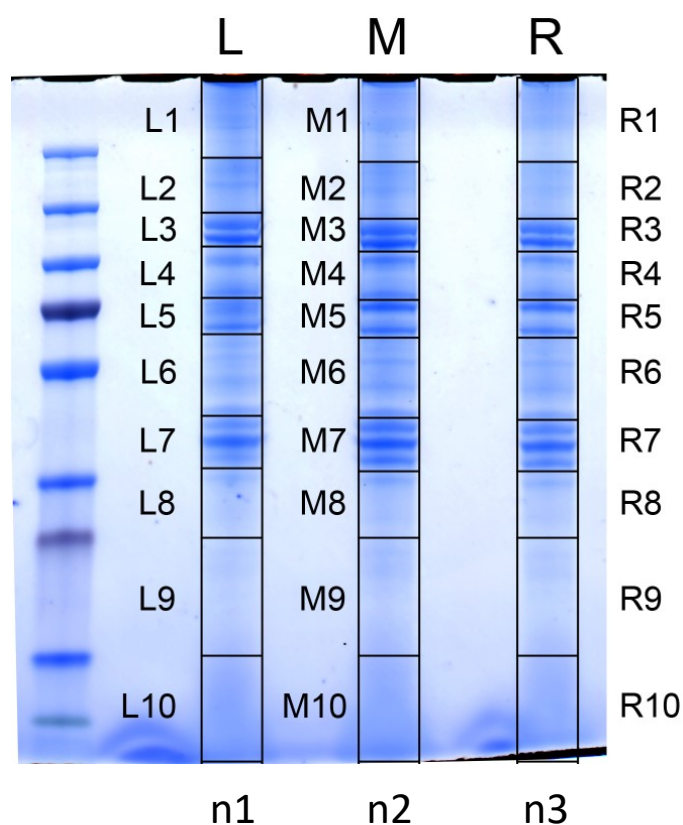
Figure 36: Coomassie-stained SDS-gel showing proteins bands from three independent SILAC-based IP eluates. After growing cells in heavy/light SILAC DMEM to P3, induction of expression by IFNγ and TNFα, cell lysis and performing IP, 25 μg of eluate in a heavy:light ratio of 1:1 was subjected to SDS-PAGE. The replicates are denoted as L (left; n1), M (middle; n2) and R (right; n3). All lanes were divided into ten gel pieces containing proteins of equal molecular weight; here denoted as L1-L10, M1-M10 and R1-R10.

Table 23: Proteins enriched ≥1.5-fold identified by SILAC-analyis of A549 par/KO (n=3)

Protein	Gene name	GO term	Ratio H/L	Intensities H/L
NADH dehydrogenase [ubiquinone] iron-sulfur protein 2, mitochondrial	NDUFS2	mitochondrial electron transport	4.67	-
Ubiquitin-like protein ISG15	ISG15	ISG15-protein conjugation	2.30	-
Tensin-3	TNS3	cell migration	1.87	-
N-acetyltransferase 10	NAT10	rRNA modification	1.81	-
Zinc finger protein 598	ZNF598	poly(A) RNA binding	1.74	-
Poly(U)-binding-splicing factor PUF60	PUF60	RNA splicing	1.65	-
Mediator of RNA polymerase II transcription subunit 18	MED18	RNA polymerase II transcription cofactor activity	1.59	-
Protein S100-A4	S100A4	actin binding	1.55	-
Nuclear factor NF-kappa-B p100 subunit; p52 subunit	NFKB2	inflammatory response	1.55	-
Nascent polypeptide-associated complex subunit alpha	NACA	transcription	1.52	-
Procollagen-lysine,2-oxoglutarate 5-dioxygenase 1	PLOD1	oxidation-reduction process	1.51	-
Intercellular adhesion molecule 1	ICAM1	cell adhesion	-	7.98
Receptor-type tyrosine-protein phosphatase kappa	PTPRK	protein dephosphorylation	-	5.98
DNA-directed RNA polymerase I subunit RPA2	POLR1B	positive regulation of gene expression	-	4.74

Table 23 continued from previous page

Protein	Gene name	GO term	Ratio H/L	Intensities H/L
RanBP2-like and GRIP domain-containing protein 3/4	RGPD3/ RGPD4	Ran GTPase binding	-	3.47
Nucleoporin SEH1	SEH1L	nuclear pore organization	1.19	3.30
Nuclear pore complex protein Nup133	NUP133	nuclear pore organization	-	3.22
Zinc finger C2HC domain-containing protein 1A	ZC2HC1A	protein binding	-	2.63
Poly [ADP-ribose] polymerase 2	PARP2	protein ADP-ribosylation, DNA repair	-	2.61
UPF0488 protein C8orf33	C8orf33	Alternative splicing	-	2.54
ATP synthase subunit d, mitochondrial	ATP5H	ATP biosynthetic process	-	2.50
Dystrophin	DMD	structural constituent of cytoskeleton	-	2.44
Translocon-associated protein subunit delta	SSR4	Protein processing in endoplasmic reticulum	-	2.43
Replication protein A 14 kDa subunit	RPA3	DNA replication, DNA repair	-	2.35
Ubiquitin-like modifier-activating enzyme 1	UBA1	ubiquitin-protein transferase activity	-	2.26
Leucine-rich repeat-containing protein 59	LRRC59	cell-cell adhesion	-	2.12
Peptidyl-tRNA hydrolase ICT1, mitochondrial	ICT1	aminoacyl-tRNA hydrolase activity	-	2.04
RNA-binding protein 42	RBM42	negative regulation of mRNA splicing	1.16	2.03
Cytoplasmic polyadenylation element-binding protein 2	CPEB2	poly(A) RNA binding	-	2.02

Table 23 continued from previous page

Protein	Gene name	GO term	Ratio H/L	Intensities H/L
Myotubularin-related protein 1	MTMR1	phosphatidylinositol biosynthetic process	-	1.97
39S ribosomal protein L23, mitochondrial	MRPL23	mitochondrial translation	1.01	1.91
Tripartite motif-containing protein 5	TRIM5	ubiquitin-protein transferase activity	-	1.91
Vascular endothelial zinc finger 1	VEZF1	angiogenesis	-	1.91
Antigen KI-67	MKI67	cell proliferation	1.20	1.87
Probable global transcription activator SNF2L1	SMARCA1	DNA replication, recombination, and repair	1.13	1.84
Nucleoporin GLE1	GLE1	mRNA export from nucleus	0.94	1.80
ATP-dependent RNA helicase DDX24	DDX24	RNA secondary structure unwinding	1.18	1.76
Egl nine homolog 1	EGLN1	response to hypoxia	-	1.75
Mammalian ependymin-related protein 1	EPDR1	cell-matrix adhesion	1.07	1.70
PHD finger protein 14	PHF14	negative regulation of transcription by RNA polymerase II	1.23	1.62
Phosphatidylinositol 4-phosphate 5-kinase type-1 alpha	PIP5K1A	phosphatidylinositol biosynthetic process	0.98	1.55
28S ribosomal protein S28, mitochondrial	MRPS28	mitochondrial translational elongation	1.02	1.52

4.8   Analysis of extracellular vesicles derived from A549 par/KO cells

In the previous section, HERC5 has been shown to interact with 42 proteins through ISGylation. The exact mechanism of how HERC5 is involved in tumor progression and metastasis formation through its role in ISGylation of proteins, however, remains to be elucidated. Exosomes have been previously described as a mediator of preparing the metastatic niche for tumor cells which have been able to detach from their primary tumors [66]. Furthermore, according to a study by Villarroya-Beltri *et al.*, ISGylation is connected to a decrease in exosome secretion through aggregation and degradation of proteins involved in multivesicular body (MVB) formation [107]. Through this interaction, MVB fusion with the plasma membrane and therefore exosome release is impaired. Since HERC5 acts as the main ISG15 E3 ligase in the cell, it was further investigated whether HERC5 is also involved in the secretion of exosomes. For this, supernatant from A459 parental and HERC5 KO cells was collected which had been treated with pro-inflammatory cytokines IFNγ and TNFα to upregulate the components of the ISGylation machinery. EVs from the supernatant were subsequently isolated by ultracentrifugation and analyzed using different methods for detection.

4.8.1   Influence of HERC5 expression on extracellular vesicle release

After isolation of extracellular vesicles by ultracentrifugation, isolated particles were first quantified by NTA (Nanoparticle Tracking Analysis) to evaluate particle homogeneity and size distribution. An exemplary measurement is shown in Figure 37A, showing a peak in size distribution at 122 nm, corresponding to a typical size of an exosome and therefore confirming sample purity. Particle concentrations from the samples were furthermore compared and shown for four independent biological replicates. Fold-changes were calculated of KO/par particle concentrations (Figure 37B) and show an average increase in exosome release of 1.6 (SD= 0.43). By performing SDS-PAGE and subsequent Coomassie-staining of equal amounts of EV lysate, an enrichment in total protein load can be observed (Figure 37C). Combined, the results indicate that HERC5 KO cells secrete more vesicles, supporting the previous finding of the role of ISG15 in exosome secretion. Therefore, also HERC5 might be involved in secretion of extracellular vesicles as in HERC5 KO cells more vesicles are secreted as detected by NTA.

4.8.2   Analysis of extracellular vesicles protein content by SILAC

SILAC-based proteome analyses have revealed differentially enriched proteins ISGylated specifically by HERC5. Furthermore, as shown by Villarroya-Beltri *et al.* [107] and in section 4.8.1, HERC5 expression seems to have an influence on EV release. Whether
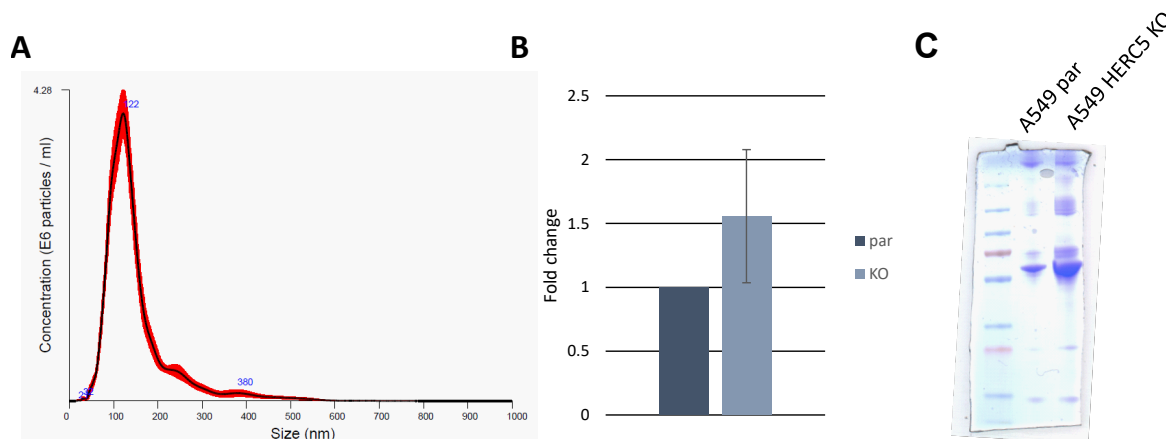
Figure 37: Quantitative differences of EVs derived from A549 par/KO cell lines. Expression of the ISGylation machinery was induced by IFNγ and TNFα for 48 h before isolation of EVs from supernatant. **A)** Exemplary image of NTA measurement, depicting good particle homogeneity and a size distribution peak at 122 nm. **B)** Fold changes of A549 KO EV particle concentration analyzed by NTA measurements (n=4, SD= 0.43) normalized to A549 par EV particle concentration. **C)** Coomassie-stained SDS-gel containing equal volumes of total protein lysates from A549 par and KO EVs show differences in protein load.

not only the amount of particles released by A549 cell lines is influenced by different HERC5 protein levels, but also if EV protein content is changed was analyzed in this section. For this, similar to previous SILAC-studies, after complete incorporation of ^{13}C-labeled amino acids, cells were treated with inflammatory cytokines IFNγ and TNFα for 48 h. FCS used for cell culture naturally contains extracellular vesicles from bovine sources. EV-depleted FCS for analyses of vesicles is commercially available, however, FCS used for SILAC approaches needs to be dialyzed in order for the serum to be completely free of contaminating, non-labeled amino acids. Since EV-depleted SILAC FCS is not readily available, FCS was mixed with SILAC DMEM to a final dilution of 30% according to Théry *et al.* [117] and subjected to ultracentrifugation at 100,000 g for 16 h at 4 °C. Cell culture was subsequently performed using the supernatant of the EV-depleted FCS in SILAC DMEM (10% final FCS concentration). Three biological replicates were used to collect supernatant from the different cell lines, while each cell line was seeded into two T175 flasks in order to produce sufficient amount of EVs from 75 mL of culture media. Ultracentrifugation was subsequently performed according to section 3.5.1. EV pellets were lysed in SDC buffer and A549 par and KO samples were mixed in a ratio of 1:1 for subsequent MS analysis. Measurements have shown a large fraction of analyzed peptides which were still unlabeled, indicating either the fact

that incorporation of ^{13}C-labeled amino acids was not complete or that contamination from bovine EVs and other contaminants such as lipoproteins in FCS has occured. Since incorporation rates had been previously analyzed, contamination of bovine EVs is the more likely cause of the low fraction of heavy-labeled peptides in the sample. Therefore, only one replicate was analyzed and peptides were screened against human as well as bovine databases in order to exclude false positive hits deriving from bovine EVs. Those proteins possibly deriving from bovine sources were hence removed from the analyses so that only peptides mappable to the human genome were used for enrichment analysis. In total, using a fold-change cut-off value of 1.5, 39 proteins could be identified to be enriched in KO EV samples, but none were enriched in parental samples (A549 par $\hat{=}$ heavy (H), A549 KO $\hat{=}$ light (L)) (see Table 24).

Of note, using the aforementioned enrichment cut-off criteria, none of the 39 identified proteins in EVs were found among the 42 previously listed ISGylated proteins and vice versa.

Table 24: Proteins enriched ≥1.5-fold identified by SILAC-analyis of A549 par/KO EVs (n=1). Classifiers are listed to categorize GO terms into pathways connected to immunity (⋆), cell adhesion (○), EV secretion (◇), and angiogenesis (▷).

Protein	Gene name	GO term	Classi-fier	Ratio H/L
Macrophage migration inhibitory factor	MIF	inflammatory response	⋆	0.032
Keratin 2	KRT2	intermediate filament organization	○	0.063
Keratin 8	KRT8	intermediate filament organization	○	0.068
Nucleophosmin	NPM1	nucleocytoplasmic transport		0.075
Profilin-1	PFN1	actin cytoskeleton organization	○	0.171
Glyceraldehyde-3-phosphate dehydrogenase	GAPDH	gluconeogenesis		0.186
C-C motif chemokine 5	CCL5	inflammatory response	⋆	0.221
Fibronectin	FN1	angiogenesis/ cell adhesion	▷ ○	0.252
Heat shock 70 kDa protein 6	HSPA6	cellular response to unfolded protein		0.294
Galectin-3-binding protein	LGALS3BP	platelet degranulation/ cell adhesion	○	0.308
Programmed cell death protein 6	PDCD6	regulation of exosomal secretion	◇	0.322
Complement decay-accelerating factor	CD55	innate immune response	⋆	0.355
CD81 antigen	CD81	cell adhesion	○ ◇	0.405
BRO1 domain-containing protein BROX	BROX	-		0.408
Laminin subunit gamma-1	LAMC1	cell adhesion	○	0.408

Table 24 continued from previous page

Protein	Gene name	GO term	Classi-fier	Ratio H/L
HLA class I histocompatibility antigen, B-18 alpha chain	HLA-B	antigen processing and presentation	⋆	0.409
Heparan Sulfate Proteoglycan 2	HSPG2	extracellular matrix organization	∘	0.439
TNFAIP3-interacting protein 1	TNIP1	inflammatory response	⋆	0.452
Syndecan-4	SDC4	signal transduction		0.457
HLA class I histocompatibility antigen, A-34 alpha chain	HLA-A	antigen processing and presentation	⋆	0.468
CD59 glycoprotein	CD59	regulation of complement activation	⋆	0.477
Collagen alpha-1(XVIII) chain	COL18A1	angiogenesis	▷	0.477
Collagen alpha-2(IV) chain	COL4A2	angiogenesis	▷	0.482
Syntenin-1	SDCBP	cell-cell adhesion	∘	0.484
Laminin subunit alpha-5	LAMA5	regulation of cell adhesion	∘	0.486
Clusterin	CLU	chaperone-mediated protein folding		0.504
Lysosome-associated membrane glycoprotein 2	LAMP2	chaperone-mediated autophagy		0.525
Glypican-1	GPC1	heparan sulfate proteoglycan catabolic process		0.531
60S ribosomal protein L13a	RPL13A	cellular response to interferon-gamma	⋆	0.532
Major vault protein	MVP	protein transport		0.544
Complement C1q tumor necrosis factor-related protein 1	C1QTNF1	negative regulation of platelet activation		0.547
Protein S100-A11	S100A11	regulation of cell proliferation		0.557

Table 24 continued from previous page

Protein	Gene name	GO term	Classifier	Ratio H/L
Annexin A1	ANXA1	inflammatory response	⋆	0.586
CD9 antigen	CD9	cell adhesion	○ ◇	0.591
Phospholipid scramblase 1	PLSCR1	positive regulation of innate immune response	⋆	0.609
Integrin alpha-3	ITGA3	cell adhesion	○	0.617
Signal peptide peptidase-like 2A	SPPL2A	signal peptide processing		0.636
CD44 antigen	CD44	cell adhesion	○	0.658
Agrin	AGRN	glycosaminoglycan catabolic process		0.664

From these preliminary results, GO term analysis was performed in order to categorize enriched proteins into biological pathways or molecular functions. By searching the GO annotation database, usually several functions are assigned to proteins due to a variety of activity of each protein. Of these, selected functions matching experimental parameters and relevant for this study were listed in Table 24. These annotations were furthermore categorized into the most frequently observed pathways immunity ($\star$), cell adhesion ($\circ$), EV secretion ($\diamond$), and angiogenesis ($\triangleright$). Notably, 26% (10/39) of proteins identified were assigned to a function concerning immunological pathways, or are induced as a result of IFNγ or TNFα activation, confirming connection of HERC5 to innate immunity. A connection to cell-adhesion has been found in an even greater number of proteins, here, 33% (13/39) were assigned to this pathway. Furthermore, GO term enrichment analysis was performed with PANTHER database using the complete set of differentially sorted proteins into EVs by using search parameters for biological processes. Results and p-values <0.05 after FDR correction were listed in Table 25. In total, 48 GO biological processes were identified to be enriched. After classification of pathways into immunity, cell adhesion, EV secretion and angiogenesis, one third of these processes is connected to immune regulation (16/48) and 8% to exosomal (4/48) secretion.

Table 25: GO term enrichment analysis performed by using PANTHER database with significant results after FDR correction. Classifiers are listed to categorize GO terms into pathways connected to immunity (⋆), cell adhesion (○), EV secretion (◇), and angiogenesis (▷).

GO biological process	Classifier	raw P-value	P-value (FDR)
extracellular matrix organization (GO:0030198)	◇	2.10E-08	1.24E-05
neutrophil degranulation (GO:0043312)	⋆	2.79E-08	1.53E-05
glycosaminoglycan catabolic process (GO:0006027)		1.85E-07	6.86E-05
inflammatory response (GO:0006954)	⋆	5.10E-07	1.50E-04
leukocyte migration (GO:0050900)	⋆	6.29E-07	1.76E-04
regulation of macrophage migration (GO:1905521)	⋆	1.64E-06	3.57E-04
platelet degranulation (GO:0002576)		6.04E-06	1.00E-03
protein stabilization (GO:0050821)		3.75E-05	4.42E-03
protein targeting to lysosome involved in chaperone-mediated autophagy (GO:0061740)		3.74E-05	4.45E-03
peptide cross-linking (GO:0018149)		5.20E-05	5.53E-03
glycosaminoglycan biosynthetic process (GO:0006024)		5.49E-05	5.71E-03
positive regulation of extracellular exosome assembly (GO:1903553)	◇	5.61E-05	5.73E-03
retinoid metabolic process (GO:0001523)		5.90E-05	5.95E-03
myoblast fusion involved in skeletal muscle regeneration (GO:0014905)		7.84E-05	7.14E-03
response to hydrostatic pressure (GO:0051599)		7.84E-05	7.18E-03

Table 25 continued from previous page

GO biological process	Classifier	raw P-value	P-value (FDR)
positive regulation of CD4-positive, alpha-beta T cell proliferation (GO:2000563)	⋆	7.84E-05	7.22E-03
regulation of extracellular exosome assembly (GO:1903551)	⋄	1.04E-04	9.09E-03
negative regulation of amyloid fibril formation (GO:1905907)		1.04E-04	9.14E-03
substrate adhesion-dependent cell spreading (GO:0034446)	∘	1.37E-04	1.13E-02
regulation of complement-dependent cytotoxicity (GO:1903659)	⋆	1.67E-04	1.33E-02
leukocyte cell-cell adhesion (GO:0007159)	⋆ ∘	1.81E-04	1.39E-02
positive regulation of epithelial cell migration (GO:0010634)	∘	2.00E-04	1.49E-02
antigen processing and presentation of exogenous peptide antigen via MHC class I, TAP-independent (GO:0002480)	⋆	2.04E-04	1.51E-02
interaction with host (GO:0051701)		2.56E-04	1.83E-02
regulation of ERK1 and ERK2 cascade (GO:0070372)		2.77E-04	1.94E-02
negative regulation of complement activation (GO:0045916)	⋆	2.89E-04	2.00E-02
negative regulation of platelet aggregation (GO:0090331)		3.37E-04	2.25E-02
antigen processing and presentation of endogenous peptide antigen via MHC class I via ER pathway, TAP-independent (GO:0002486)	⋆	3.37E-04	2.27E-02
antigen processing and presentation of endogenous peptide antigen via MHC class Ib (GO:0002476)	⋆	3.88E-04	2.54E-02
viral process (GO:0016032)	⋆	4.10E-04	2.66E-02
angiogenesis (GO:0001525)	▷	4.18E-04	2.69E-02

Table 25 continued from previous page

GO biological process	Classi-fier	raw P-value	P-value (FDR)
interferon-gamma-mediated signaling pathway (GO:0060333)	⋆	4.29E-04	2.75E-02
positive regulation of exosomal secretion (GO:1903543)	◇	5.02E-04	3.10E-02
negative regulation of DNA damage response, signal transduction by p53 class mediator (GO:0043518)		5.02E-04	3.12E-02
endoderm development (GO:0007492)		5.19E-04	3.19E-02
interaction with symbiont (GO:0051702)		5.58E-04	3.34E-02
negative regulation of myeloid cell apoptotic process (GO:0033033)		5.64E-04	3.35E-02
regulation of translational initiation (GO:0006446)		5.58E-04	3.35E-02
negative regulation of intrinsic apoptotic signaling pathway in response to DNA damage by p53 class mediator (GO:1902166)		5.64E-04	3.36E-02
positive regulation of peptidyl-tyrosine phosphorylation (GO:0050731)		5.80E-04	3.42E-02
positive regulation of protein kinase activity (GO:0045860)		6.22E-04	3.59E-02
positive regulation of MAPK cascade (GO:0043410)		6.59E-04	3.79E-02
cellular response to low-density lipoprotein particle stimulus (GO:0071404)		6.98E-04	3.94E-02
regulation of leukocyte apoptotic process (GO:2000106)	⋆	7.32E-04	4.09E-02
regulation of cytokine secretion (GO:0050707)	⋆	8.34E-04	4.53E-02
positive regulation of T cell cytokine production (GO:0002726)	⋆	8.47E-04	4.56E-02
skin development (GO:0043588)		8.99E-04	4.81E-02
myelin assembly (GO:0032288)		9.26E-04	4.89E-02

4.9   Influence of pre-analytic factors in liquid biopsy

The identification of novel markers for detection of cancer as well as the determination of function of those proteins involved in malignant transformation are important steps towards the elucidation of disease mechanisms and finding druggable targets. However, in order to be able to advance in the field of cancer diagnostics and therapy, not only structural and functional information can give rise to possibilities for designing e.g. new drugs, moreover, the possibility of detecting mutations or epigenetic changes at an early time point could influence treatment strategies and increase overall survival. Since mortality rates strongly correlate with disease stage, these early detection tools are becoming more and more important [40].

So-called pre-analytic parameters have been shown to have a great impact on early stage analyses in the liquid biopsy field. It is therefore important that standardized procedures concerning e.g. blood draw, stability of liquid biomarkers or detection methods will be established. Efforts regarding these issues of standardization have already been made, for example by the European consortium Cancer-ID, and are still the topic of current research [73, 111]. Two studies in line with these attempts were conducted here as part of the Cancer-ID consortium and have already been accepted for publication [111, 118]. The main focus of the first study was to evaluate whether a combined analysis of CTCs, ctDNA, miRNA and extracellular vesicles from one single blood tube is possible. Furthermore, the impact of preservatives that are present in blood-collection tubes on the different liquid biomarkers was investigated to determine the most suitable tube for analysis. The second study conducted here deals with the establishment of standardized parameters for CTC detection using a semi-automated scanning microscope [111, 118].

4.9.1   Establishment of a single tube assay for multi-parameter liquid biopsy detection in melanoma patients

Blood collection tubes have been shown to increase stability of different analytes present in the blood of cancer patients such as CTCs, ctDNA, miRNAs or EVs. All of these analytes can give valuable information on characteristics of a tumor or distant metastases and can furthermore change during disease progression. Since different blood collection tubes can influence these biomarkers in a distinct way, this study deals with differences in stability, composition or concentrations deriving from preservatives present in EDTA, Streck or Transfix blood collection tubes and if a combined analysis of all four mentioned biomarkers can be performed from 7.5 mL of blood from a single tube [118].

Blood from 20 metastatic melanoma (MM) patients and 5 healthy donors (HD) was drawn in the aforementioned tubes. First, the influence of plasma removal from blood

prior to CTC isolation with the ClearCell FX1 System was analyzed. For this, spiking experiments using 50 GFP-positive H1975 cells were performed using healthy donor blood in EDTA and Streck tubes. Mean recovery rates were 47.0% ± 9.3 without plasma removal in EDTA tubes (n=4) and 46.8% ± 12.7 with plasma removal (n=4, p=0.85, Wilcoxon signed-rank test). In Streck tubes recovery rates were 52% and 26% in two replicates with plasma removal, however, in experiment 2 errors (*) in the ClearCell device occurred during blood processing and were therefore not included into calculation of the mean (see Table 26).

Table 26: ClearCell recovery rates after spiking of 50 H1975-GFP into 7.5 mL blood with or without plasma removal in EDTA and Streck tubes.

Run	Tube	Plasma removal	Exp. 1 recovery	Exp. 2 recovery	mean ± SD
1	EDTA	no	38%	40%	47.0% ± 9.3
2	EDTA	no	56%	54%	
3	EDTA	yes	30%	48%	46.8%± 12.7
4	EDTA	yes	48%	61%	
5	Streck	yes	52%	26%*	52 (39)%

CTC and ctDNA analyses have been performed by Lelia Lück and in summary have shown no differences in ctDNA concentration in plasma between EDTA and Streck tubes (mean EDTA: 3.3 ng/µL ± 4.6, Streck: 3.0 ng/µL ± 4.7 , p=0.96, Wilcoxon signed-rank test, data not shown). Plasma removal of Transfix tubes was not possible due to elevated levels of hemolysis. Analysis of mutations in ctDNA has furthermore not shown differences in variant allele frequencies (VAF) derived from tube preservatives with the exception of one patient. Here, a *BRAF K601E* mutation could be found only in the EDTA tube (VAF: 0.7%) and a *MAP2K1 I111S* mutation only in the ctDNA from the Streck tube (VAF: 0.3%) (data processed by Lelia Lück). CTC analyses revealed enhanced recovery rates of CTCs in EDTA blood (3/20 patients) compared to Streck and Transfix tubes in which no CTCs could be detected when using the microfluidics-based ClearCell FX1 System for CTC enrichment (data was processed by Lelia Lück, not shown). After isolation by ultracentrifugation, EV particle concentration and morphology were analyzed by NTA measurements and subsequent transmission electron microscopy (data processed by Orion Pharma, Finland). The mean concentrations of EV particles detected in blood from EDTA tubes were 3.33 x 10^{11} ± 2.77 x 10^{11} and for Streck 2.84 x 10^{11} ± 2.31 x 10^{11} particles/mL. Wilcoxon signed-rank test showed furthermore no differences in particle concentrations of HD and MM patients (p=0.31 (HD), p=0.92 (MM)). Using transmission electron microscopy, no differences in EV morphology, sizes and purity could be observed.

NGS analysis of total miRNAs was performed from plasma samples as well as EV fractions of 10 MM patients and 5 HDs (Qiagen) using EDTA and Streck blood collection tubes. Since NGS analysis itself can be influenced by many factors, for normalization of the data, two different algorithms were used to increase robustness of the outcome. Venn diagrams using normalization algorithms geNorm [112] and NormFinder [113] depict the number of differentially regulated miRNAs depending on the tube, sample type and normalization (Figure 38). In total, 10 miRNAs had differential expression using both normalization methods in EDTA plasma samples, whereas 5 were found in Streck plasma samples. Between plasma samples, no overlap of miRNAs could be found. In EV samples, six miRNAs were found to be differentially regulated using both algorithms and both tubes: hsa-miR-375, hsa-miR-215-5p, hsa-miR-141-3p, hsa-miR-200a-3p, hsa-miR-200b-3p and hsa-miR-200c-3p. These diagrams furthermore visualize the low amount of miRNAs that are overlapping between the two tubes, indicating a substantial influence of blood collection tube on the stability and composition of miRNAs present in plasma and EVs. MiRNas were also plotted by their p-values against fold-changes of MM/HD giving rise to volcano plots of plasma and EV samples from EDTA and Streck tubes (Figure 39). In EDTA plasma and EV samples, 8 and 46 miRNAs were found, respectively, which fit parameters of fold changes >2 and p-values <0.5 while in Streck plasma and EV samples 5 and 62 significant miRNAs were fitting these cut-off values.
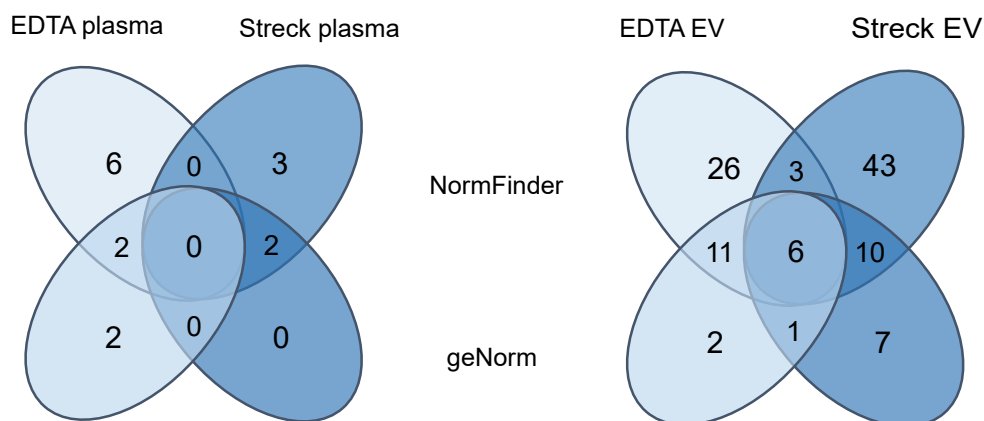
Figure 38: NGS analysis of differentially regulated miRNAs in MM patients compared to HD. Venn diagrams illustrate the amount of differentially regulated miRNAs from different algorithms as well as EDTA (light blue) and Streck (dark blue) tubes (left: plasma samples, right: EV samples). Plasma samples show no overlap of significant miRNAs, whereas in EV samples, six miRNAs were found to be differentially regulated in both tubes and were identified by both algorithms.
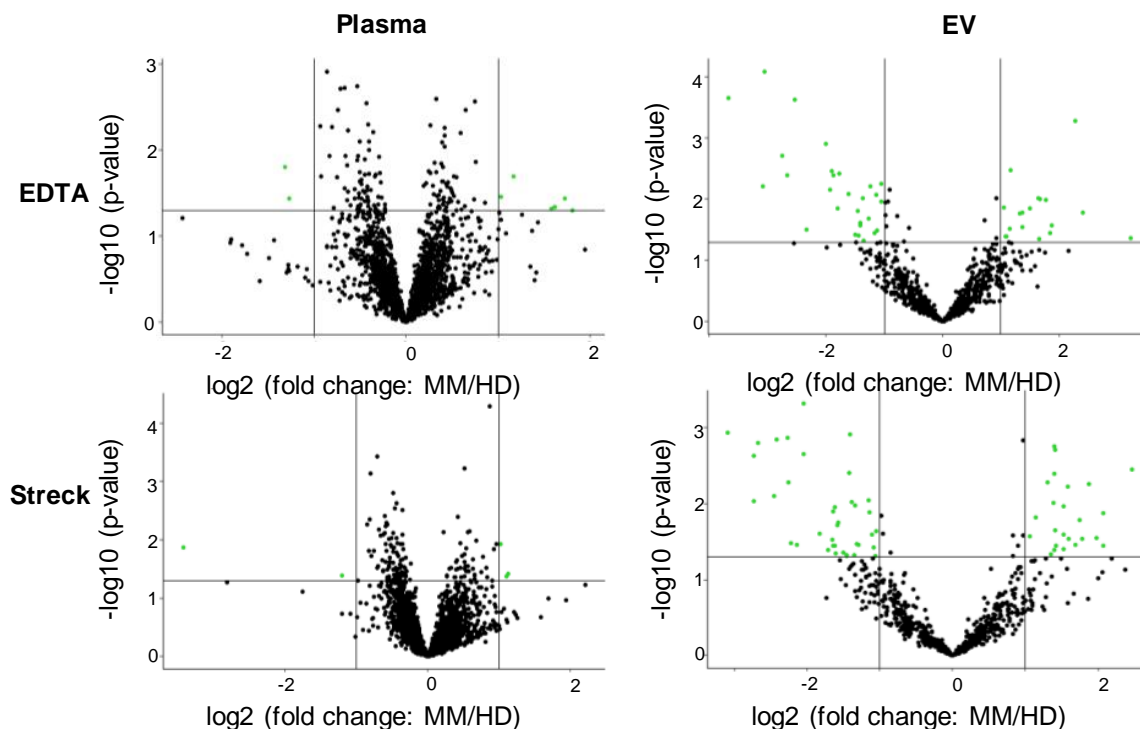
Figure 39: NGS analysis of differentially regulated miRNAs in MM patients compared to HD. Volcano plots show significant differentially expressed miRNAs after normalization with NormFinder. Cut-off values of fold changes >2 and p-values <0.5 were applied. Green dots represent those miRNAs suiting these parameters while black dots represent miRNAs below these thresholds. EDTA plasma and EV samples show 8 and 46 miRNAs, respectively, while in Streck plasma and EV samples 5 and 62 significant miRNAs were identified.

Even though miRNA NGS results were different in EDTA and Streck tubes, significant results could nevertheless be obtained. This can be underlined by the fact that when applying dynamic PCA (principle component analysis) using cut-off values of fold-changes >2 and p-values <0.5 it becomes clear that a good spatial separation between patients samples and expression in HDs can be achieved in both tubes and in both plasma and EV samples (Figure 40).

Orthogonal validation of three (hsa-miR-375, hsa-miR-215-5p, and hsa-miR-200c-3p) of the six miRNAs that were identified in EV samples from EDTA and Streck tubes, as well as both normalization methods was subsequently performed. By using RT-qPCR of reverse transcribed miRNAs and normalization against reference miRNAs hsa-miR-103a-3p and hsa-miR-93-5p, hsa-miR-200c-3p was found to be down-regulated (1.97-fold) compared to healthy donors in Streck EV samples. In EDTA EV samples hsa-miR-375 and hsa-miR-200c-3p were down-regulated (2.23-fold and 2.48-fold, respectively). No
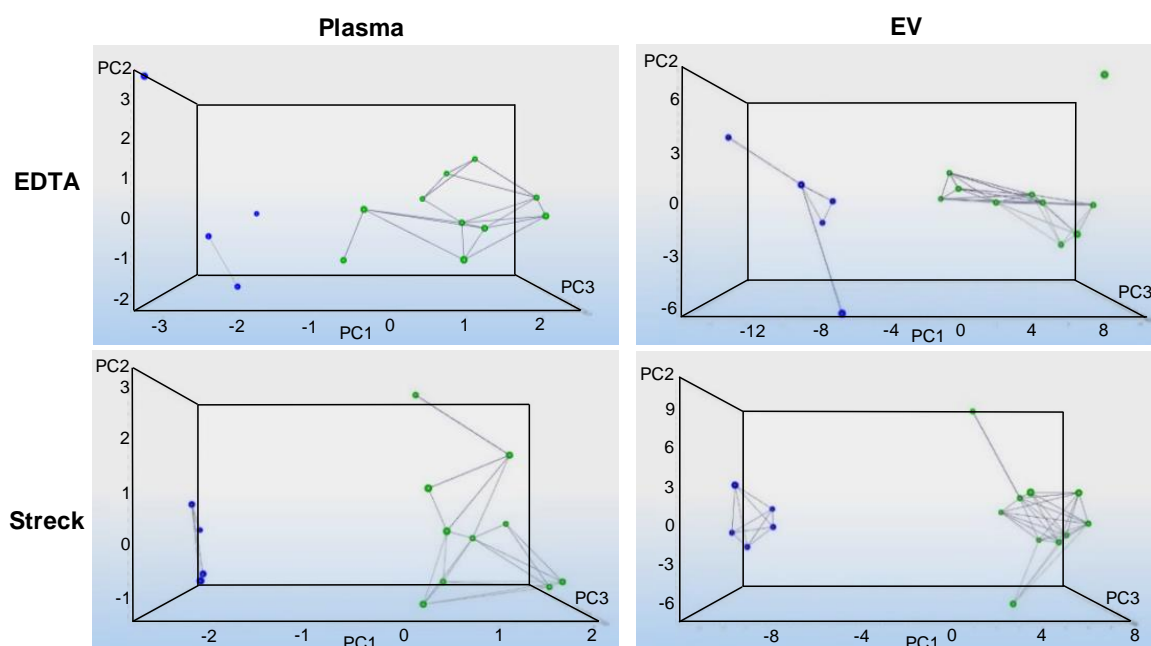
Figure 40: Dynamic PCA analysis of differentially regulated miRNAs in MM patients and healthy donors. The four groups EDTA-plasma, EDTA-EV, Streck-plasma and Streck-EV were analyzed and cut-off values of fold changes >2 and p-values <0.5 were applied. Healthy donors are depicted in blue, while green dots represent MM patients.

differential regulation of hsa-miR-215-5p in neither of the tubes could be observed (Table 27). In the corresponding NGS data, hsa-miR-200c-3p was downregulated 5.19 and 6.40-fold in Streck and EDTA tubes, respectively. Hsa-miR-375 was downregulated 6.57 (Streck) and 5.50-fold (EDTA). In the NGS data of MM patients, hsa-miR-215-5p was downregulated 3.96 (Streck) and 2.76- fold (EDTA).

Table 27: RT-qPCR analysis of relative miRNA expression in healthy donors (HD) in comparison to melanoma patients (MM) in either Streck or EDTA EV samples

Sample	hsa-miR-200c-3p	hsa-miR-215-5p	hsa-miR-375
HD Streck/MM Streck	1.97	0.76	1.05
HD EDTA/MM EDTA	2.48	0.95	2.23

4.9.2   Establishment of a semi-automated detection method for CTCs

The field of pre-analytics in liquid biopsy not only encompasses studies on stability of different biomarkers but also deals with standardization of detection methods. Circulating tumor cells (CTCs) have been shown to harbor prognostic value for disease development as their presence in the blood of cancer patients strongly correlates with the development of distant metastases [50]. Enumeration of these biomarkers can give valuable information as well as expression of specific markers such as epithelial cell surface proteins [50]. To date, the only FDA-approved CTC detection platform is the CellSearch system, which detects and enumerates CTCs according to their EpCAM (epithelial cell adhesion molecule) expression status. Since not all CTCs actually express EpCAM, CTC detection methods that are marker-independent are needed and have to be evaluated. In the following study, performed by Claudia Koch *et al.*, the label-free and size dependent enrichment device Parsortix® was used to investigate the influence of pre-analytical factors and their compatibility in clinical settings [111]. As a part of this study, a workflow for semi-automated CTC detection using the XCyto® 10 quantitative cell imager was established. So far, the detection of CTCs has been performed manually using Axioplan 2 (Zeiss) microscope and by scanning the whole slide for keratin-positive/CD45-negative cells. This manual enumeration is, however, time consuming and also introduces bias into the detection, since the interpretation of keratin staining intensity in combination with the lack of CD45 expression is subjective plus manual screening may miss cells. In order to fill the need for an automated detection system, a protocol has been established which makes use of defining thresholds of the different expression intensities of both cell populations.

For this, first spiking experiments have been performed using 1000 MCF-7 cells and 300,000 PBMCs, which were stained with tumor cell marker pan-keratin-AF488 and negative exclusion marker CD45-APC. Using the XCyto® 10 imager and 4x objective, the whole section of the slide was scanned and each cell can be plotted according to their expression in the different fluorescence channels while using DAPI signal for identification of cellular shape. Similar to FACS analysis, gating can be applied to separate those cells fitting search parameters and can subsequently be used for further analysis. Gates have been established by plotting CD45-APC signal intensities against pan-keratin-AF488 intensities for separation of tumor cells from leukocytes (Figure 41A). Cells inside these gates were subsequently overlayed with the original scanned image for adjustment of the gating parameters until all tumor cells were included (Figure 41B). Once cells were identified, they can be re-analyzed with 20x objective for higher resolution and therefore distinction of true positive hits can be ensured (Figure 41C).
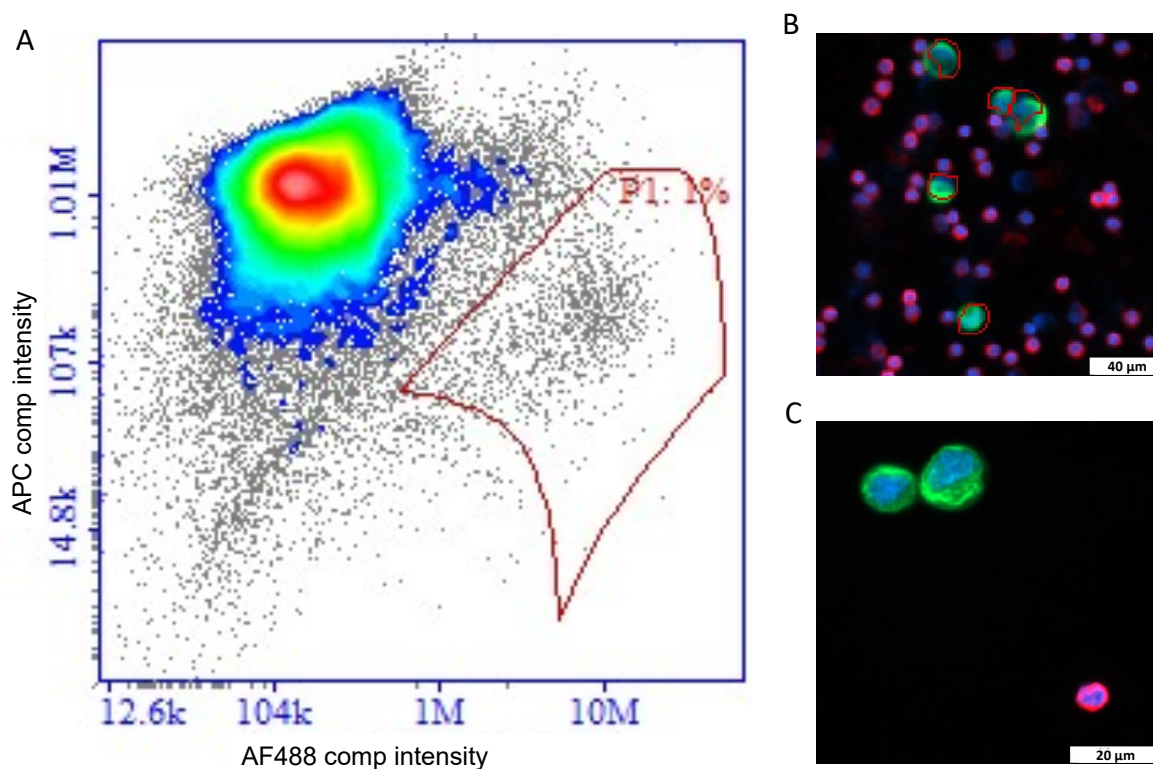
Figure 41: Establishment of gating parameters from MCF-7 cell line using XCyto® 10 semi-automated scanning microscope. Using spike-in controls of 1000 MCF-7 cells in a background of 300,000 PBMCs, stained slides were imaged by the XCyto® 10 imager. **A)** Gating of pan-keratin-positive MCF-7 tumor cells from a background of CD45-positive leukocytes. By plotting APC (-CD45) against AF488 (-pan-cytokeratin) intensities, a gate containing only tumor cells with CK-high (AF488) and CD45-low (APC) signals was established. **B)** Overlay of gating parameters established in A and scanned microscope image show positively gated MCF-7 cells (green) among un-gated leukocytes (red). Image was taken with 4x objective of XCyto® 10. Scale bar represents 40 μm. **C)** After gating, possible tumor cells can be re-analyzed by using 20x objective. MCF-7 cells are shown here as an example for image resolution. Scalebar represents 20 μm.

After setting up thresholds for staining intensities with a cell line system, it was further evaluated whether these pre-established gates could be suitable for the analysis of patient samples. Slides of blood from seven metastatic breast cancer (mBC) patients was processed through the Parsortix® device and subsequently scanned by XCyto® 10 imager. The same previously established gating was applied and it was investigated whether the same amount of cells could be identified by XCyto® 10 as by using Axioplan2 (Zeiss) microscope (Figure 42A). Application of gating for patient no. 7 gave rise to an image gallery of small image details containing only the classified objects (Figure 42B). Screening of this image gallery was already less time consuming than scanning of the whole slide manually and has proven to include all objects of possible CTC candidates. Gated cells were analyzed by overlay of gates and original image for identification of CTCs with the 4x objective (Figure 42C) but can possibly be re-analyzed with the 20x objective for increased resolution. However, using Axioplan2 (Zeiss) microscope and 20x objective, the same cell could clearly be identified as a CTC, underlining the feasibility of semi-automated detection with the XCyto® 10 microscope. This patient represents an optimal example with strong pan-keratin staining signal in combination with very low background which is not always the case.
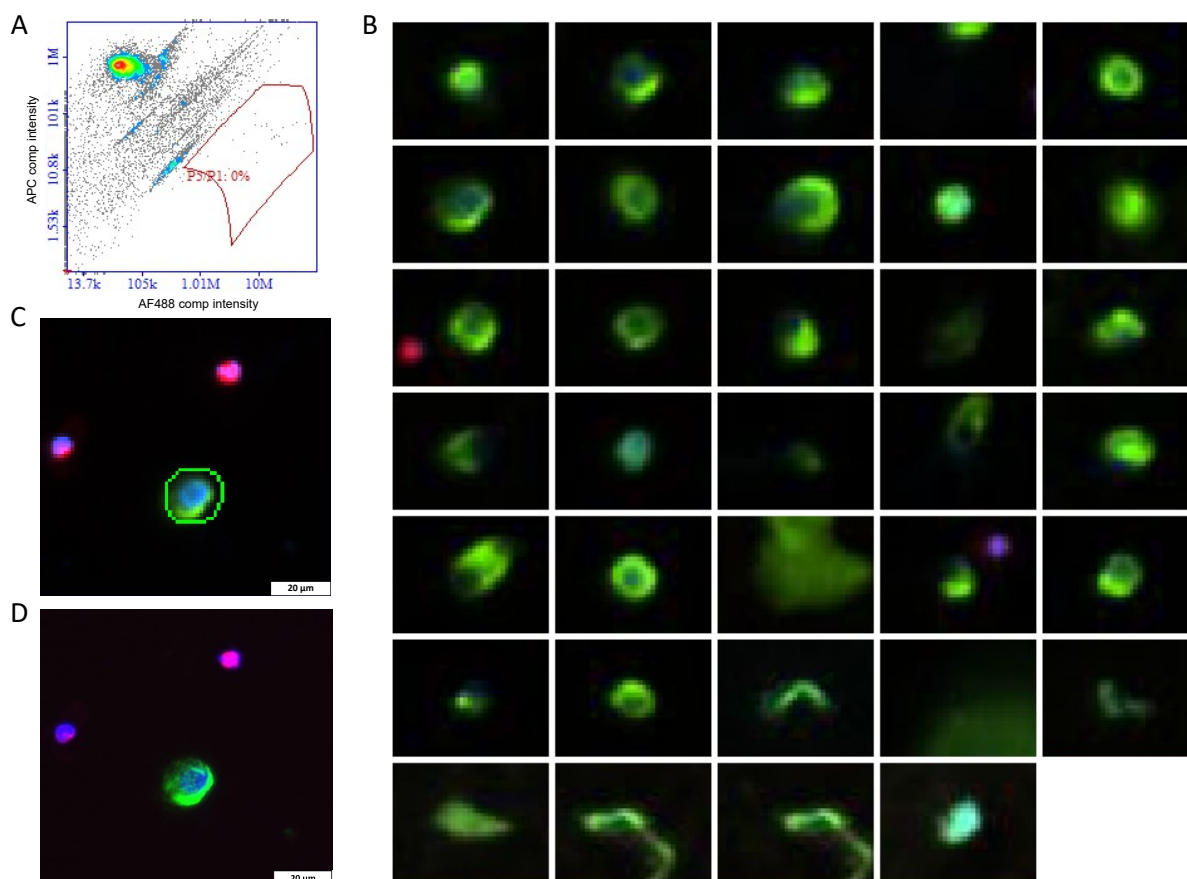
Figure 42: Image analysis of patient sample no. 7 using XCyto® 10. After processing of the patient sample through the Parsortix® device and applying IF staining protocol, the whole slide was scanned by XCyto® 10. **A)** Gating parameters established from MCF-7 cell line were used to identify possible CTCs in patients. APC intensities are plotted here against AF488 intensities and gate from Figure 41A was overlayed to distinguish keratin-positive cells from PBMCs. **B)** Application of gating gives rise to an image gallery consisting of those 34 objects which fit gating parameters of APC-low and AF488-high signals. Positive hits can subsequently be analyzed manually to further narrow down possible CTCs. **C)** Image overlay of possible gated CTC and XCyto® 10 microscope image using 4x objective. The cell corresponds to the second image in the first row of the image gallery in B. Scale bar represents 20 µm. **D)** The same cell was imaged using Axioplan2 (Zeiss) microscope and 20x objective showing a higher resolution and confirming CTC status on the identified cell. Scale bar represents 20 µm.

In total, stained slides from seven metastatic breast cancer patients were scanned by the XCyto® 10 imager and compared by manual screening with Axioplan2 (Zeiss) microscope. In total, all CTCs that were identified by manual screening could be found by application of pre-established gating parameters (see Table 28). In addition to that, four CTCs were identified by XCyto® 10 only, meaning that their expression might have been weak and therefore not easily identified or just overseen by manual screening. Overall, the results show the suitability of XCyto® 10-based semi-automated screening for CTC detection.

Table 28: Summary of mBC patient samples and their CTC counts analyzed by either manual or XCyto® 10 -based semi-automated screening.

Sample No.	CTCs identified by manual screening	CTCs identified by XCyto® 10
1	2	2
2	1	1
3	5	5
4	0	1
5	0	0
6	4	4
7	14	17

5 Discussion

Early metastasis is the primary reason for the high lung cancer mortality. Critical in understanding the course of metastasization is knowledge on specific gene mutations of metastasis suppressor genes, epigenetic events, pathway alterations connected to early dissemination and the interplay of the microenvironment. Previous results from our group indicated that loss of HERC5 chromosomal location as well as its promoter hypermethylation correlate with shortened DSF and OS in NSCLC and moreover lead to an increase in DTCs and occurrence of brain metastases [99, 105, 106]. Until today, the majority of publications have attributed regulation of the innate immune response to the putative metastasis suppressor gene HERC5, while its connection to cancer and dissemination has been scarcely described so far. One of the major aims of this thesis therefore was to investigate HERC5 function in the context of NSCLC progression, taking into account the brain and bone microenvironment as major sites of metastasis, as well as the relation of innate immunity connected to HERC5 function. Therefore, whether traits of carcinogenicity and metastasization are related to differential HERC5 expression was investigated in various functional assays. Since HERC5 is the main E3 ligase of posttranslational modifier ISG15 in the cell, identification of novel ISGylation target proteins of HERC5 was performed in cancer cells. Recent studies connected ISG15 as well as ISGylation to multivesicular body (MVB) formation. The impact of HERC5-dependent ISGylation was therefore investigated in the context of quantitative EV secretion and proteome analysis of EV content. Furthermore, initial studies on pre-analytical parameters influencing the outcome of liquid biopsy studies were performed. These studies included determining the feasibility of obtaining several biological analytes from a single blood draw as well as establishing a semi-automated CTC detection approach, with the final goal of establishment of a HERC5-based liquid biopsy assay.

5.1 Influence of HERC5 expression levels on tumorigenicity

In order to study whether HERC5 could function as a metastasis suppressor gene, different *in vitro* cell lines were chosen as model systems based on their basal mRNA and protein expression. The successful establishment of two overexpressing (HTB56 and H1395) and one knock-out (A549) cell line was validated by Western blot and RT-qPCR. Afterwards, the effect of differential HERC5 expression on different oncogenic properties was measured in several functional assays. In general, proliferation remained unaffected by modified HERC5 expression regardless of the model cell line. HTB56 HERC5 OE cells showed a decreased clonogenic potential as well as a reduced capacity of forming colonies under anchorage-independent conditions in comparison to its corresponding empty vector control. Migratory behavior was furthermore elevated under low HERC5

levels in both modified HTB56 and A549 cell lines, while invasive potential remained unchanged. Taken together, the increase of clonogenic and anchorage-independent growth as well as migration further supports the notion that HERC5 acts as a metastasis suppressor [99]. Metastasis suppressor genes are defined to regulate the escape of cancer cells from primary sites, and the invasion and growth in secondary organs without affecting primary tumor growth [119]. Since no enhancement of proliferative traits could be observed, HERC5 might thus not function as a tumor suppressor gene which are defined to inhibit cell cycle progression, proliferation and division [120].

A second overexpression system was established to validate the initial observation of elevated aggressiveness of HTB56 cells due to HERC5 depletion. The H1395 cells were chosen as an additional model system based on their low endogenous HERC5 expression level. However, the parental H1395 cells did not exhibit an aggressive phenotype and overexpression of HERC5 in this cell line did not alter these characteristics, making functional investigation unfeasible. Only few studies exist on H1395 cells, although in these studies the cells showed the ability to form colonies under anchorage-independent growth conditions [121]. In the study by Starczynowski *et al.*, up to 10^4 cells were seeded, while we used 3×10^3 cells, which is a standard cell number used for the other cell lines. Migratory capability has furthermore been described for H1395 cells before. Again, in a published study a very high number of cells was used (10^5 instead of 2×10^4 used here) and a prolonged incubation time of 24 h instead of 16 h [122]. Hence, assays could be repeated using different experimental parameters, however, the biological relevance of such experiments is questionable.

Since low HERC5 levels in NSCLC patients have been connected to occurrence of brain metastases and DTCs in the bone marrow [99, 106], it is conceivable that also microenvironmental factors play a major role in influencing metastatic outgrowth in a HERC5-dependent manner. By repeating the functional assays with conditioned media from primary astrocytes and murine pre-osteoblasts it was investigated whether secreted factors from osteoblasts or astrocytes have an influence on HERC5-related aggressive phenotype. In this setting, no significant differences resulting from modified HERC5 expression could be observed in any of the functional assays. Previously found differences in standard media setting were even diminished under these conditions.

Using conditioned media, variances between replicates are increased in all assays in comparison to standard media, possibly caused by variations in cytokine release during collection of the media of different cell passages and storage [123]. Cytokines are highly prone to degradation over time, however, their storage is necessary during the course of performing different biological replicates. These variations could lead to increased variance. Significance is thus reduced since calculation of p-values is based on variance and dispersion of the data in both student's t-test as well as in

Wilcoxon-rank-sum test applied in this context. The use of astrocytes and murine pre-osteoblasts is moreover a mere approach of modeling the microenvironment of brain and bone, respectively. This model might be, however, insufficient when trying to mimic the intricate interplay of the vast variety of cells present in these respective organs. Apart from endothelial cells, astrocytes, microglia and pericytes form the blood-brain-barrier, which selectively separates the brain from the blood circulation [124]. Astrocyte function includes support and protection of neurons as well as interaction with endothelial cells, thereby regulating tight junction maintenance and thus barrier tightness [125]. Microglia, which are a part of the blood-brain-barrier as well, participate in immune surveillance of the central nervous system. They are macrophages which are capable of e.g. engulfing microorganisms as well as secreting pro-inflammatory mediators such as interleukin 1 beta (IL-1β) and TNFα [124]. These cells might therefore be more suitable for the usage of conditioned media in the diverse functional assays performed here as their secreted inflammatory cytokines might more strongly influence HERC5 expression levels, a topic that will be discussed in more detail in the following sections. The usage of immortalized murine pre-osteoblasts furthermore might not represent the optimal cell line for functional assays, and human cells might reflect species-specific growth factors and cytokines much better. Moreover, it is of interest to analyze cellular behavior upon differential HERC5 expression with further differentiation states of different cells present in the bone marrow such as osteoblasts or osteoclasts [126].

Based on the finding that cells with a low endogenous HERC5 expression (HTB56 EC) show an increased clonogenic potential, anchorage-independent growth and migratory capacity compared to HERC5 overexpressing cells, the influence of possible changes of global gene expression affected by modified HERC5 expression was assessed by RNAseq in these cell lines. Surprisingly, the expression of only two genes was found significantly altered besides *HERC5* after correction for multiple testing. Fibroblast Growth Factor 7 (*FGF7*) was found to be upregulated in OE cells, while Collagen Type XII Alpha 1 Chain (*COL12A1*) was downregulated. *COL12A1* is a member of the fibril-associated collagens [127]. It is found in type I collagen containing tissue and thus collagen XIIA is involved in the regulation of mechanical properties of collagen fibril bundles [127]. It is furthermore necessary for osteoblast/osteocyte differentiation. Hence, its downregulation has been described to cause muscle weakness and skeletal abnormalities [127]. Its upregulation, however, has been described in also numerous epithelial carcinomas such as gastric, breast and renal cancer and is also associated with poor overall survival and metastasis formation in these entities [128, 129, 130, 131]. Although the mode of action is not completely understood, collagen XIIA was described to promote cell migration via a positive feedback sustained by MAPK pathway in gastric cancer [132]. Since upregulation of *COL12A1* is likewise observed in NSCLC cells with low endogenous HERC5 expression

(HTB56 EC), the previously observed increase in migratory potential in these cells might be partially associated with *COL12A1* upregulation. FGF7 is a paracrine growth factor that exerts its function through activation of receptor tyrosine kinase FGFR2b [133]. Upon binding, different signaling pathways resulting in mitogenic and cell survival are activated [134]. In the context of cancer, FGF7 seems to play different roles depending on the specific entity. Loss of FGFR2b signaling was associated with prostate cancer progression [135], while in ovarian and cervical cancer FGF7 is highly expressed and promotes cell proliferation and metastasis [134, 136]. *COL12A1* and *FGF7* should therefore be further investigated in other cell lines by also modifying their expression or by pharmacological inhibition. However, the amount of differentially expressed genes found by RNAseq was unexpectedly low given the observed phenotypical changes in functional assays. Since HERC5 has so far been predominantly described as a mediator of post-translational modification due to transfer of ISG15, this function might lead to changes in the proteome, resulting in increased aggressive traits possibly related to metastasization. HERC5 might therefore predominantly act on protein rather than on mRNA levels.

Taken together, the functional analyses of cell lines with modified HERC5 expression show that HERC5 depletion causes more aggressive traits, elevating the potential to migrate, to grow limitlessly in the absence of neighboring cells and without attachment to a solid surface. These characteristics were not altered in the presence of brain and bone microenvironments. Downstream analysis of alterations in gene expression revealed two genes which could be involved in rendering cells more aggressive when HERC5 levels are low. The low number of genes, however, leads to the assumption that HERC5 is involved in protein rather than mRNA regulation.

5.2   HERC5 expression in the immune response

Due to the fact that HERC5 plays a role within immunological responses e.g. in viral infections, here it was investigated whether the potential metastasis suppressive effects of HERC5 in NSCLC is mediated through an interaction with the immune system. Inflammation of the lung is observed in most lung cancer patients due to tobacco consumption. Chronic inflammatory lung diseases such as COPD have been furthermore linked to malignant transformation and both smoking and COPD cause innate as well as adaptive immune responses [137]. Thus, the tumor microenvironment of the lung is comprised of a heterogenous and complex interplay of tumor and stromal cells [138]. The cellular components of the stroma includes endothelial cells, cancer-associated fibroblasts (CAFs), immune cells such as tumor-associated macrophages (TAMs), regulatory T cells, NK cells, dendritic cells, and tumor-infiltrating lymphocytes [15, 138, 139]. These inflammatory

cells are responsible for releasing a variety of cytokines, which in turn regulate different signaling pathways and contribute to growth and survival or apoptosis.

Different cytokines have been described to upregulate HERC5 expression in e.g. endothelial cells but also A549 NSCLC cell line. These include IFNα, IFNβ, IL-1β TNFα and LPS [78, 80, 81]. Even though all of the aforementioned cytokines are mainly related to innate immunity, they exhibit multifunctional but distinct biological effects. IFNα and IFNβ are type I IFNs and predominantly involved in antiviral defense mechanisms. Activation of their signaling pathways via receptors IFNAR-1 and -2 ultimately leads to transcription of IFN-stimulated response element genes to establish an antiviral state [140]. Induction by LPS mainly occurs in bacterial infections since it is an integral component of the outer membrane of gram-negative bacteria [141]. While viral and bacterial infections have not been described as the main cause of lung cancer tumorigenesis, however, innate immune responses in general play a role in lung cancer progression [142].

Besides, the connection of adaptive immunity and lung cancer can be observed due to the significant improvements of primary and metastatic lung cancer management with the introduction of immune checkpoint blockade therapies using e.g. PD-1 or CTLA-4 targeting drugs. The use of these immuno-oncology drugs in turn leads to induction of IFNγ expression [143]. Both innate and adaptive immune responses thus act in corporation and are often overlapping during tumorigenesis and treatment response.

Nevertheless, proteomic analyses of cytokines from lung cancer serum samples revealed the presence of various types of interleukins (ILs), vascular endothelial growth factor, TNFα and IFNγ [144]. Here, the focus was to study the effect of IFNγ and TNFα treatment in different cell lines with genetically modified HERC5 expression. We could show that stimulation with IFNγ alone leads to a strong induction of *HERC5* mRNA expression in HTB56 cells, which cannot be observed under TNFα treatment or combination of both cytokines. Interestingly, on the protein level no upregulation of HERC5 is observed and furthermore does not lead to an increase in neither free ISG15 nor ISGylated proteins. This discrepancy between mRNA levels and protein levels under IFNγ leads to the assumption that translation is perturbed to at least some extent. This discrepancy was, however, not observed in A549 cell line. *HERC5* mRNA levels in these cells was more strongly induced under TNFα than IFNγ treatment, but showed the highest induction when cytokines were combined. The same pattern was observed for HERC5 protein expression and furthermore showed a strong increase in ISGylated protein levels. A synergistic cooperative effect of TNFα and IFNγ has been previously described [116]. IFNγ exerts its function through binding to receptor dimer IFNGR1 and IFNGR2, and subsequent cross-activation of Jak1 and Jak2 kinases. Through phosphorylation, STAT1 homodimers form and transcription of IFNγ-activated site genes is

induced after translocation into the nucleus [145]. TNFα activates NF-κB signaling lead-ing to transcription of inflammation-related genes [146]. Their combination, however, leads to interactions between both families of transcription factors which cooperatively regulate the transcription of a large number of important immunoregulatory genes such as class I MHC [116]. This described synergistic effect could explain the enhancement HERC5 up-regulation in NSCLC cell lines.

HERC5 expression in A549 KO cells remained low or undetectable under IFNγ treatment, but showed a slight upregulation using TNFα. However, no upregulation was expected due to CRISPR-Cas9 induced knockout of *HERC5* gene. PCR and subse-quent Sanger sequencing analysis of different knockout clones showed deletions leading to frameshift mutations. Different clones were then combined in order to reduce the influence of possible off-target effects. Nevertheless, it is possible that knock-out was not successful in one of the 4q alleles in A549 cells. Chromosomal imbalance has been reported for this cell line, which displays an aneuploid karyotype with five copies of chromosome 4 [147]. Additional deeper sequencing could therefore validate the total *HERC5* knockout in the established A549 cell line after combination of several clones as well as after passaging the cells over time.

Induction of free, unconjugated ISG15 expression by TNFα and IFNγ was further-more most strongly observed in A549 KO cells in comparison to other cell lines. More-over, the amount of ISGylation was comparatively low in A549 KO cells using both cytokines in combination. Due to HERC5 depletion in A549 KO cells, the ratio between free ISG15 and ISGylated proteins is thus most strongly shifted towards free ISG15 levels since it cannot be transferred onto target proteins, resulting in diminished ISGyla-tion. In the corresponding parental cells, the strongest induction of ISGylated proteins is observed, indicating that HERC5 acts as the main ISG15 E3 ligase in this NSCLC cell line. Due to low endogenous HERC5 and ISG15 expression within these cells, the combination of TNFα and IFNγ thus represents a suitable system for the induction of protein ISGylation.

Additional NSCLC cell lines were analyzed on either mRNA (H1975) or protein level (H1395) after treatment with TNFα and IFNγ. In H1975 cells, *HERC5* expression levels remained unchanged under cytokine treatment. H1395 cells unexpectedly exhibited a strong increase in HERC5 protein levels as well as ISGylation under TNFα and combined cytokine treatment. In previous studies of our group, this cell line showed homozygous promoter hypermethylation of the *HERC5* gene [99], thus HERC5 expression should in principle be repressed. Its upregulation could possibly result from methylation pattern changes under inflammatory conditions, as this phenomenon has been observed for TNFα. This cytokine is able to induce DNA demethylation of *IL-32* gene in HEK293 cells, mediated by a methylcytosine dioxygenase in an NF-κB-dependent manner [148].

Nevertheless, more research is necessary in this respect to understand these mechanisms of transcription or translation initiation and whether cytokine treatment can also induce demethylation in NSCLC. In order to evaluate changes between transcriptional and translational levels in more detail, H1395 and H1975 cell lines should be included in further studies.

Here, it was shown that by treatment with inflammatory cytokines IFNγ and TNFα, HERC5 mRNA as well as protein expression can be induced in different NSCLC cell lines. HERC5 has been described as the main E3 ISGylase in the cell and therefore as a regulator of the innate immune system. As ISGylation of protein targets is induced within different NSCLC cells, HERC5 could therefore be involved in innate immune responses in lung cancer. By TNFα and IFNγ treatment, free, unconjugated ISG15 protein levels were most prominently increased in a HERC5 KO model, while the amount of ISGylated proteins was highest in the corresponding parental cell line. This indicates that HERC5 acts as the main ISG15 ligase also in these lung cancer cells. Furthermore, through cytokine treatment the establishment of a robust ISGylation system could be achieved, which can be used for subsequent analysis of HERC5-dependent ISGylation targets.

5.3   HERC5-dependent ISGylation of target proteins

The expression of ISG15 and its conjugating enzymes is deregulated in various cancer entities [107]. It was therefore investigated in this study whether HERC5-dependent ISGylation might be of importance in NSCLC progression as well. Since RNAseq data did not show alterations of global gene expression, the function of HERC5 in post-translational modification and its ISGylation targets might thus give more insight into the previously observed association with metastatic spread.

The combination of TNFα and IFNγ resulted in the highest induction of HERC5 expression as well as ISGylation levels in A549 parental cell line. In order to detect proteins specifically ISGylated by HERC5, this cell line model was therefore selected along with its KO counterpart for the establishment of an ISG15 IP assay. After having validated the feasibility of enriching ISGylated proteins, mass spectrometry-based SILAC approach was used to identify HERC5 ISGylated target proteins. Here, 42 targets were found including the positive control ISG15.

The proteins that were uniquely identified in this study did not show any enrichment of common specific pathways or biological processes. However, some of the ISGylation targets represent interesting proteins that could be worthy of a further evaluation. The highest H/L ratio among the identified proteins was found for NADH Dehydrogenase [Ubiquinone] Iron-Sulfur Protein 2, Mitochondrial (NDUFS2), which is a part of mitochondrial respiratory chain complex I. It catalyzes the initial transfer of electrons in the

transport chain and in database meta-analysis, high NDUFS2 expression correlates with shortened OS in lung, breast and ovarian cancers [149]. Interestingly, its interaction with another target protein identified in this study has been recently described. S100 calcium-binding protein A4 (S100A4) is a metastasis-promoting protein that - apart from cell differentiation and apoptosis - is also involved in mitochondrial metabolism [150, 151]. In NSCLC, S100A4 is capable of reprogramming energy metabolism and promoting lung cancer invasion and metastasis by up-regulating NDUFS2 expression also in A549 cells [151].

Three previous studies about ISGylation which used a similar experimental approach were published by Zhao *et al.*, Giannakopoulos *et al.*, and Wong *et al.* identified 158, 76, and 174 proteins, respectively. In these studies, Hela cells (cervical adenocarcinoma), U973 cells (histiocytic lymphoma), murine embryonic fibroblasts, and A549 cells were used. Combined, 300 unique protein targets were found, with little overlap between the studies [81, 87, 88]. Also in these studies, no clear prediction of biological function for protein ISGylation could be made with a broad variety of pathways being affected such as cytoskeletal organization, stress responses, translation and transcription or RNA splicing [89].

Little overlap between the 42 proteins identified in this study and those proteins from the aforementioned studies was found. Only three proteins were described in at least one other publication. Nascent Polypeptide Associated Complex Subunit Alpha (NACA) was identified in the proteomics study by Zhao *et al.* [87]. It acts as a cytosolic chaperone and binds to unfolded nascent proteins emerging from ribosomes which lack signal peptide sequences [152]. It is furthermore upregulated in e.g. breast adenocarcinomas and exerts anti-apoptotic function in several types of cancer cells [152, 153]. In the same study by Zhao *et al.*, Procollagen-Lysine,2-Oxoglutarate 5-Dioxygenase 1 (PLOD1) was likewise identified [87]. PLOD1 catalyzes the hydroxylation of lysyl residues in collagen-like peptides which in turn provides attachment sites for carbohydrates, hence regulating collagen cross-linking and extracellular matrix formation [154]. Increased collagen cross-linking enhances cancer cell migration and invasion and has been shown to be highly expressed in e.g. gastric and colorectal cancers [154, 155]. Interestingly, Ubiquitin Like Modifier Activating Enzyme 1 (UBA1) was independently identified by Giannakopoulos *et al.* and Wong *et al.* apart from this study [81, 88]. UBA1 is the E1 ubiquitin conjugating enzyme to target cellular proteins for degradation. As an integral part of the proteasomal pathway, it is involved in almost all functions in the human cell but shows increased activity in cancer cells [156]. Inhibition of its E1 enzyme was described to delay leukemia tumor growth in mouse models [157].

In comparison to the three described proteomics studies, the amount of ISGylated target proteins in this study is rather low. It has to be noted that all studies established

different systems and cell lines for enrichment and analysis of target proteins, which makes the comparison challenging. Furthermore, IFNβ was used in all other studies, while in this study, cells were treated with TNFα and IFNγ in order to induce ISGylation. Furthermore, in the other studies, the detection of target proteins was conducted by direct mass spectrometry approaches, whereas here a SILAC-based mass spectrometry approach was chosen. This proteomics analysis has been shown to enhance specificity by strongly reducing the background of false-positive interactions [158]. In SILAC-based experiments, two proteomes are distiguishable by growing one cell population in medium containing normal or 'light' amino acids while the other population is grown using medium with 'heavy' amino acids. Proteins from both populations are mixed in a 1:1 ratio and analyzed by mass spectrometry. Peptides found in both populations appear as a pair in the mass spectra, characterized by a shift induced by their weight difference, and their peak intensities are directly proportional to their abundance [158]. This SILAC-based method should therefore be more specific compared to the other studies, possibly explaining the lower amount of identified proteins. Clearly here expression of HERC5 was induced artificially using two cytokines and thus different types of activation could obviously lead to a different set of ISGylated proteins and a bigger overlap with the other studies. In order to reduce this bias of cytokine induction, robust *in vitro* ISGylation could also be achieved by overexpression of all proteins of the ISGylation machinery [82]. The choice of cell lines naturally leads to differences in ISGylation targets as well, as also indicated by the low amount of overlap between results presented here and previously mentioned studies.

Some of the proteins found by SILAC-based mass spectrometry were chosen to be validated by Western blot analysis. This approach has, however, not been successful so far. Protein ISGylation causes a mass shift of 15 kDa which should appear as an additional band above the unconjugated protein on the Western blot. Only a small fraction of proteins is ISGylated in comparison to the overall pool of a specific target protein, making their detection challenging [87]. Usually, long exposure times are needed to detect ISGylated target proteins but this approach is oftentimes not sufficient. It has been described that ISGylation is observable when cells are transfected with a plasmid system consisting of the target protein, E1, E2 and E3 ligases as well as ISG15 [89].

Unlike the immense knowledge available on ubiquitin, the role of ubiquitin-like modifier ISG15 within the cell as well as in tumorigenesis remains much more unclear. Several different roles of protein ISGylation have been described so far [159]. ISGylation of viral proteins seems to impact viral protein-protein interactions thereby destabilizing capsid formation, impairing viral RNA processing or counteracting host translational shutoff by viruses [89, 92, 160]. Many effectors of IFN signaling in the human host cell

such as Stat1 are ISGylated, supporting sustained activation of this pathway [161]. Apart from anti-viral activity, Zhao *et al.* furthermore suggested a possible cross-talk between ISG15 and ubiquitin pathways as in their proteomic study, another protein involved in ubiquitin conjugation (Ubc13) was also identified [87]. ISGylation does not seem to direct proteins for degradation by the proteasome, instead, blocking of ISG15 protein conjugation increases levels of polyubiquitinated proteins, hence negatively regulating proteasomal degradation [162]. Overall, while no structural consequence of ISGylated substrates is known, ISGylation might result in their aggregation, changes in subcellular localization or in the inability to interact with binding partners [107]. Interestingly, ISGylation of Tumor Susceptibility 101 (TSG101), an important component of the ESCRT (Endosomal Sorting Complexes Required for Transport) machinery and MVBs, has been reported to inhibit exosome secretion [107]. Of note, TSG101 was not found in the SILAC analysis of ISGylated proteins conducted here.

To conclude, in an IP approach with ISG15 as bait, 42 different protein targets of HERC5-mediated ISGylation were identified under treatment of TNFα and IFNγ. Even though no clear involvement in specific signaling pathways could be found, some of the ISGylation target proteins have been previously associated with deregulation in several cancer entities. However, the fate of these ISGylated proteins is still unclear and thus how these proteins are functionally linked to NSCLC carcinogenesis and especially to immune response still has to be resolved.

5.4   Influence of HERC5 protein on EV secretion

Exosome-mediated signaling affects many aspects of tumorigenesis and metastasis formation [163]. Communication between tumor and stromal cells in the TME can for example induce differentiation of fibroblasts into their cancer-associated form (CAF) which can promote tumor growth and metastasis [164]. Furthermore, proliferative and angiogenic pathways can be promoted and immune suppression or activation can be induced [165, 166]. Exosomes furthermore play a role in initiation of metastatic niches [167]. They have been shown to educate cells and inducing a pro-metastatic phenotype by activation of oncoproteins [167]. Furthermore, cells are able to uptake tumor-derived exosomes which carry organ-specific integrins thereby influencing organotropism of metastasis [67].

In HEK293 cells, ISGylation of TSG101 was shown to lead to a decrease in exosomal secretion by re-routing multivesicular bodies (MVB) to lysosomes, leading to their degradation [107]. Due to the suggested role of ISGylation in exosomal secretion, it was investigated whether differential HERC5 expression could lead to impairments of this pathway as well. Here, it could be shown that under inflammatory cytokines TNFα

and IFNγ, diminished HERC5 expression leads to an increase in EV release. Protein cargo in EVs is furthermore modified, indicating an important role of HERC5 in the immune response. By using induction of the ISGylation machinery by TNFα and IFNγ, analysis of the amount of EV secretion was performed. Results were obtained by NTA measurements and SDS-PAGE. Our results indicate that low HERC5 levels in A549 KO cells leads to elevated particle concentrations as well as protein load, thus to an increase in released EVs in comparison to parental cells.

It was further investigated whether not only the amount of particles is enhanced in KO cells but also if there is a qualitative difference in protein content compared to parental cells. Contrary to the assumption that exosomes and EVs are a mere reflection of the cellular overall state, they are reported to selectively influence their cargo and can furthermore reflect changes in the cell microenvironment [165], which might aid in understanding HERC5-related cancer progression. Even though exact mechanisms are still poorly understood, EV composition can thus influence cell-cell communication [165].

By using ultracentrifugation-based enrichment from cellular supernatant of cells grown in SILAC heavy or light media, EVs were subjected to SILAC mass spectrometry measurements. In SILAC-based proteomics studies, dialyzed FCS has to be used so that no contaminating, non-labeled amino acids impair incorporation of heavy amino acids. This medium still contains bovine-derived EVs which needs to be depleted for an accurate identification of differences in EV content due to the high sensitivity of SILAC measurements [158]. However, even after depletion using a protocol by Théry *et al.* [117], a large fraction of unlabeled peptides was identified. Depletion of bovine EVs was therefore not optimal leading to a strong contamination and thus impairing data quality. Even though the results were screened against a bovine database it cannot be excluded that some homologous proteins from bovine and human species can be completely distinguished and the experiments have to be repeated.

Nevertheless, preliminary results from one replicate were obtained, identifying 39 proteins enriched in EVs from KO samples while no enrichment in parental cells was found. The most prominent finding was the enrichment of Macrophage migration inhibitory factor (MIF) in KO exosomes. MIF is a regulator of the innate immune responses which exerts its function through cytokine-like activation of ERK1-ERK2-MAPK pathway [168]. Its upregulation has been described in many cancer entities, including NSCLC [169].
Interestingly, Integrin alpha-3 (ITGA3) was identified in EVs from KO cells in this study, a protein whose upregulation has been frequently described in the context of cancer and metastasis as well [170]. Moreover, integrins were described to have an impact of organotropism of metastasis [67]. Tetraspanins CD9 and CD81 were identified

in the samples as well, providing evidence that at least a fraction of the enriched EVs consists of exosomes. It was not expected, however, to find enrichment of these exosomal markers in the KO samples, as the amount of analyzed EVs should be equal, while the protein cargo independent of differential EV amounts should be assessed. Due to the probable presence of bovine EVs and other contaminations in the sample, measurements of protein concentrations might have therefore been impaired as well, underlining once more the preliminary nature of these results.

In contrast to SILAC analysis of ISGylated proteins of the cell lysates, in EVs enrichment of several affected pathways could be identified by GO term annotation analysis. First, from each differentially enriched protein in the EVs, GO term annotation was analyzed for each target protein. After categorization into the most prominent findings, frequencies were assessed and revealed the connection to immunity-related pathways in 26% of the proteins. Terms connected to cell-adhesion were even more common (33%). Additionally, PANTHER database was searched for GO term enrichment analysis which confirmed connection to innate immune regulation in 33% of the pathways. Furthermore, exosomal secretion pathways as well as cell adhesion and angiogenesis could be identified. As many of these pathways can be related to tumorigenesis, these findings indicate that metastatic traits in HERC5-depleted cells could be related to altered protein cargo. Low HERC5 levels can furthermore be connected to an increased cross-talk with innate immune processes.

One of the anti-viral functions of ISGylation includes blocking budding of viral particles in order to prevent the spread of the pathogens [159]. In a similar manner, ISGylation could lead to inhibition of exosome secretion in cancer settings, thereby minimizing cell-to-cell communication and altering immune modulation. Due to the obtained preliminary results that KO cells with diminished ISGylation release more EVs and potentially carry transformative protein cargo, the role of HERC5 in the context of ISGylation and EV release could therefore give valuable information on NSCLC disease progression and metastasis formation and should be investigated further.

While ISGylation of TSG101 was shown to be sufficient to reduce exosome secretion, here, release of EVs was analyzed. EV is a general term for particles of various sites containing a lipid bilayer without the ability to replicate and without a nucleus [117]. Exosomes are type of EVs derived from endosomal MVB compartments, about 50 - 100 nm in size and defined as important mediators of intercellular communication [159]. Their biological cargo includes proteins, nucleic acids and lipids [165]. A possible way to confirm that enriched vesicles consist of exosomes is the detection of exosomal markers tetraspanins CD9, CD63, CD81 or the previously described, ESCRT-related TSG101 e.g. on Western blots or by IF staining [107, 165]. Apart from the detection of exosomal markers, evaluation of particle purity needs to be assessed. Here, NTA

measurements were performed to analyze the size distributions of the obtained particles. These analyses showed peaks of around 120 nm, which is still as expected and of an acceptable size due to the known heterogeneity in exosomal sizes [117]. However, in oncological settings, many studies are based on heterogeneous populations of EVs, most of which have actually shown to play a role [163]. Thus, ultracentrifugation was chosen as it is still considered the gold standard which is used for enrichment of vesicles of different nature.

In summary, due to a previous study which linked ISGylation to inhibition of ex-osomal secretion [107], in this thesis the effect of HERC5 expression on quantitative and qualitative EV secretion was assessed. Here, it was shown that in HERC5-depleted NSCLC cells, EV release is elevated in an inflammatory setting using TNFα and IFNγ, indicating a suppressive influence of HERC5 on vesicle secretion in connection to immune responses. Preliminary results furthermore showed that EV protein cargo differs between HERC5-depleted NSCLC cells and the corresponding parental cell line, and some of these identified proteins have been associated with tumorigenesis before. HERC5-depletion might therefore induce the directional transfer of specific proteins possibly involved in cancer progression onto surrounding cells, thus actively altering their protein composition. The effect of this transfer remains, however, unclear. In contrast to the SILAC analysis of cells, EV SILAC analyses showed an enrichment in various signaling pathways and thus a possible connection between HERC5 expression and the immune response.

5.5   Assessment of pre-analytical parameters in liquid biopsy

Apart from analysis of HERC5 and its role in NSCLC progression, different pre-analytical variables influencing liquid biopsy results were furthermore analyzed. The studies were performed with blood taken from metastatic melanoma, or metastatic breast cancer patients as well as cell lines from the respective tumor entity.

The first study dealt with the feasibility of a combined analysis of several biological analytes from a single blood draw. CTCs, ctDNA and miRNAs from total plasma as well as EVs were assessed. It was furthermore analyzed whether different blood collection tubes (EDTA, Streck and Transfix tubes) give different results concerning these analytes. Many different studies exist today evaluating optimal protocols for single analytes. However, due to the overlapping and additive nature of many of the biomarkers a greater clinical power and accuracy can be obtained when combining several parameters. The potential great power of such multianalyte analyses was lately shown by e.g. Yang *et al.* By applying machine learning algorithms to multi-analyte liquid biopsy data in pancreatic cancer patients the study achieved significantly higher accuracy for disease

staging (84%) than imaging alone (accuracy = 64%; p <0.05) [171]. To our knowledge our study was, however, the first of its kind combining CTC, ctDNA and miRNA liquid biopsy data from a single tube.

Here we could show that due to increased hemolysis observed in Transfix tubes, only CTC analysis could be performed from these tubes. Obviously although Transfix tubes are very well suited for certain CTC detection methods [111] they are not suitable for multi-analyte analysis. CTC counts were in general very low in comparison to other melanoma studies with a similar enrichment technique [172, 173, 174]; in only 15% of EDTA blood samples CTCs were identified while Streck and Transfix tubes were negative for CTCs. Similarly to NSCLC, melanoma CTCs harbor a great heterogeneity of marker expression, therefore, their detection could be optimized by using a different enrichment system or staining protocol and including antibodies targeting further markers and improving detection sensitivity [175, 176, 177]. Analysis of ctDNA in general did not show significant differences in neither concentration nor in mutation frequencies, which is not of a surprise as the samples were processed immediately. Stability of ctDNA has been shown to decrease over time, but is highly dependent on the blood collection tube [178, 179]. In one patient a discrepancy in ctDNA mutations was observed, however, a replicate could not be performed to rule out the possibility of a technical error. Differences in size distributions, morphology and sample purity of EVs could neither be observed between EDTA and Streck tubes. However, miRNA NGS results showed lower UMI counts in Streck samples, indicating a diminished detection sensitivity compared to EDTA tubes. Analysis of differential miRNA expression was performed by using geNorm as well as Normfinder normalization algorithms. Irrespective of either tube or normalization method, less differentially regulated miRNAs were found in plasma samples in comparison to EV samples. Furthermore, in plasma samples no overlap of miRNAs could be detected while miRNAs from EVs showed six differentially, indicating that miRNAs from plasma are more heavily influenced by pre-analytic factors such as the choice of blood collection tube and data processing than compared to miRNAs in EVs.

In addition, the suitability of EV analyses for biomarker detection and prediction could be shown by an orthogonal validation approach. From those miRNAs shared between EDTA and Streck EV samples as well as both normalization methods, 2 of 3 analyzed miRNAs could be confirmed by RT-qPCR. Both hsa-miR-200c and hsa-miR-375 are reported to be deregulated in melanoma development and progression [180, 181]. To be mentioned, large differences in identification of differential miRNAs were observed between the two normalization algorithms. In both plasma and EV samples, only a small fraction of miRNAs were overlapping between the two algorithms. Analysis of differential expression is therefore also largely dependent on the choice of normalization

method, and therefore adding a level of complexity when assessing the potential clinical suitability of different miRNAs as liquid biopsy biomarkers. Therefore, for an optimal workflow and in order to obtain standardized results, strict SOPs need to be established and used throughout a study.

In addition to evaluation of blood collection tube influence on liquid biomarkers, a semi-automated screening method of CTCs enriched by the Parsortix® device was established [118]. CTCs represent a rare and heterogenous population of blood-based analytes, which differ in size, frequency, and expression depending on disease state and cancer entity. Their enumeration and characterization is usually performed by analysis of immuno-fluorescence staining of epithelial markers such as EpCAM or keratins. Since the identification is often performed manually, this process induces errors and user biases, and needs to be standardized to improve comparability across different laboratories. Accurate and re-producible assessment thus requires image analysis tools. Surprisingly, so far only few studies exist on automated CTC calling, since most approaches require machine learning techniques to successfully discriminate between tumor cells and contaminating blood cells [182, 183].

Here, in order to reduce bias from manual evaluation of CTC enumeration, the XCyto® 10 quantitative cell imager was used. This device allows setting up detection thresholds of different expression intensities from several cell populations in a similar manner as FACS analyses. However, the addition of visual inspection of the chosen cells and higher resolution imaging of individual cells allows an accurate validation of the initial gating results. Here, CTC populations were distinguished according to their pan-keratin staining intensity and distinction from CD45-positive contaminating leukocytes.

First, gating parameters were established which successfully separated pan-keratin positive tumor cells from CD45-positive leukocytes in a cell line-based model. Using the same gating, blood from breast cancer patients was then analyzed with the XCyto® 10 and compared with manual screening using Axioplan 2 microscope. The feasibility of using the semi-automated approach could be validated due to the high concordance between both enumeration methods. XCyto® 10-based screening could even detect CTCs which were not found manually, underlining the suitability of this identification method.

Taken together, here we could show that the analysis of ctDNA, CTC, and miRNAs is possible from one blood collection tube, but the outcome of the analysis is strongly dependent of the blood collection tube. The establishment of a semi-automated CTC screening workflow furthermore enables precise and standardized enumeration while reducing bias from individual image analysis. The combination of both studies therefore represent valuable prerequisites for the planned establishment of HERC5-based liquid biopsy analyses in the future.

5.6   Conclusion & Outlook

Metastasis formation is a complex process which involves the acquisition of phenotypic changes enabling the adaptation and survival in new environments. These processes usually involve deregulation of so-called metastasis promoting or suppressing genes. In principle, metastasis suppressor genes can influence any aspect of the metastatic cascade which includes escape from the primary site and intravasation, circulation in the bloodstream, endurance of pressure in blood vessels, extravasation, and survival and growth in distant organs [31].

Previous studies have proposed that HERC5 may act as a metastasis suppressor gene in NSCLC [99]. In this study, many different aspects of HERC5 function have been investigated to further elucidate its role within the metastatic cascade *in vitro*. The metastasis suppressing function rather than tumor suppressing function was supported by the fact that no effect on proliferative capacity was seen when HERC5 expression was manipulated in the NSCLC cell lines. It was, however, shown that HERC5 suppresses migratory traits which might enable tumor cells to evade from the primary tumor site. Anchorage-independent growth potential is furthermore increased which could lead to colony outgrowth prior to attachment at a secondary site. Clonogenic potential is elevated as well, indicating an increased ability to renew an entire cell population from a single cell. In summary, HERC5 depletion induces carcinogenic changes within different parts of the metastatic cascade (see Figure 43). These characteristics were also studied using conditioned media from astrocytes and pre-osteoblasts and were found to be diminished in the microenvironments of brain and bone. Hence, brain and bone microenvironmental factors do not seem to have an influence on HERC5-dependent aggressiveness.

The study of interactions between the different cell populations could, however, be improved. Different types of cells present in brain or bone microenvironment could be included in the assays. The assay set-up could be changed as well, replacing the usage of conditioned media to reduce the cytokine variations induced by passaging and degradation during storage. Co-culturing systems use cell cultivation set-ups while two or more cell populations have some form of contact between them [184]. While migration and invasion transwell assays already represent forms of co-culturing by allowing cells seeded at the bottom of the wells to secrete e.g. cytokines directionally into the vicinity of the cells in the chamber, proliferation, colony formation and anchorage-independent growth assays or 3D cultures would need other forms of co-culturing. One possibility could be here to utilize microfluidic systems e.g. fluid channel separation or membrane separation. This way, diffusible molecules could be exchanged between the different cell populations but are still spatially separated without disrupting communication [184].

RNAseq analysis of an overexpressing and control cell line (HTB56) was performed to assess potential alterations of transcription. On mRNA levels HERC5 influence on downstream pathways seem to be limited since only two genes, *COL12A1* and *FGF7*, were found to be deregulated. Although being identified after correction for multiple testing, it is necessary to verify these findings in an orthogonal validation approach by e.g. RT-qPCRs. Additional NSCLC cell lines would also need to be analyzed in order to confirm whether these mRNAs are in fact altered by differential HERC5 expression. While *COL12A1* and *FGF7* have been described in cancer settings, none of them have been identified as bona fide metastasis activating or suppressing genes so far. However, both could be associated with the observed aggressive phenotype of NSCLC cells with low HERC5 expression to some extent. Through the transfer of ISG15 onto target proteins, HERC5 predominantly acts on the post-translational modification level and thus might not be as relevant for changes in gene expression.

HERC5 function has so far been mainly connected to immune response mechanisms, e.g. defense against viral infections due to its role as an E3 ligase of ubiquitin-like modifier ISG15. SILAC-based proteomic analysis was chosen to minimize unspecific interactions e.g. through purification from antibodies in the IP pull-down assay. By the use of an ISG15-IP, covalent ISGylation could be achieved and in combination with induction by TNFα and IFNγ, a robust, standardized assay for HERC5-dependent ISGylation could be established. However, through of the activation by specific cytokines different types of pathways are activated, which leads to a biased approach. Thus, in order to analyze intrinsic ISGylated proteins, this setting could be optimized e.g. by overexpression of all proteins involved in the ISGylation machinery. Here, under inflammatory conditions several specific targets of HERC5-dependent ISGylation have been identified, which were increased in parental cell line samples compared to HERC5 KO cells. Even though no specific pathway was affected in this setting, some of these targets have been previously associated with an carcinogenic or metastatic phenotype. If the identified proteins are mediators of the observed aggressive phenotype, has yet to be validated by e.g. genetically altering the expression of these target proteins. However, the influence of ISGylation on target proteins is unclear and thus the exact role of ISGylation in the context of NSCLC remains elusive. Since different functions of ISGylation have been described depending on the target protein and setting [159], the role of ISGylation of each target might have to be analyzed individually.

To conclude, the influences of three cell types, which can be found in the different microenvironments on HERC5 function have been studied. While in our data brain and bone microenvironmental factors do not indicate an effect on tumorigenicity, influences of an inflammatory microenvironment elevating HERC5 expression as well as HERC5-dependent ISGylation could be confirmed in an NSCLC setting (see Figure 43).

Since HERC5 protein harbors two different functional domains, it remains elusive whether HERC5-induced phenotypical changes are connected to transfer of ISG15 through its HECT domain or whether its RLD domain has an influence as well. The ISGylation active site is located within the HERC5 HECT domain in which the conjugation onto target proteins is catalyzed by cysteine residue 994 [81]. In order to study the significance of ISGylation, this cysteine is commonly mutated to an alanine residue [81]. It should be thus investigated whether this active site is of importance in the context of NSCLC as well by site directed mutagenesis assays, inducing a mutation in HERC5 ISGylation active site and repeating functional assays. However, first attempts in cloning of a construct including this C994A alteration have not been successful so far.

While in the SILAC-based proteome study, cellular influences regarding HERC5 ISGylation targets have been analyzed, changes of EV composition were assessed from the same samples in parallel. Results indicate that HERC5 depletion induces quantitative and qualitative changes in EV release in an inflammatory setting. Some of the identified EV proteins have been attributed to carcinogenesis, however, the exact consequence on cell-cell-communication has to be investigated further. Functional annotation enrichment analysis indicated assigned the majority of pathways to immune response mechanism. This enrichment might, however, derive from specific cytokine induction and should thus be analyzed under different experimental settings. Overall, within the cell, mRNA expression changes as well as the amount altered pathways due to cytokine-induced ISGylation was low in comparison to extracellular changes, indicating a higher impact on extrinsic mechanisms of HERC5.

The analysis of EV content by SILAC-based methods was, however, hampered by the contamination of residual bovine FCS. In order to estimate the amount of contaminating EVs, depletion should thus be monitored more carefully. In general, ultracentrifugation-based enrichment methods are still considered the gold standard in EV enrichment, however they are known to enrich also vesicles of different sizes as well as contaminations such as lipoproteins [185]. Ultracentrifugation approaches could therefore be combined with an additional purification technique such as size exclusion chromatography. Apart from technical improvements regarding EV enrichment, the functional role of HERC5-dependent release of EVs in metastasis and immune modulation should be investigated further. Alterations in particle concentrations and protein cargo could elevate cross-talk with (immune) cells in the tumor microenvironment. These EVs might therefore be important mediators in either the establishment of a pre-metastatic niche or immune evasion evasion.

While SILAC analysis of EVs should be repeated to confirm protein cargo, the actual impact of EVs deriving from differential HERC5 expression under immune stimulation should be assessed as well. To evaluate a possible cross-talk with immune cells, EVs

from A549 parental and KO cells could be isolated. Co-cultures with PBMCs could be established to analyze whether these cells can be differentially activated by the EV cargo. By staining and subsequent FACS analysis, it could be investigated if the PBMCs have developed into different sub-populations. Another similar approach of assessing the cross-talk with immune cells could include immuno-profiling of PBMCs from NSCLC patients. The composition of PBMCs in blood from these patients could be analyzed by FACS. Subsequent correlation with HERC5 expression levels could reveal whether HERC5 has an influence on this composition. In case certain types of immune cells are activated by differential HERC5 expression, it should be also analyzed whether this activation could be mediated by the secretion of inflammatory cytokines. A possible way of investigation could be the usage of the highly sensitive Olink-technology, in which a large number of proteins can be analyzed simultaneously. Here, target proteins are recognized by pairs of antibodies which are conjugated to DNA oligonucleotides. Only if two matching antibodies are brought into proximity, DNA can amplified, thus achieving a high sensitivity and the possibility of multiplexing of multiple targets.

As previous studies have provided evidence that HERC5 has clinical relevance in NSCLC patients, this aspect could be investigated in more detail by the use of *in vivo* models. Preliminary mouse experiments have already been performed in our group by Angelika Mojzisch. In order to mimic a metastatic disease setting, luciferase-tagged A549 parental and HERC5 KO cells were used for intracardial injections in two groups of five nude mice each. The tumor growth was monitored according to luciferase expression assessed by BLI (bioluminescence imaging). At time of sacrifice, signals were significantly higher in mice injected with A549 HERC5 KO cells in brain and adrenal glands. The blood was furthermore screened for CTCs and the total amount of these cells was increased in mice injected with A549 KO cells as well. These preliminary results indicate a specific effect of HERC5 in early tumor dissemination. In further experiments, expression profiling of overt metastases could be performed to analyze a possible influence of differential HERC5 expression as well. As an indication for early dissemination, other organs should also be analyzed for the presence of micrometastases.

In principle, HERC5 levels in CTCs could be assessed for correlation of expression and survival. However, the lack of a suitable antibody for HERC5 IF staining has so far hampered this analysis. Metastasis suppressor genes often harbor epigenetic modifications such as methylation. *HERC5* has been further identified as a target gene often silenced by methylation [99]. Moreover, the methylation of a specific CpG island was shown to be of prognostic value which was furthermore correlated with early tumor dissemination and bad prognosis [99]. Thus, it should be assessed whether *HERC5* could be used as liquid biomarker on ctDNA for monitoring early relapse and prognosis. Methylation could e.g. be assessed here by highly sensitive digital
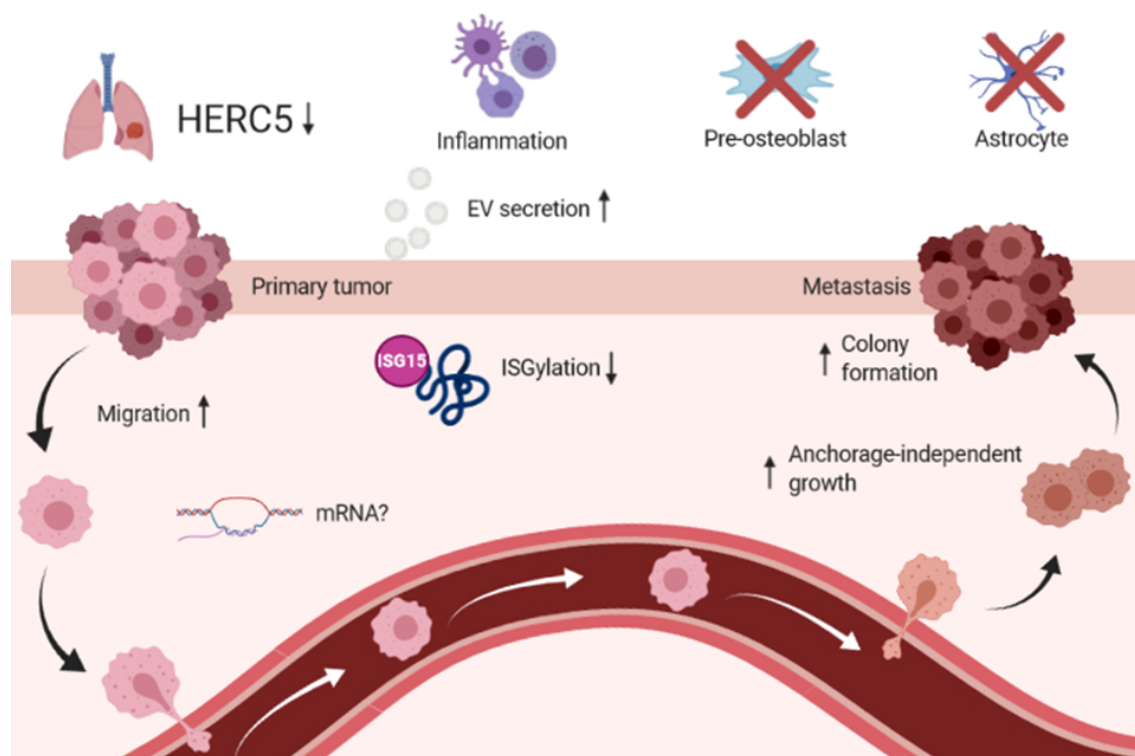
Figure 43: Schematic overview of different mode of carcinogenic actions of HERC5 in NSCLC metastasis. In cells with low HERC5 expression, migration, anchorage-independent growth and colony formation are elevated. These traits, however, are not influenced by either pre-osteoblast or astrocyte microenvironments. HERC5 levels have limited influence on mRNA expression of other proteins, whereas ISGylation of target proteins is largely dependent on HERC5 activity. Under inflammatory conditions ISGylation of proteins is diminished and EV secretion is elevated. The protein cargo is also changed with many proteins involved in pathways associated with immune response mechanisms. Image created in BioRender.com.

droplet PCR (ddPCR) approaches after bisulfite conversion of the ctDNA which induces the chemical conversion of unmethylated cytosines into thymidine, while methylated cytosines remain unchanged. This method therefore allows to distinguish between unmethylated and methylated state. The assessment of *HERC5* ctDNA methylation status in metastatic NSCLC patients before and during treatment could reveal changes in methylation patterns to correlate it to treatment response and to help understand its significance in the course of NSCLC progression.

To conclude, this thesis highlighted various novel aspects of HERC5-mediated tumorigenicity in lung cancer. An elevated aggressive phenotype could be observed which might be linked to different steps within the metastatic cascade. While its impact on cellular signaling pathways through post-translational modification remains unclear, a

strong role in cell-cell-communication in an immunomodulatory setting was suggested. However, more knowledge on the exact mechanisms of how HERC5 is involved in metastasization as well as its possible interaction with the tumor microenvironment is needed. This knowledge could be valuable for the development of a blood-based liquid biopsy assay, contributing to early detection of relapse and disease monitoring of NSCLC in the future.

References

[1] J Michael Bishop and Robert A Weinberg. *Molecular oncology*. Scientific American, 1996.

[2] Douglas Hanahan and Robert A Weinberg. The hallmarks of cancer. *Cell*, 100(1):57–70, 2000.

[3] Douglas Hanahan and Robert A Weinberg. Hallmarks of cancer: the next generation. *cell*, 144(5):646–674, 2011.

[4] Klaus Pantel and Catherine Alix-Panabières. Liquid biopsy and minimal residual disease—latest advances and implications for cure. *Nature Reviews Clinical Oncology*, 16(7):409–424, 2019.

[5] Freddie Bray, Jacques Ferlay, Isabelle Soerjomataram, Rebecca L Siegel, Lindsey A Torre, and Ahmedin Jemal. Global cancer statistics 2018: GLOBOCAN estimates of incidence and mortality worldwide for 36 cancers in 185 countries. *CA: a cancer journal for clinicians*, 68(6):394–424, 2018.

[6] Rebecca L Siegel, Kimberly D Miller, and Ahmedin Jemal. Cancer statistics, 2020. *CA: A Cancer Journal for Clinicians*, 70(1):7–30, 2020.

[7] N Howlader, AM Noone, M Krapcho, J Garshell, N Neyman, SF Altekruse, CL Kosary, M Yu, J Ruhl, Z Tatalovich, et al. SEER cancer statistics review, 1975–2010. *Bethesda, MD: National Cancer Institute*, 21:12, 2013.

[8] Lindsey A Torre, Rebecca L Siegel, and Ahmedin Jemal. Lung cancer statistics. In *Lung cancer and personalized medicine*, pages 1–19. Springer, 2016.

[9] Ahmedin Jemal, Elizabeth M Ward, Christopher J Johnson, Kathleen A Cronin, Jiemin Ma, A Blythe Ryerson, Angela Mariotto, Andrew J Lake, Reda Wilson, Recinda L Sherman, et al. Annual report to the nation on the status of cancer, 1975–2014, featuring survival. *JNCI: Journal of the National Cancer Institute*, 109(9):djx030, 2017.

[10] Anthony J Alberg, Malcolm V Brock, Jean G Ford, Jonathan M Samet, and Simon D Spivack. Epidemiology of lung cancer: Diagnosis and management of lung cancer: American college of chest physicians evidence-based clinical practice guidelines. *Chest*, 143(5):e1S–e29S, 2013.

[11] Majid Ezzati, S Jane Henley, Alan D Lopez, and Michael J Thun. Role of smoking in global and regional cancer epidemiology: current patterns and data needs. *International journal of cancer*, 116(6):963–971, 2005.

[12] Darren R Brenner, John R McLaughlin, and Rayjean J Hung. Previous lung diseases and lung cancer risk: a systematic review and meta-analysis. *PloS one*, 6(3), 2011.

[13] Ann G Schwartz, Michele L Cote, Angela S Wenzlaff, Alison Van Dyke, Wei Chen, John C Ruckdeschel, Shirish Gadgeel, and Ayman O Soubani. Chronic obstructive lung diseases and risk of non-small cell lung cancer in women. *Journal of Thoracic Oncology*, 4(3):291–299, 2009.

[14] Corey J Langer, Benjamin Besse, Antonio Gualberto, Elizabeth Brambilla, and Jean-Charles Soria. The evolving role of histology in the management of advanced non–small-cell lung cancer. *Journal of clinical oncology*, 28(36):5311–5320, 2010.

[15] Steven L Wood, Maria Pernemalm, Philip A Crosbie, and Anthony D Whetton. The role of the tumor-microenvironment in lung cancer-metastasis and its relationship to potential therapeutic targets. *Cancer treatment reviews*, 40(4):558–566, 2014.

[16] Morgan R Davidson, Adi F Gazdar, and Belinda E Clarke. The pivotal role of pathology in the management of lung cancer. *Journal of thoracic disease*, 5(Suppl 5):S463, 2013.

[17] Wanyin Lim, Carole A Ridge, Andrew G Nicholson, and Saeed Mirsadraee. The 8th lung cancer TNM classification and clinical staging system: review of the changes and clinical implications. *Quantitative imaging in medicine and surgery*, 8(7):709, 2018.

[18] Peter Goldstraw, Kari Chansky, John Crowley, Ramon Rami-Porta, Hisao Asamura, Wilfried EE Eberhardt, Andrew G Nicholson, Patti Groome, Alan Mitchell, Vanessa Bolejack, et al. The IASLC lung cancer staging project: proposals for revision of the TNM stage groupings in the forthcoming (eighth) edition of the TNM classification for lung cancer. *Journal of Thoracic Oncology*, 11(1):39–51, 2016.

[19] Fred R Hirsch, Giorgio V Scagliotti, James L Mulshine, Regina Kwon, Walter J Curran Jr, Yi-Long Wu, and Luis Paz-Ares. Lung cancer: current therapies and new targeted treatments. *The Lancet*, 389(10066):299–311, 2017.

[20] Faria Nasim, Bruce F Sabath, and George A Eapen. Lung cancer. *Medical Clinics*, 103(3):463–473, 2019.

[21] Nithya Ramnath, Thomas J Dilling, Loren J Harris, Anthony W Kim, Gaetane C Michaud, Alex A Balekian, Rebecca Diekemper, Frank C Detterbeck, and Douglas A Arenberg. Treatment of stage III non-small cell lung cancer: diagnosis and management of lung cancer: American college of chest physicians evidence-based clinical practice guidelines. *Chest*, 143(5):e314S–e340S, 2013.

[22] Mark A Socinski, Tracey Evans, Scott Gettinger, Thomas A Hensing, Lecia VanDam Sequist, Belinda Ireland, and Thomas E Stinchcombe. Treatment of stage IV non-small cell lung cancer: Diagnosis and management of lung cancer: American college of chest physicians evidence-based clinical practice guidelines. *Chest*, 143(5):e341S–e368S, 2013.

[23] Ahmet Zehir, Ryma Benayed, Ronak H Shah, Aijazuddin Syed, Sumit Middha, Hyunjae R Kim, Preethi Srinivasan, Jianjiong Gao, Debyani Chakravarty, Sean M Devlin, et al. Mutational landscape of metastatic cancer revealed from prospective clinical sequencing of 10,000 patients. *Nature medicine*, 23(6):703, 2017.

[24] Nancy E Hynes and Heidi A Lane. ERBB receptors and cancer: the complexity of targeted inhibitors. *Nature Reviews Cancer*, 5(5):341–354, 2005.

[25] Deric L Wheeler, Emily F Dunn, and Paul M Harari. Understanding resistance to EGFR inhibitors—impact on future treatment strategies. *Nature reviews Clinical oncology*, 7(9):493, 2010.

[26] Thomas J Lynch, Daphne W Bell, Raffaella Sordella, Sarada Gurubhagavatula, Ross A Okimoto, Brian W Brannigan, Patricia L Harris, Sara M Haserlat, Jeffrey G Supko, Frank G Haluska, et al. Activating mutations in the epidermal growth factor receptor underlying responsiveness of non–small-cell lung cancer to gefitinib. *New England Journal of Medicine*, 350(21):2129–2139, 2004.

[27] Roy S Herbst, Daniel Morgensztern, and Chris Boshoff. The biology and management of non-small cell lung cancer. *Nature*, 553(7689):446–454, 2018.

[28] Susumu Kobayashi, Titus J Boggon, Tajhal Dayaram, Pasi A Jänne, Olivier Kocher, Matthew Meyerson, Bruce E Johnson, Michael J Eck, Daniel G Tenen, and Balázs Halmos. EGFR mutation and resistance of non–small-cell lung cancer to gefitinib. *New England Journal of Medicine*, 352(8):786–792, 2005.

[29] Haidong Dong, Scott E Strome, Diva R Salomao, Hideto Tamura, Fumiya Hirano, Dallas B Flies, Patrick C Roche, Jun Lu, Gefeng Zhu, Koji Tamada, et al. Tumor-associated B7-H1 promotes T-cell apoptosis: a potential mechanism of immune evasion. *Nature medicine*, 8(8):793–800, 2002.

[30] Edward B Garon, Naiyer A Rizvi, Rina Hui, Natasha Leighl, Ani S Balmanoukian, Joseph Paul Eder, Amita Patnaik, Charu Aggarwal, Matthew Gubens, Leora Horn, et al. Pembrolizumab for the treatment of non–small-cell lung cancer. *New England Journal of Medicine*, 372(21):2018–2028, 2015.

[31] Jawad Fares, Mohamad Y Fares, Hussein H Khachfe, Hamza A Salhab, and Youssef Fares. Molecular principles of metastasis: a hallmark of cancer revisited. *Signal transduction and targeted therapy*, 5(1):1–17, 2020.

[32] Joan Massagué and Anna C Obenauf. Metastatic colonization by circulating tumour cells. *Nature*, 529(7586):298–306, 2016.

[33] Oumar Camara, Andreas Kavallaris, Helmut Nöschel, Matthias Rengsberger, Cornelia Jörke, and Katharina Pachmann. Seeding of epithelial cells into circulation during surgery for breast cancer: the fate of malignant and benign mobilized cells. *World journal of surgical oncology*, 4(1):67, 2006.

[34] Simon A Joosse, Tobias M Gorges, and Klaus Pantel. Biology, detection, and clinical implications of circulating tumor cells. *EMBO molecular medicine*, 7(1):1–11, 2015.

[35] M Angela Nieto, Ruby Yun-Ju Huang, Rebecca A Jackson, and Jean Paul Thiery. EMT: 2016. *Cell*, 166(1):21–45, 2016.

[36] Jean Paul Thiery, Hervé Acloque, Ruby YJ Huang, and M Angela Nieto. Epithelial-mesenchymal transitions in development and disease. *Cell*, 139(5):871–890, 2009.

[37] Klaus Pantel, Bernward Passlick, Judith Vogt, Peter Stosiek, Matthias Angstwurm, Rita Seen-Hibler, K Häussinger, Olaf Thetter, Jakob R Izbicki, and G Riethmüller. Reduced expression of plakoglobin indicates an unfavorable prognosis in subsets of patients with non-small-cell lung cancer. *Journal of clinical oncology*, 16(4):1407–1413, 1998.

[38] Aristidis Moustakas and Carl-Henrik Heldin. Signaling networks guiding epithelial–mesenchymal transitions during embryogenesis and cancer progression. *Cancer science*, 98(10):1512–1520, 2007.

[39] Wai Leong Tam and Robert A Weinberg. The epigenetics of epithelial-mesenchymal plasticity in cancer. *Nature medicine*, 19(11):1438, 2013.

[40] Anna C Obenauf and Joan Massagué. Surviving at a distance: organ-specific metastasis. *Trends in cancer*, 1(1):76–91, 2015.

[41] Matias Riihimäki, A Hemminki, Mahdi Fallah, Hauke Thomsen, Kristina Sundquist, Jan Sundquist, and Kari Hemminki. Metastatic sites and survival in lung cancer. *Lung cancer*, 86(1):78–84, 2014.

[42] Héctor Peinado, Haiying Zhang, Irina R Matei, Bruno Costa-Silva, Ayuko Hoshino, Goncalo Rodrigues, Bethan Psaila, Rosandra N Kaplan, Jacqueline F Bromberg, Yibin Kang, et al. Pre-metastatic niches: organ-specific homes for metastases. *Nature Reviews Cancer*, 17(5):302–317, 2017.

[43] Klaus Pantel and Catherine Alix-Panabières. Tumour microenvironment: informing on minimal residual disease in solid tumours. *Nature Reviews Clinical Oncology*, 14(6):325–326, 2017.

[44] Klaus Pantel and Catherine Alix-Panabières. Circulating tumour cells in cancer patients: challenges and perspectives. *Trends in molecular medicine*, 16(9):398–406, 2010.

[45] Sabine Riethdorf, Harriet Wikman, and Klaus Pantel. Biological relevance of disseminated tumor cells in cancer patients. *International journal of cancer*, 123(9):1991–2006, 2008.

[46] Klaus Pantel, M Angstwurm, G Riethmüller, B Passlick, J Izbicki, Olaf Thetter, and K Häussinger. Frequency and prognostic significance of isolated tumour cells in bone marrow of patients with non-small-cell lung cancer without overt metastases. *The Lancet*, 347(9002):649–653, 1996.

[47] Sabine Kasimir-Bauer, Katharina Reiter, Bahriye Aktas, Ann-Kathrin Bittner, Stephan Weber, Thomas Keller, Rainer Kimmig, and Oliver Hoffmann. Different prognostic value of circulating and disseminated tumor cells in primary breast cancer: Influence of bisphosphonate intake? *Scientific reports*, 6:26355, 2016.

[48] Simon A Joosse and Klaus Pantel. Tumor-educated platelets as liquid biopsy in cancer patients. *Cancer cell*, 28(5):552–554, 2015.

[49] Alberto Bardelli and Klaus Pantel. Liquid biopsies, what we do not know (yet). *Cancer cell*, 31(2):172–179, 2017.

[50] Evi Lianidou and Klaus Pantel. Liquid biopsies. *Genes, Chromosomes and Cancer*, 58(4):219–232, 2019.

[51] Songdong Meng, Debasish Tripathy, Eugene P Frenkel, Sanjay Shete, Elizabeth Z Naftalis, James F Huth, Peter D Beitsch, Marilyn Leitch, Susan Hoover, David Euhus, et al. Circulating tumor cells in patients with breast cancer dormancy. *Clinical cancer research*, 10(24):8152–8162, 2004.

[52] Ana Barradas and Leon WMM Terstappen. Towards the biological understanding of CTC: capture technologies, definitions and potential to create metastasis. *Cancers*, 5(4):1619–1642, 2013.

[53] Brigitte Rack, Christian Schindlbeck, Julia Jückstock, Ulrich Andergassen, Philip Hepp, Thomas Zwingers, Thomas WP Friedl, Ralf Lorenz, Hans Tesch, Peter A Fasching, et al. Circulating tumor cells predict survival in early average-to-high risk breast cancer patients. *Journal of the National Cancer Institute*, 106(5):dju066, 2014.

[54] Matthew G Krebs, Robert L Metcalf, Louise Carter, Ged Brady, Fiona H Blackhall, and Caroline Dive. Molecular analysis of circulating tumour cells—biology and biomarkers. *Nature reviews Clinical oncology*, 11(3):129, 2014.

[55] Jianwei Huang, Ke Wang, Jianjun Xu, Jian Huang, and Tao Zhang. Prognostic significance of circulating tumor cells in non-small-cell lung cancer patients: A meta-analysis. *PLoS ONE*, 8(11), 2013.

[56] Tobias M Gorges, Nicole Penkalla, Thomas Schalk, Simon A Joosse, Sabine Riethdorf, Johannes Tucholski, Klaus Lücke, Harriet Wikman, Stephen Jackson, Nora Brychta, et al. Enumeration and molecular characterization of tumor cells in lung cancer patients using a novel in vivo device for capturing circulating tumor cells. *Clinical Cancer Research*, 22(9):2197–2206, 2016.

[57] Catherine Alix-Panabières and Klaus Pantel. Clinical applications of circulating tumor cells and circulating tumor DNA as liquid biopsy. *Cancer discovery*, 6(5):479–491, 2016.

[58] Frank Diehl, Kerstin Schmidt, Michael A Choti, Katharine Romans, Steven Goodman, Meng Li, Katherine Thornton, Nishant Agrawal, Lori Sokoll, Steve A Szabo, et al. Circulating mutant DNA to assess tumor dynamics. *Nature medicine*, 14(9):985, 2008.

[59] Tony Mok, Yi-Long Wu, Jin Soo Lee, Chong-Jen Yu, Virote Sriuranpong, Jennifer Sandoval-Tan, Guia Ladrera, Sumitra Thongprasert, Vichien Srimuninnimit, Meilin Liao, et al. Detection and dynamic changes of EGFR mutations from circulating tumor DNA as a predictor of survival outcomes in NSCLC patients treated with first-line intercalated erlotinib and chemotherapy. *Clinical Cancer Research*, 21(14):3196–3203, 2015.

[60] Bethany N Hannafon and Wei-Qun Ding. Intercellular communication by exosome-derived microRNAs in cancer. *International journal of molecular sciences*, 14(7):14240–14269, 2013.

[61] Heidi Schwarzenbach, Naohiro Nishida, George A Calin, and Klaus Pantel. Clinical relevance of circulating cell-free microRNAs in cancer. *Nature reviews Clinical oncology*, 11(3):145, 2014.

[62] Patrick S Mitchell, Rachael K Parkin, Evan M Kroh, Brian R Fritz, Stacia K Wyman, Era L Pogosova-Agadjanyan, Amelia Peterson, Jennifer Noteboom, Kathy C O'Briant, April Allen, et al. Circulating microRNAs as stable blood-based markers for cancer detection. *Proceedings of the National Academy of Sciences*, 105(30):10513–10518, 2008.

[63] Guo-Liang Huang, Jiancong Sun, Yan Lu, Yuke Liu, Huiyuan Cao, Huanyu Zhang, and George A Calin. MiR-200 family and cancer: From a meta-analysis view. *Molecular Aspects of Medicine*, 2019.

[64] P Fonseca, I Vardaki, A Occhionero, and T Panaretakis. Metabolic and signaling functions of cancer cell-derived extracellular vesicles. In *International review of cell and molecular biology*, volume 326, pages 175–199. Elsevier, 2016.

[65] Hadi Valadi, Karin Ekström, Apostolos Bossios, Margareta Sjöstrand, James J Lee, and Jan O Lötvall. Exosome-mediated transfer of mRNAs and microRNAs is a novel mechanism of genetic exchange between cells. *Nature cell biology*, 9(6):654–659, 2007.

[66] Xu Zhang, Xiao Yuan, Hui Shi, Lijun Wu, Hui Qian, and Wenrong Xu. Exosomes in cancer: small particle, big player. *Journal of hematology & oncology*, 8(1):83, 2015.

[67] Ayuko Hoshino, Bruno Costa-Silva, Tang-Long Shen, Goncalo Rodrigues, Ayako Hashimoto, Milica Tesic Mark, Henrik Molina, Shinji Kohsaka, Angela Di Giannatale, Sophia Ceder, et al. Tumour exosome integrins determine organotropic metastasis. *Nature*, 527(7578):329–335, 2015.

[68] Martin HD Neumann, Sebastian Bender, Thomas Krahn, and Thomas Schlange. ctDNA and CTCs in liquid biopsy–current status and where we need to progress. *Computational and structural biotechnology journal*, 16:190–195, 2018.

[69] Christina Alidousty, Danielle Brandes, Carina Heydt, Svenja Wagener, Maike Wittersheim, Stephan C Schäfer, Barbara Holz, Sabine Merkelbach-Bruse, Reinhard Büttner, Jana Fassunke, et al. Comparison of blood collection tubes from three different manufacturers for the collection of cell-free DNA for liquid biopsy mutation testing. *The Journal of Molecular Diagnostics*, 19(5):801–804, 2017.

[70] Robert Hawkins. Managing the pre-and post-analytical phases of the total testing process. *Annals of laboratory medicine*, 32(1):5–16, 2012.

[71] Barbara Mesquita, Dominic G Rothwell, Deborah J Burt, Francesca Chemi, Fabiola Fernandez-Gutierrez, Daniel Slane-Tan, Jenny Antonello, Mathew Carter, Louise Carter, Marina Parry, et al. Molecular analysis of single circulating tumour cells following long-term storage of clinical samples. *Molecular oncology*, 11(12):1687–1697, 2017.

[72] Joost H van Ginkel, Daan A van den Broek, Joyce van Kuik, Dorothé Linders, Roel de Weger, Stefan M Willems, and Manon MH Huibers. Preanalytical blood sample workup for cell-free DNA analysis using droplet digital PCR for future molecular cancer diagnostics. *Cancer medicine*, 6(10):2297–2307, 2017.

[73] Vera Kloten, Martin HD Neumann, Francesca Di Pasquale, Markus Sprenger-Haussels, Jonathan M Shaffer, Martin Schlumpberger, Andrei Herdean, Fay Betsou, Wim Ammerlaan, Taija af Hällström, et al. Multicenter evaluation of circulating plasma MicroRNA extraction technologies for the development of clinically feasible reverse transcription quantitative PCR and next-generation sequencing analytical work flows. *Clinical Chemistry*, 65(9):1132–1140, 2019.

[74] FR Garcia-Gonzalo and JL Rosa. The HERC proteins: functional and evolutionary insights. *Cellular and Molecular Life Sciences CMLS*, 62(16):1826–1838, 2005.

[75] Jon M Huibregtse, Martin Scheffner, Sylvie Beaudenon, and Peter M Howley. A family of proteins structurally and functionally related to the E6-AP ubiquitin-protein ligase. *Proceedings of the National Academy of Sciences*, 92(7):2563–2567, 1995.

[76] Kaoru Mitsui, Makoto Nakanishi, Satoshi Ohtsuka, Thomas H Norwood, Ken Okabayashi, Chikara Miyamoto, Keiji Tanaka, Akihiko Yoshimura, and Motoaki Ohtsubo. A novel human gene encoding HECT domain and RCC1-like repeats interacts with cyclins and is potentially regulated by the tumor suppressor proteins. *Biochemical and biophysical research communications*, 266(1):115–122, 1999.

[77] Karin Hochrainer, Herbert Mayer, Ulrike Baranyi, BerndR Binder, Joachim Lipp, and Renate Kroismayr. The human HERC family of ubiquitin ligases: novel members, genomic organization, expression profiling, and evolutionary aspects. *Genomics*, 85(2):153–164, 2005.

[78] Renate Kroismayr, Ulrike Baranyi, Christian Stehlik, Andrea Dorfleutner, Bernd R Binder, and Joachim Lipp. HERC5, a HECT E3 ubiquitin ligase tightly regulated in LPS activated endothelial cells. *Journal of cell science*, 117(20):4749–4756, 2004.

[79] Yi-Chieh Perng and Deborah J Lenschow. ISG15 in antiviral immunity and beyond. *Nature Reviews Microbiology*, 16(7):423–439, 2018.

[80] Anahita Dastur, Sylvie Beaudenon, Melissa Kelley, Robert M Krug, and Jon M Huibregtse. Herc5, an interferon-induced HECT E3 enzyme, is required for conjugation of ISG15 in human cells. *Journal of Biological Chemistry*, 281(7):4334–4338, 2006.

[81] Joyce Jing Yi Wong, Yuh Fen Pung, Newman Siu-Kwan Sze, and Keh-Chuang Chin. HERC5 is an IFN-induced HECT-type E3 protein ligase that mediates type i IFN-induced ISGylation of protein targets. *Proceedings of the National Academy of Sciences*, 103(28):10735–10740, 2006.

[82] Larissa A Durfee, Nancy Lyon, Kyungwoon Seo, and Jon M Huibregtse. The ISG15 conjugation system broadly targets newly synthesized proteins: implications for the antiviral function of ISG15. *Molecular cell*, 38(5):722–732, 2010.

[83] Jennifer L Potter, Jana Narasimhan, Liane Mende-Mueller, and Arthur L Haas. Precursor processing of pro-ISG15/UCRP, an interferon-β-induced ubiquitin-like protein. *Journal of Biological Chemistry*, 274(35):25061–25068, 1999.

[84] Weiming Yuan and Robert M Krug. Influenza B virus NS1 protein inhibits conjugation of the interferon (IFN)-induced ubiquitin-like ISG15 protein. *The EMBO journal*, 20(3):362–371, 2001.

[85] Chen Zhao, Sylvie L Beaudenon, Melissa L Kelley, M Brett Waddell, Weiming Yuan, Brenda A Schulman, Jon M Huibregtse, and Robert M Krug. The UbcH8 ubiquitin E2 enzyme is also the E2 enzyme for ISG15, an IFN-α/β-induced ubiquitin-like protein. *Proceedings of the National Academy of Sciences*, 101(20):7578–7582, 2004.

[86] Michael P Malakhov, Oxana A Malakhova, Keun Il Kim, Kenneth J Ritchie, and Dong-Er Zhang. UBP43 (USP18) specifically removes ISG15 from conjugated proteins. *Journal of Biological Chemistry*, 277(12):9976–9981, 2002.

[87] Chen Zhao, Carilee Denison, Jon M Huibregtse, Steven Gygi, and Robert M Krug. Human ISG15 conjugation targets both IFN-induced and constitutively expressed proteins functioning in diverse cellular pathways. *Proceedings of the National Academy of Sciences*, 102(29):10200–10205, 2005.

[88] Nadia V Giannakopoulos, Jiann-Kae Luo, Vladimir Papov, Weiguo Zou, Deborah J Lenschow, Barbara S Jacobs, Ernest C Borden, Jun Li, Herbert W Virgin, and Dong-Er Zhang. Proteomic identification of proteins conjugated to ISG15 in mouse and human cells. *Biochemical and biophysical research communications*, 336(2):496–506, 2005.

[89] Larissa A Durfee and Jon M Huibregtse. Identification and validation of ISG15 target proteins. In *Conjugation and Deconjugation of Ubiquitin Family Modifiers*, pages 228–237. Springer, 2010.

[90] Keith R Loeb and Arthur L Haas. The interferon-inducible 15-kda ubiquitin homolog conjugates to intracellular proteins. *Journal of Biological Chemistry*, 267(11):7806–7813, 1992.

[91] YuJie Tang, Gongxun Zhong, Lianhui Zhu, Xing Liu, Yufei Shan, Huapeng Feng, ZhiGao Bu, Hualan Chen, and Chen Wang. Herc5 attenuates influenza a virus by catalyzing ISGylation of viral NS1 protein. *The Journal of Immunology*, 184(10):5777–5790, 2010.

[92] Chen Zhao, Tien-Ying Hsiang, Rei-Lin Kuo, and Robert M Krug. ISG15 conjugation system targets the viral NS1 protein in influenza a virus–infected cells. *Proceedings of the National Academy of Sciences*, 107(5):2253–2258, 2010.

[93] Atsushi Okumura, Gengshi Lu, Ian Pitha-Rowe, and Paula M Pitha. Innate antiviral response targets HIV-1 release by the induction of ubiquitin-like protein ISG15. *Proceedings of the National Academy of Sciences*, 103(5):1440–1445, 2006.

[94] Chen Zhao, Haripriya Sridharan, Ran Chen, Darren P Baker, Shanshan Wang, and Robert M Krug. Influenza b virus non-structural protein 1 counteracts ISG15 antiviral activity by sequestering isgylated viral proteins. *Nature communications*, 7(1):1–12, 2016.

[95] Anna M Mielech, Andy Kilianski, Yahira M Baez-Santos, Andrew D Mesecar, and Susan C Baker. MERS-CoV papain-like protease has deISGylating and deubiquitinating activities. *Virology*, 450:64–70, 2014.

[96] K Hochrainer, R Kroismayr, U Baranyi, BR Binder, and J Lipp. Highly homologous HERC proteins localize to endosomes and exhibit specific interactions with hPLIC and Nm23B. *Cellular and molecular life sciences*, 65(13):2105–2117, 2008.

[97] EH Postel, SJ Berberich, SJ Flint, and CA Ferrone. Human c-myc transcription factor PuF identified as nm23-H2 nucleoside diphosphate kinase, a candidate suppressor of tumor metastasis. *Science*, 261(5120):478–480, 1993.

[98] Feng Xue, Brandon W Higgs, Jiaqi Huang, Chris Morehouse, Wei Zhu, Xin Yao, Philip Brohawn, Zhan Xiao, Yinong Sebastian, Zheng Liu, et al. HERC5 is a prognostic biomarker for post-liver transplant recurrent human hepatocellular carcinoma. *Journal of translational medicine*, 13(1):379, 2015.

[99] Michaela Wrage, Wolfgang Hagmann, Dirk Kemming, Faik G Uzunoglu, Sabine Riethdorf, Katharina Effenberger, Manfred Westphal, Katrin Lamszus, Soo-Zin Kim, Natalia Becker, et al. Identification of HERC5 and its potential role in NSCLC progression. *International journal of cancer*, 136(10):2264–2272, 2015.

[100] JB Andersen and BA Hassel. The interferon regulated ubiquitin-like protein, ISG15, in tumorigenesis: friend or foe? *Cytokine & growth factor reviews*, 17(6):411–421, 2006.

[101] Klaas Kok, Robert Hofstra, Alison Pilz, Anke van den Berg, Peter Terpstra, CH Buys, and Ben Carritt. A gene in the chromosomal region 3p21 with greatly reduced expression in lung cancer is similar to the gene for ubiquitin-activating enzyme. *Proceedings of the National Academy of Sciences*, 90(13):6071–6075, 1993.

[102] Pamela MJ McLaughlin, Wijnand Helfrich, Klaas Kok, Marcel Mulder, Soesja W Hu, Marja GL Brinker, Marcel HJ Ruiters, Lou FMH de Leij, and Charles HCM Buys. The ubiquitin-activating enzyme E1-like protein in lung cancer cell lines. *International journal of cancer*, 85(6):871–876, 2000.

[103] Yongli Guo, Fadzai Chinyengetere, Andrey V Dolinko, Alexandra Lopez-Aguiar, Yun Lu, Fabrizio Galimberti, Tian Ma, Qing Feng, David Sekula, Sarah J Freemantle, et al. Evidence for the ubiquitin protease UBP43 as an antineoplastic target. *Molecular cancer therapeutics*, 11(9):1968–1977, 2012.

[104] Hye Gyeong Han, Hye Won Moon, and Young Joo Jeon. ISG15 in cancer: Beyond ubiquitin-like protein. *Cancer letters*, 438:52–62, 2018.

[105] Michaela Wrage, Salla Ruosaari, Paul P Eijk, Jussuf T Kaifi, Jaakko Hollmen, Emre F Yekebas, Jakob R Izbicki, Ruud H Brakenhoff, Thomas Streichert, Sabine Riethdorf, et al. Genomic profiles associated with early micrometastasis in lung cancer: relevance of 4q deletion. *Clinical Cancer Research*, 15(5):1566–1574, 2009.

[106] Faik G Uzunoglu, Ebba Dethlefsen, Annkathrin Hanssen, Michaela Wrage, Lena Deutsch, Katharina Harms-Effenberger, Yogesh K Vashist, Matthias Reeh, Guido Sauter, Ronald Simon, et al. Loss of 4q21. 23-22.1 is a prognostic marker for disease free and overall survival in non-small cell lung cancer. *PloS one*, 9(12), 2014.

[107] Carolina Villarroya-Beltri, Francesc Baixauli, María Mittelbrunn, Irene Fernández-Delgado, Daniel Torralba, Olga Moreno-Gonzalo, Sara Baldanta, Carlos Enrich, Susana Guerra, and Francisco Sánchez-Madrid. ISGylation controls exosome secretion by promoting lysosomal degradation of MVB proteins. *Nature communications*, 7(1):1–11, 2016.

[108] Priya Choudhry. High-throughput method for automated colony and cell counting by digital image analysis based on edge detection. *PloS one*, 11(2), 2016.

[109] Camilo Guzman, Manish Bagga, Amanpreet Kaur, Jukka Westermarck, and Daniel Abankwa. Colonyarea: an ImageJ plugin to automatically quantify colony formation in clonogenic assays. *PloS one*, 9(3), 2014.

[110] Fatemeh Momen-Heravi, Leonora Balaj, Sara Alian, Pierre-Yves Mantel, Allison E Halleck, Alexander J Trachtenberg, Cesar E Soria, Shanice Oquin, Christina M Bonebreak, Elif Saracoglu, et al. Current methods for the isolation of extracellular vesicles. *Biological chemistry*, 394(10):1253–1262, 2013.

[111] Claudia Koch, Simon A Joosse, Svenja Schneegans, Okka JW Wilken, Melanie Janning, Desiree Loreth, Volkmar Müller, Katharina Prieske, Malgorzata Banys-Paluchowski, Ludwig J Horst, et al. Pre-analytical and analytical variables of

label-independent enrichment and automated detection of circulating tumor cells in cancer patients. *Cancers*, 12(2):442, 2020.

[112] Jo Vandesompele, Katleen De Preter, Filip Pattyn, Bruce Poppe, Nadine Van Roy, Anne De Paepe, and Frank Speleman. Accurate normalization of real-time quantitative RT-PCR data by geometric averaging of multiple internal control genes. *Genome biology*, 3(7):research0034–1, 2002.

[113] Claus Lindbjerg Andersen, Jens Ledet Jensen, and Torben Falck Ørntoft. Normalization of real-time quantitative reverse transcription-PCR data: a model-based variance estimation approach to identify genes suited for normalization, applied to bladder and colon cancer data sets. *Cancer research*, 64(15):5245–5250, 2004.

[114] Soheil Madadi, Heidi Schwarzenbach, Johan Lorenzen, and Meysam Soleimani. MicroRNA expression studies: challenge of selecting reliable reference controls for data normalization. *Cellular and Molecular Life Sciences*, pages 1–18, 2019.

[115] Jennifer A Doudna and Emmanuelle Charpentier. The new frontier of genome engineering with CRISPR-Cas9. *Science*, 346(6213):1258096, 2014.

[116] Raymond W Ganster, Zhong Guo, Lifang Shao, and David A Geller. Differential effects of TNF-α and IFN-γ on gene transcription mediated by NF-κB-Stat1 interactions. *Journal of interferon & cytokine research*, 25(11):707–719, 2005.

[117] Clotilde Théry, Kenneth W Witwer, Elena Aikawa, Maria Jose Alcaraz, Johnathon D Anderson, Ramaroson Andriantsitohaina, Anna Antoniou, Tanina Arab, Fabienne Archer, Georgia K Atkin-Smith, et al. Minimal information for studies of extracellular vesicles 2018 (MISEV2018): a position statement of the international society for extracellular vesicles and update of the MISEV2014 guidelines. *Journal of extracellular vesicles*, 7(1):1535750, 2018.

[118] Svenja Schneegans, Lelia Lück, Katharina Besler, Leonie Bluhm, Julia-Christina Stadler, Janina Staub, Rüdiger Greinert, Beate Volkmer, Mikael Kubista, Christoffer Gebhardt, Alexander Sartori, Darryl Irwin, Elina Serkkola, Taija af Hällström, Evi Lianidou, Markus Sprenger-Haussels, Melanie Hussong, Peter Mohr, Stefan W. Schneider, Jonathan Shaffer, Klaus Pantel, and Harriet Wikman. Pre-analytical factors affecting the establishment of a single tube assay for multiparameter liquid biopsy detection in melanoma patients. *Molecular Oncology*, 14(5):1001–1015, 2020.

[119] Jinchun Yan, Qin Yang, and Qihong Huang. Metastasis suppressor genes. *Histology and histopathology*, 28(3):285, 2013.

[120] Geoffrey M Cooper and RE Hausman. A molecular approach. *The Cell. 2nd ed. Sunderland*, *MA: Sinauer Associates*, 2000.

[121] Daniel T Starczynowski, William W Lockwood, Sophie Deléhouzée, Raj Chari, Joanna Wegrzyn, Megan Fuller, Ming-Sound Tsao, Stephen Lam, Adi F Gazdar, Wan L Lam, et al. TRAF6 is an amplified oncogene bridging the RAS and NF-κB pathways in human lung cancer. *The Journal of clinical investigation*, 121(10):4095–4105, 2011.

[122] Jian Feng, Liqin Xu, Songshi Ni, Jun Gu, Huijun Zhu, Haiying Wang, Shu Zhang, Wei Zhang, and Jianfei Huang. Involvement of FoxQ1 in NSCLC through regulating EMT and increasing chemosensitivity. *Oncotarget*, 5(20):9689, 2014.

[123] Wenyan Xu, Xiaoyu Yu, Jiewei Zhang, Sasi Bhushan, Siddalinga Prasad, KN Prasad, Fan Wu, Jun Yuan, and H Fai Poon. Soy hydrolysate mimic autocrine growth factors effect of conditioned media to promote single CHO-K1 cell proliferation. *Tissue and Cell*, 58:130–133, 2019.

[124] Nevenka Dudvarski Stankovic, Marcin Teodorczyk, Robert Ploen, Frauke Zipp, and Mirko HH Schmidt. Microglia–blood vessel interactions: a double-edged sword in brain pathologies. *Acta neuropathologica*, 131(3):347–363, 2016.

[125] James Keaney and Matthew Campbell. The dynamic blood–brain barrier. *The FEBS journal*, 282(21):4067–4079, 2015.

[126] Yvonne Schüler, Cornelia Lee-Thedieck, Konstanze Geiger, Tatjana Kaiser, Yoshinori Ino, Wilhelm K Aicher, and Gerd Klein. Osteoblast-secreted factors enhance the expression of dysadherin and CCL2-dependent migration of renal carcinoma cells. *International journal of cancer*, 130(2):288–299, 2012.

[127] Matthias Chiquet, David E Birk, Carsten G Bönnemann, and Manuel Koch. Collagen XII: protecting bone and muscle integrity by organizing collagen fibrils. *The international journal of biochemistry & cell biology*, 53:51–54, 2014.

[128] Shijie Duan, Baocheng Gong, Pengliang Wang, Hanwei Huang, Lei Luo, and Funan Liu. Novel prognostic biomarkers of gastric cancer based on gene expression microarray: COL12A1, GSTA3, FGA and FGG. *Molecular medicine reports*, 18(4):3727–3736, 2018.

[129] Ten-Yang Yen, Nicole Haste, Leslie C Timpe, Christina Litsakos-Cheung, Roger Yen, and Bruce A Macher. Using a cell line breast cancer progression system to identify biomarker candidates. *Journal of proteomics*, 96:173–183, 2014.

[130] Hongjuan Zhao, Börje Ljungberg, Kjell Grankvist, Torgny Rasmuson, Robert Tibshirani, and James D Brooks. Gene expression profiling predicts survival in conventional renal cell carcinoma. *PLoS Med*, 3(1):e13, 2005.

[131] Sridhar Ramaswamy, Ken N Ross, Eric S Lander, and Todd R Golub. A molecular signature of metastasis in primary solid tumors. *Nature genetics*, 33(1):49–54, 2003.

[132] Zhen Xiang, Jun Li, Shuzheng Song, Jiexuan Wang, Wei Cai, Wenjun Hu, Jun Ji, Zhenggang Zhu, Lu Zang, Ranlin Yan, et al. A positive feedback between IDO1 metabolite and COL12A1 via MAPK pathway to promote gastric cancer metastasis. *Journal of Experimental & Clinical Cancer Research*, 38(1):314, 2019.

[133] Moosa Mohammadi and Allen Zinkle. Structural biology of the FGF7 subfamily. *Frontiers in genetics*, 10:102, 2019.

[134] Anquan Shang, Cheng Zhou, Ganxia Bian, Wei Chen, Wenying Lu, Weiwei Wang, and Dong Li. miR-381-3p restrains cervical cancer progression by downregulating FGF7. *Journal of cellular biochemistry*, 120(1):778–789, 2019.

[135] Cong Wang, Ziying Liu, Yuepeng Ke, and Fen Wang. Intrinsic FGFR2 and ectopic FGFR1 signaling in the prostate and prostate cancer. *Frontiers in genetics*, 10, 2019.

[136] Jun Wu, Wei Han, Weiwei Yang, Hongyu Liu, Chunhong Li, Ling Guo, Yan Jin, Ruijie Zhang, He Chen, et al. Keratinocyte growth factor binding to fibroblast growth factor receptor 2-IIIb promotes epithelial ovarian cancer cell proliferation and invasion. *Journal of cancer research and therapeutics*, 14(9):347, 2018.

[137] A McGarry Houghton. Mechanistic links between COPD and lung cancer. *Nature Reviews Cancer*, 13(4):233–245, 2013.

[138] Lysanne Lievense, Joachim Aerts, and Joost Hegmans. Immune therapy. In *Lung Cancer and Personalized Medicine*, pages 59–90. Springer, 2016.

[139] Sook Shien Lee and Yoke Kqueen Cheah. The interplay between MicroRNAs and cellular components of tumour microenvironment (TME) on non-small-cell lung cancer (NSCLC) progression. *Journal of immunology research*, 2019, 2019.

[140] Akinori Takaoka and Tadatsugu Taniguchi. New aspects of IFN-α/β signalling in immunity, oncogenesis and bone metabolism. *Cancer science*, 94(5):405–411, 2003.

[141] Bruce Beutler and Ernst Th Rietschel. Innate immune sensing and its roots: the story of endotoxin. *Nature Reviews Immunology*, 3(2):169–176, 2003.

[142] Simon Milette, Pierre O Fiset, Logan A Walsh, Jonathan D Spicer, and Daniela F Quail. The innate immune architecture of lung tumors and its implication in disease progression. *The Journal of pathology*, 247(5):589–605, 2019.

[143] Ling Ni and Jian Lu. Interferon gamma in cancer immunotherapy. *Cancer medicine*, 7(9):4509–4516, 2018.

[144] Ángela Marrugal, Laura Ojeda, Luis Paz-Ares, Sonia Molina-Pinelo, and Irene Ferrer. Proteomic-based approaches for the study of cytokines in lung cancer. *Disease markers*, 2016, 2016.

[145] Leonidas C Platanias. Mechanisms of type-I-and type-II-interferon-mediated signalling. *Nature Reviews Immunology*, 5(5):375–386, 2005.

[146] Ya-di Wu and BP Zhou. TNF-α/NF-κB/Snail pathway in cancer cell migration and invasion. *British journal of cancer*, 102(4):639–644, 2010.

[147] Takahiro Isaka, Andrea L Nestor, Tadahiro Takada, and David C Allison. Chromosomal variations within aneuploid cancer lines. *Journal of Histochemistry & Cytochemistry*, 51(10):1343–1353, 2003.

[148] Zuodong Zhao, Mengying Lan, Jingjing Li, Qiang Dong, Xiang Li, Baodong Liu, Gang Li, Hailin Wang, Zhuqiang Zhang, and Bing Zhu. The proinflammatory cytokine TNFα induces DNA demethylation–dependent and–independent activation of interleukin-32 expression. *Journal of Biological Chemistry*, 294(17):6785–6795, 2019.

[149] LD Li, HF Sun, Y Bai, SP Gao, HL Jiang, and W Jin. Significant prognostic values of nuclear genes encoding mitochondrial complex I subunits in tumor patients. *Neoplasma*, 63(4):548–558, 2016.

[150] Noona Ambartsumian, Jörg Klingelhöfer, and Mariam Grigorian. The multifaceted S100A4 protein in cancer and inflammation. In *Calcium-Binding Proteins of the EF-Hand Superfamily*, pages 339–365. Springer, 2019.

[151] Lili Liu, Lei Qi, Teresa Knifley, Dava W Piecoro, Piotr Rychahou, Jinpeng Liu, Mihail I Mitov, Jeremiah Martin, Chi Wang, Jianrong Wu, et al. S100A4 alters metabolism and promotes invasion of lung cancer cells by up-regulating mitochondrial complex I protein NDUFS2. *Journal of Biological Chemistry*, 294(18):7516–7527, 2019.

[152] W Zeng, J Zhang, M Qi, C Peng, J Su, X Chen, and Z Yuan. α NAC inhibition of the FADD-JNK axis plays anti-apoptotic role in multiple cancer cells. *Cell death & disease*, 5(6):e1282–e1282, 2014.

[153] J Patrick Murphy and Devanand M Pinto. Temporal proteomic analysis of IGF-1R signalling in MCF-7 breast adenocarcinoma cells. *Proteomics*, 10(9):1847–1860, 2010.

[154] Yifei Qi and Ren Xu. Roles of PLODs in collagen synthesis and cancer progression. *Frontiers in cell and developmental biology*, 6:66, 2018.

[155] Dazhi Wang, Shuyu Zhang, and Fufeng Chen. High expression of PLOD1 drives tumorigenesis and affects clinical outcome in gastrointestinal carcinoma. *Genetic testing and molecular biomarkers*, 22(6):366–373, 2018.

[156] Wei Xu, Julie L Lukkarila, Sara R da Silva, Stacey-Lynn Paiva, Patrick T Gunning, and Aaron D Schimmer. Targeting the ubiquitin E1 as a novel anti-cancer strategy. *Current pharmaceutical design*, 19(18):3201–3209, 2013.

[157] G Wei Xu, Mohsin Ali, Tabitha E Wood, Derek Wong, Neil Maclean, Xiaoming Wang, Marcela Gronda, Marko Skrtic, Xiaoming Li, Rose Hurren, et al. The ubiquitin-activating enzyme E1 as a therapeutic target for the treatment of leukemia and multiple myeloma. *Blood, The Journal of the American Society of Hematology*, 115(11):2251–2259, 2010.

[158] Matthias Mann. Functional and quantitative proteomics using SILAC. *Nature reviews Molecular cell biology*, 7(12):952–958, 2006.

[159] Carolina Villarroya-Beltri, Susana Guerra, and Francisco Sánchez-Madrid. Isgylation–a key to lock the cell gates for preventing the spread of threats. *J Cell Sci*, 130(18):2961–2969, 2017.

[160] Anna Rahnefeld, Karin Klingel, Anett Schuermann, Nicola L Diny, Nadine Althof, Anika Lindner, Philipp Bleienheuft, Konstantinos Savvatis, Dorota Respondek, Elisa Opitz, et al. Ubiquitin-like protein ISG15 (interferon-stimulated gene of 15 kDa) in host defense against heart failure in a mouse model of virus-induced cardiomyopathy. *Circulation*, 130(18):1589–1600, 2014.

[161] Murali Ganesan, Larisa Y Poluektova, Dean J Tuma, Kusum K Kharbanda, and Natalia A Osna. Acetaldehyde disrupts interferon alpha signaling in hepatitis C virus-infected liver cells by up-regulating USP18. *Alcoholism: Clinical and Experimental Research*, 40(11):2329–2338, 2016.

[162] Shyamal D Desai, Arthur L Haas, Laurence M Wood, Yu-Chen Tsai, Sidney Pestka, Eric H Rubin, Ahamed Saleem, Alam Nur-E-Kamal, and Leroy F Liu. Elevated expression of ISG15 in tumor cells interferes with the ubiquitin/26S proteasome pathway. *Cancer research*, 66(2):921–928, 2006.

[163] Annette Becker, Basant Kumar Thakur, Joshua Mitchell Weiss, Han Sang Kim, Hector Peinado, and David Lyden. Extracellular vesicles in cancer: cell-to-cell mediators of metastasis. *Cancer cell*, 30(6):836–848, 2016.

[164] Hailong Fu, Huan Yang, Xu Zhang, and Wenrong Xu. The emerging roles of exosomes in tumor–stroma interaction. *Journal of cancer research and clinical oncology*, 142(9):1897–1907, 2016.

[165] Carolina Villarroya-Beltri, Francesc Baixauli, Cristina Gutiérrez-Vázquez, Francisco Sánchez-Madrid, and María Mittelbrunn. Sorting it out: regulation of exosome loading. In *Seminars in cancer biology*, volume 28, pages 3–13. Elsevier, 2014.

[166] Cristina Gutiérrez-Vázquez, Carolina Villarroya-Beltri, María Mittelbrunn, and Francisco Sánchez-Madrid. Transfer of extracellular vesicles during immune cell-cell interactions. *Immunological reviews*, 251(1):125–142, 2013.

[167] Héctor Peinado, Maša Alečković, Simon Lavotshkin, Irina Matei, Bruno Costa-Silva, Gema Moreno-Bueno, Marta Hergueta-Redondo, Caitlin Williams, Guillermo García-Santos, Cyrus M Ghajar, et al. Melanoma exosomes educate bone marrow progenitor cells toward a pro-metastatic phenotype through MET. *Nature medicine*, 18(6):883, 2012.

[168] Thierry Calandra and Thierry Roger. Macrophage migration inhibitory factor: a regulator of innate immunity. *Nature reviews immunology*, 3(10):791–800, 2003.

[169] Makiko Tomiyasu, Ichiro Yoshino, Ryuichi Suemitsu, Tatsuro Okamoto, and Keizo Sugimachi. Quantification of macrophage migration inhibitory factor mRNA expression in non-small cell lung cancer tissues and its clinical significance. *Clinical Cancer Research*, 8(12):3755–3760, 2002.

[170] Piti Techavichit, Yang Gao, Lyazat Kurenbekova, Ryan Shuck, Lawrence A Donehower, and Jason T Yustein. Secreted frizzled-related protein 2 (sFRP2) promotes osteosarcoma invasion and metastatic potential. *BMC cancer*, 16(1):869, 2016.

[171] Zijian Yang, Michael J LaRiviere, Jina Ko, Jacob E Till, Theresa Christensen, Stephanie S Yee, Taylor A Black, Kyle Tien, Andrew Lin, Hanfei Shen, et al. A multi-analyte panel consisting of extracellular vesicle miRNAs and mRNAs, cfDNA, and CA19-9 shows utility for diagnosis and staging of pancreatic adenocarcinoma. *Clinical Cancer Research*, 2020.

[172] Carlos A Aya-Bonilla, Gabriela Marsavela, James B Freeman, Chris Lomma, Markus H Frank, Muhammad A Khattak, Tarek M Meniawy, Michael Millward, Majid E Warkiani, Elin S Gray, et al. Isolation and detection of circulating tumour cells from metastatic melanoma patients using a slanted spiral microfluidic device. *Oncotarget*, 8(40):67355, 2017.

[173] Kazuo Koyanagi, Steven J O'Day, Peter Boasberg, Michael B Atkins, He-Jing Wang, Rene Gonzalez, Karl Lewis, John A Thompson, Clay M Anderson, Jose Lutzky, et al. Serial monitoring of circulating tumor cells predicts outcome of induction biochemotherapy plus maintenance biotherapy for metastatic melanoma. *Clinical Cancer Research*, 16(8):2402–2408, 2010.

[174] Xi Luo, Devarati Mitra, Ryan J Sullivan, Ben S Wittner, Anya M Kimura, Shiwei Pan, Mai P Hoang, Brian W Brannigan, Donald P Lawrence, Keith T Flaherty, et al. Isolation and molecular characterization of circulating melanoma cells. *Cell reports*, 7(3):645–653, 2014.

[175] G Marsavela, Carlos A Aya-Bonilla, ME Warkiani, ES Gray, and M Ziman. Melanoma circulating tumor cells: Benefits and challenges required for clinical application. *Cancer letters*, 424:1–8, 2018.

[176] Katharina Gorges, Lisa Wiltfang, Tobias M Gorges, Alexander Sartori, Lina Hildebrandt, Laura Keller, Beate Volkmer, Sven Peine, Anna Babayan, Ingrid Moll, et al. Intra-patient heterogeneity of circulating tumor cells and circulating tumor DNA in blood of melanoma patients. *Cancers*, 11(11):1685, 2019.

[177] Elin S Gray, Anna L Reid, Samantha Bowyer, Leslie Calapre, Kelvin Siew, Robert Pearce, Lester Cowell, Markus H Frank, Michael Millward, and Mel Ziman. Circulating melanoma cell subpopulations: their heterogeneity and differential responses to treatment. *Journal of Investigative Dermatology*, 135(8):2040–2048, 2015.

[178] Qing Kang, N Lynn Henry, Costanza Paoletti, Hui Jiang, Pankaj Vats, Arul M Chinnaiyan, Daniel F Hayes, Sofia D Merajver, James M Rae, and Muneesh Tewari. Comparative analysis of circulating tumor DNA stability in K3EDTA, Streck, and CellSave blood collection tubes. *Clinical biochemistry*, 49(18):1354–1360, 2016.

[179] Bente Risberg, Dana WY Tsui, Heather Biggs, Andrea Ruiz-Valdepenas Martin de Almagro, Sarah-Jane Dawson, Charlotte Hodgkin, Linda Jones, Christine Parkinson, Anna Piskorz, Francesco Marass, et al. Effects of collection and processing procedures on plasma circulating cell-free DNA from cancer patients. *The Journal of Molecular Diagnostics*, 20(6):883–892, 2018.

[180] Léon C van Kempen, Karin van den Hurk, Vladimir Lazar, Stefan Michiels, Véronique Winnepenninckx, Marguerite Stas, Alan Spatz, and Joost J van den Oord. Loss of microRNA-200a and c, and microRNA-203 expression at the invasive front of primary cutaneous melanoma is associated with increased thickness and disease progression. *Virchows Archiv*, 461(4):441–448, 2012.

[181] Joseph Mazar, Dan DeBlasio, Subramaniam S Govindarajan, Shaojie Zhang, and Ranjan J Perera. Epigenetic regulation of microRNA-375 and its role in melanoma development in humans. *FEBS letters*, 585(15):2467–2476, 2011.

[182] Sanne De Wit, Leonie L Zeune, T Jeroen N Hiltermann, Harry JM Groen, Guus Van Dalum, and Leon WMM Terstappen. Classification of cells in CTC-enriched samples by advanced image analysis. *Cancers*, 10(10):377, 2018.

[183] ST Ligthart, F-C Bidard, C Decraene, T Bachelot, S Delaloge, E Brain, M Campone, P Viens, J-Y Pierga, and LWMM Terstappen. Unbiased quantitative assessment of Her-2 expression of circulating tumor cells in patients with metastatic and non-metastatic breast cancer. *Annals of oncology*, 24(5):1231–1238, 2013.

[184] Lisa Goers, Paul Freemont, and Karen M Polizzi. Co-culture systems and technologies: taking synthetic biology to the next level. *Journal of The Royal Society Interface*, 11(96):20140065, 2014.

[185] Agustin Enciso-Martinez, Edwin Van Der Pol, Chi M Hau, Rienk Nieuwland, Ton G Van Leeuwen, Leon WMM Terstappen, and Cees Otto. Label-free identification and chemical characterisation of single extracellular vesicles and lipoproteins by synchronous rayleigh and raman scattering. *Journal of Extracellular Vesicles*, 9(1):1730134, 2020.

List of abbreviations

AD . . . . Adenocarcinoma

AF488 . . . . Alexa Fluor 488

AJCC . . . . American Joint Commission on Cancer

APC . . . . Allophycocyanin

APS . . . . Ammonium persulfate

bp . . . . Base pairs

BM . . . . Bone marrow

BSA . . . . Bovine serum albumin

COPD . . . . Chronic obstructive pulmonary disease

CTC . . . . Circulating tumor cell

ctDNA . . . . Circulating tumor DNA

C$_q$ . . . . Quantitation cycle

CK . . . . Cytokeratin

DAPI . . . . 4',6-diamidino-2-phenylindole

DSF . . . . Disease free survival

DMEM . . . . Dulbecco's Modified Eagle Medium

DMSO . . . . Dimethylsulfoxide

DNA . . . . Deoxyribonucleic acid

DNase . . . . Desoxyribonuclease

dNTP . . . . Deoxyribonucleoside triphosphate

DTC . . . . Disseminated tumor cell

EC . . . . Empty vector control

ECL . . . . Electrochemoluminescence

EDTA . . . . Ethylenediaminetetraacetic acid

EGFR . . . . Epidermal growth factor receptor

EMT . . . . Epithelial-mesenchymal transition

EpCAM . . . . Epithelial cell adhesion molecule

ESCRT . . . . Endosomal sorting complexes required for transport

EV . . . . Extracellular vesicle

FACS . . . . Fluorescence-activated cell sorting

FCS . . . . Fetal calf serum

FDA . . . . US Food and Drug Administration

fwd-Primer . . . . Forward-Primer

gDNA . . . . genomic DNA

GFP . . . . Green fluorescent protein

GO . . . . Gene ontology

HA . . . . Human influenza hemagglutinin

HD . . . . Healthy donor

HECT . . . . Homologous to E6-AP Carboxyl Terminus

HERC5 . . . . HECT and RLD domain containing E3 ubiquitin protein ligase 5

HRP . . . . Horseraddish peroxidase

IF . . . . Immunofluorescence

IFN . . . . Interferon

IP . . . . Immunoprecipitation

IRES . . . . Internal ribosomal entry site

ISG15 . . . . Interferon stimulated gene 15

ITB . . . . Institute of Tumor Biology

kb . . . . Kilo base pairs

kDa . . . . Kilodalton

KO . . . . Knockout

LCC . . . . Large cell carcinoma

LPS . . . . Lipopolysaccharide

mBC . . . . Metastatic breast cancer

MEM . . . . Modified Eagle Medium

MET . . . . Mesenchymal-epithelial transition

miRNA . . . . microRNA

MM . . . . Metastatic melanoma

MOPS . . . . 3-(N-morpholino)propanesulfonic acid

MRD . . . . Minimal residual disease

MS . . . . Mass spectrometry

MTT . . . . 3-(4,5-dimethylthiazol-2-yl)-2,5-diphenyltetrazolium bromide

MVB . . . . Multivesicular body

MW . . . . Molecular weight

NAD . . . . Nicotinamide adenine dinucleotide

NGS . . . . Next generation sequencing

NSCLC . . . . Non-small cell lung cancer

NTA . . . . Nanoparticle tracking analysis

OE . . . . Overexpression

OS . . . . Overall survival

par . . . . Parental

PBS . . . . Phosphate-buffered saline

PBS-T . . . . Phosphate-buffered saline Tween-20

PCA . . . . Principle component analysis

PCR . . . . Polymerase chain reaction

PD-1 . . . . Programmed death-1

PDL-1 . . . . Programmed death ligand-1

PEG . . . . Polyethylene glycol

PFA . . . . Paraformaldehyde

RNA . . . . Ribonucleic acid

RNase . . . . Ribonuclease

rev-Primer . . . . Reverse-Primer

RIN . . . . RNA integrity number

RIPA . . . . Radioimmunoprecipitation assay buffer

RLD . . . . Regulator of chromosome condensation 1 like domain

RT . . . . Room temperature

RT-qPCR . . . . Real-time quantitative polymerase chain reaction

SCC . . . . Squamous cell carcinoma

SCLC . . . . Small cell lung cancer

SDS . . . . Sodium dodecyl sulfate

SDS-PAGE . . . . Sodium dodecyl sulfate polyacrylamide gelelectrophoresis

SILAC . . . . Stable isotope labeling by amino acids in cell culture

TAE . . . . Tris-acetate-EDTA buffer

Taq-Polymerase . . . . *Thermus aquaticus* DNA-Polymerase

TEMED . . . . N,N,N',N'-Tetramethylethylenediamine

TBS . . . . Tris-buffered saline

TBS-T . . . . Tris-buffered saline Tween-20

TKI . . . . Tyrosine kinase inhibitors

TNF . . . . Tumor necrosis factor

Tris . . . . Tris(hydroxymethyl)aminomethane

TSG101 . . . . Tumor susceptibility gene 101

Ub1L . . . . Ubiquitin-activating enzyme E1-like protein

UbcH8 . . . . Ubiquitin-carrier protein H8

UBL . . . . Ubiquitin-like modifier

UICC . . . . Union for International Cancer Control

UKE . . . . University Medical Center Hamburg-Eppendorf

UMI . . . . Unique molecular index

UV . . . . Ultraviolet

VAF . . . . Variant allele frequency

Appendix

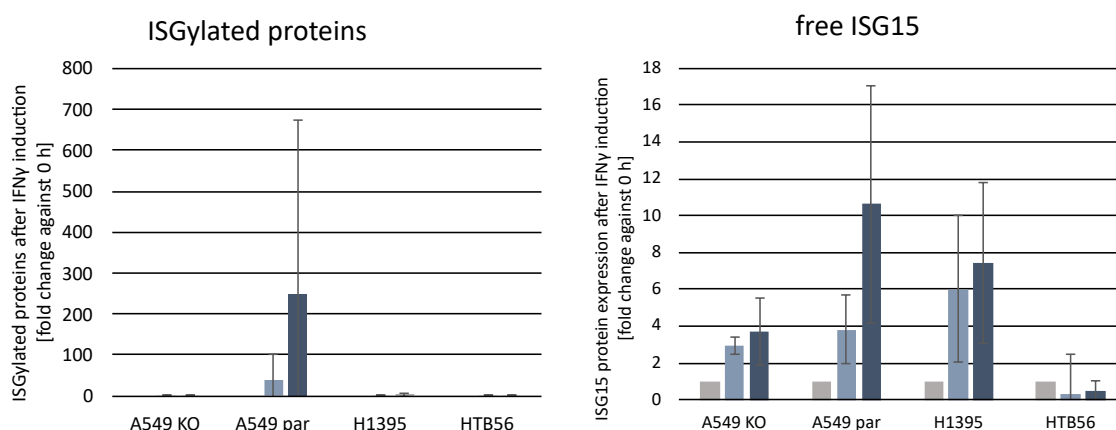## IFNγ-induced regulation of ISG15 expression

Figure 44: Protein quantification after IFNγ treatment. A549 KO, A549 par, H1395 and HTB56 cell lines treated with 10 ng/mL IFNγ for 24 h (light blue) and 48 h (dark blue). Expression was normalized to 0 h (gray). Left: ISGylated proteins, right: free ISG15. Averaged values are shown from three biological replicates (n=3) with error bars depicting corresponding standard deviations.

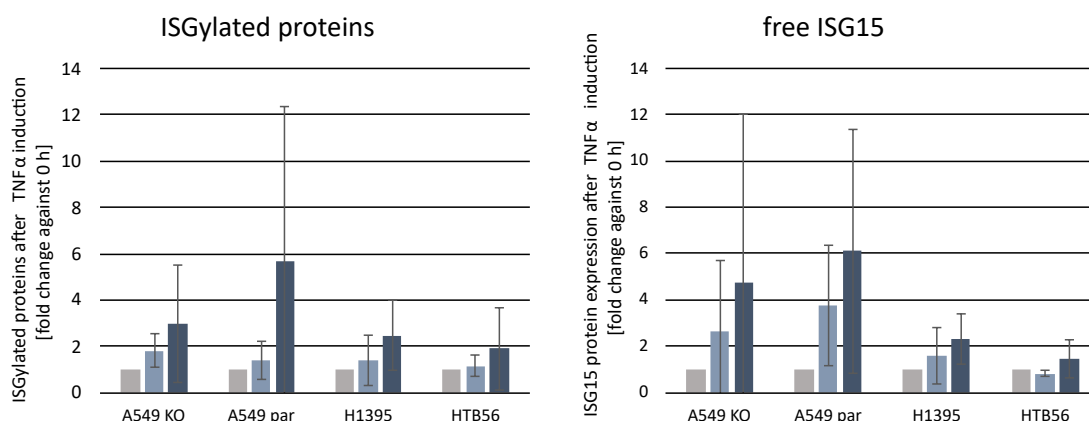## TNFα-induced regulation of ISG15 expression

Figure 45: Protein quantification after TNFα treatment. A549 KO, A549 par, H1395 and HTB56 cell lines treated with 10 ng/mL TNFα for 24 h (light blue) and 48 h (dark blue). Expression was normalized to 0 h (gray). Left: ISGylated proteins, right: free ISG15. Averaged values are shown from three biological replicates (n=3) with error bars depicting corresponding standard deviations.
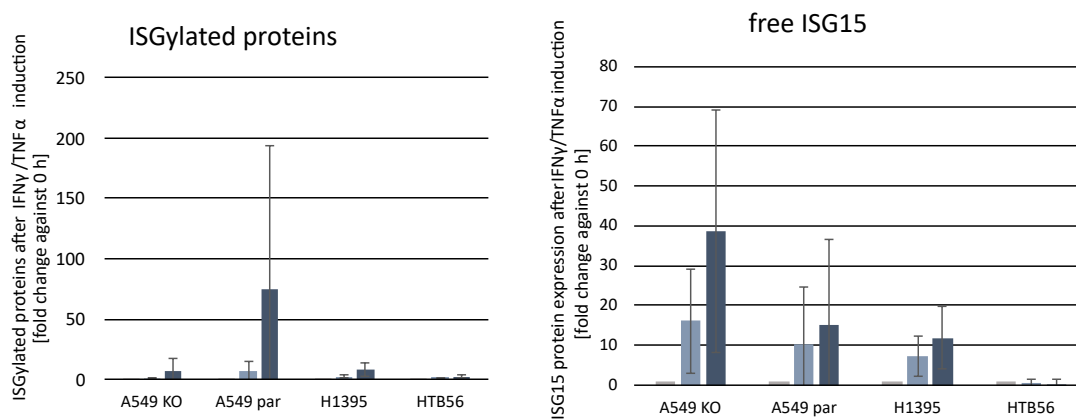
IFNγ and TNFα-induced regulation of ISG15 expression

Figure 46: Protein quantification after IFNγ and TNFα treatment. A549 KO, A549 par, H1395 and HTB56 cell lines treated with 10 ng/mL IFNγ and TNFα for 24 h (light blue) and 48 h (dark blue). Expression was normalized to 0 h (gray). Left: ISGylated proteins, right: free ISG15. Averaged values are shown from three biological replicates (n=3) with error bars depicting corresponding standard deviations.

Danksagung

Die intensive Zeit meiner Promotion hat mich sicherlich nicht nur fachlich, sondern auch persönlich geprägt. Eine der wichtigsten Erkenntnisse ist jedoch, dass gute Forschung immer das Ergebnis der Zusammenarbeit von vielen Einzelnen ist. Daher möchte ich mich bei all denjenigen bedanken, die zu dieser Arbeit beigetragen haben.

Ein großer Dank gilt Herrn Prof. Dr. Klaus Pantel für die mir gegebene Möglichkeit, meine Promotion in einem so faszinierenden Forschungsfeld im Institut für Tumorbiologie durchführen zu dürfen. Die gemeinsamen Institutsseminare boten mir stets spannende Diskussionen um die Forschung voranzutreiben.

Bedanken möchte ich mich ebenso bei meiner Betreuerin Prof. Dr. Haiju Wikman, dass ich die Gelegenheit hatte, an einem für mich so spannenden Thema in den letzten vier Jahren forschen zu dürfen. Dabei gab es stets die Gelegenheit, auch über das Thema hinaus neue Projekte kennenzulernen, um so meinen Wissensstand im Bereich der Krebsforschung zu erweitern.

Großer Dank gilt vor allem auch Dr. Stefan Werner, der ebenfalls kontinuierlich mit einem guten Rat beiseite stand und unsere Gruppe betreut hat. Ich bin euch für die Möglichkeit dankbar, an mehreren Konferenzen teilgenommen zu haben, vor allem natürlich, so eine tolle Reise mit euch nach Chicago erlebt zu haben!

Bei Frau Prof. Dr. Susanne Dobler bedanke ich mich herzlich für die Begutachtung meiner Dissertation und der kurzfristigen Bereiterklärung, Teil meiner Prüfungskommission zu sein.

Mein besonderer Dank gilt außerdem allen Mitgliedern der AG Wikman. Insbesondere danke ich dir, Jolanthe, für deine tatkräftige Unterstützung und dass du immer für uns da warst. Ich bin sehr dankbar für Katharina und Lena, die mich den größten Teil meiner Promotion begleitet haben. Wir haben nicht nur den Laboralltag, sondern auch viele schöne private Momente geteilt und ihr seid sehr gute Freundinnen geworden. Mit euch bin ich durch alle Höhen und Tiefen gegangen, die das Doktorandenleben so mit sich bringt, das wird mir ewig in Erinnerung bleiben. Yassine, ich danke dir für deine dauerhaft gute Laune und Unterstützung (unter anderem auch durch die unzähligen Kekse!) und dass du es mit den Wikman-girls so lange ausgehalten hast. Bedanken möchte ich mich ebenso bei Desiree für die Korrekturhilfen und Unterstützung, aber auch für die willkommenen Ablenkungen während unserer Kaffeepausen. Ich danke außerdem Thais für die Unterstützung unserer Arbeitsgruppe. Nicht zu vergessen sind natürlich auch die zahlreichen Medizin-Doktoranden und MLS-Studenten, die uns in letzten Jahren im Labor unterstützt haben. Ein großer Dank gilt dabei Lelia für die Kooperation und Hilfe unserer gemeinsamen Publikation. Besonders

danke ich auch meiner Masterstudentin Angelika, die dieses Projekt im Rahmen ihrer Masterarbeit unterstützt hat.

Für sehr hilfreiche fachliche Unterstützung der SILAC Analysen danke ich außerdem Dr. Kai Bartkowiak. Ebenso möchte ich mich bei Hannah Voß für die Hilfe bei den massenspektrometrischen Messungen der EVs bedanken.

Ich danke Dr. Linda Scarrott für die Durchsicht der Diskussion und für das Erstellen des Englisch-Zertifikats in so kurzer Zeit.

Bedanken möchte ich mich beim gesamten Tumorbiologie-Team für die Unterstützung bei allen technischen und wissenschaftlichen Fragen, das nette Arbeitsklima und die gute Zusammenarbeit. Vielen Dank an euch alle!

Ein besonderer Dank gilt außerdem all meinen Doktoranden-KollegInnen, mit denen ich diese besondere Zeit teilen durfte. Ich bedanke mich daher bei Sonja, Johanna, Pari, Ines, Leonie, Lucija, Yang, Sebastian, Claudia, Jana, Maha, Mais und Gresa. Ihr habt meine Promotionszeit unvergesslich gemacht!

Ich möchte mich vor allem auch bei meinen Freundinnen Sarah, Judith, Nadine, Ina und Julia bedanken, dass ihr mich stets bestärkt und durchgehend begleitet habt. Ich danke euch sehr für die zahlreichen Korrekturhilfen, für die täglichen Hundevideos, gifs, und natürlich für eure Unterstützung und Freundschaft!

Mein besonderer Dank gilt meiner Familie, für den Glauben an mich, für das Verständnis meiner häufigen Abwesenheit und für eure Unterstützung.

Mein abschließender Dank gilt meinem Freund Katsuya. Ich möchte dir von ganzem Herzen dafür danken, dass du mich unermüdlich unterstützt und motiviert hast. Danke, dass du mir in den guten, aber auch den schwierigen Phasen beigestanden, und stets Rücksicht auf meine Arbeit genommen hast. Deine Gelassenheit, Objektivität und deine Fürsorge haben mich immer wieder aufgemuntert und daran erinnert, das Wesentliche im Leben nicht aus den Augen zu verlieren. ありがとう

Eidesstattliche Versicherung

Hiermit erkläre ich an Eides statt, dass ich die vorliegende Dissertationsschrift selbst verfasst und keine anderen als die angegebenen Quellen und Hilfsmittel benutzt habe.

Hamburg, den .... 2020 ....

Dr. Linda Scarrott
Borselstraße 32
22765 Hamburg

Universitätsklinikum Hamburg-Eppendorf
Institut für Tumorbiologie
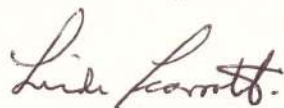Martinistraße 52, 20246 Hamburg

Hamburg, 21.04.2020

Subject: English Language Thesis Certification for Svenja Schneegans

To whom it may concern,

Svenja Schneegans, who was born on 28.06.1990 in Hamburg, Germany, is submitting her doctoral dissertation in English. The title of the thesis is "The putative role of HERC5 in NSCLC metastasis and its potential utility as a liquid biopsy marker".

I hereby certify as a native English speaker and molecular biologist that the English language used in this thesis is sufficiently correct for submission.

Yours Sincerely,

Dr. Linda Scarrott